The Hong Kong Polytechnic University
Department of Health Technology and Informatics

Assessment of Articular Cartilage Using Optical Coherence Tomography and High Frequency Ultrasound

By

Shuzhe, Wang

A thesis submitted in partial fulfilment of the requirements for the degree of Master of Philosophy

March, 2009

CERTIFICATE OF ORIGINALITY

I hereby declare that this thesis is my own work and that, to the best of my knowledge and belief, it reproduces no material previously published or written, nor material that has been accepted for the award of any other degree or diploma, except where due acknowledgement has been made in the text.

_____ (Signed)

Wang Shuzhe (Name of student)

ABSTRACT

Abstract of thesis titled

"Assessment of Articular Cartilage Using Optical Coherence Tomography and High Frequency Ultrasound"

Submitted by Shuzhe, Wang

for the Degree of Master of Philosophy

at The Hong Kong Polytechnic University

in March 2009

Articular cartilage is a thin complex tissue covering the bony ends of joints. Optical coherence tomography (OCT) has recently attracted researchers' attention for the assessment of articular cartilage due to its characteristics of having miniaturized probe and high resolution and being non-contact. However, little has been reported on the basic characteristics of articular cartilage determined using OCT. High frequency ultrasound has also been a useful tool to assess the condition of articular cartilage. Little systematical study has been done, however, to investigate the relationships between morphological, acoustic and mechanical properties of articular cartilage. No study has been reported to use both OCT and ultrasound simultaneously for the assessment of articular cartilage.

In this study, an OCT system with a central wavelength of 1310 nm was employed to investigate the refractive index (RI), OCT roughness index

(ORI), and stiffness of cartilage. A high frequency ultrasound system (55 MHz) and an ultrasound water jet indentation system (20 MHz) were also used to measure the ultrasound roughness index (URI), acoustic parameters, thickness, and stiffness of cartilage.

In the experiment of the depth and degeneration dependences of RI assessment, articular cartilage plugs were collected from bovine patella (n=18). The cartilage layer was further prepared into two halves and three horizontal cartilage slices (n=18×2×3) with an approximately equal thickness. Forty samples for surface roughness, acoustic parameters, thickness and mechanical properties measurements were prepared from twenty bovine patellae (n=20×2). The enzymes, collagenase and trypsin, were applied to remove the collagen fibrils and proteoglycans in cartilage, respectively, to simulate cartilage degeneration.

It was found that the RI was significantly different among the three layers for both normal and enzyme-treated articular cartilage, while the enzyme treatments didn't lead to a significant change. Both ORI and URI results showed significant increase of roughness index in the collagenase digestion group. No significant difference was observed in the trypsin digestion group. The results of mechanical properties of articular cartilage showed that stiffness reduced significantly in both enzyme treatment groups. Histological analysis revealed that most of the proteoglycans were depleted after the trypsin digestion. Images of scanning electron microscopy (SEM) suggested a degradation of cartilage surface after the collagenase digestion.

A linear relationship was observed between ORI and URI results. Stiffness measured by both air jet and water jet indentation tests showed linear relationships with the stiffness and Young's modulus obtained by standard mechanical indentation tests. A linear relationship was noted between the integrated reflection coefficient (IRC) and URI. Inverse and power relationships were noted between stiffness and roughness index in the collagenase treatment group.

In summary, OCT and ultrasound could be useful tools to investigate the optical (OCT), acoustic (ultrasound), morphological, and mechanical properties of articular cartilage quantitatively. The combination of these two techniques may provide a comprehensive assessment of articular cartilage. Future studies are needed to further investigate properties of cartilage from different sites and species. The studies of quantitative assessments of cartilage properties *in vivo* using endoscope-based OCT and ultrasound are also necessary in the future.

Keywords: Optical coherence tomography; OCT; ultrasound; indentation; articular cartilage; osteoarthritis; cartilage degeneration; refractive index; roughness index; stiffness; air jet; water jet.

ACKNOWLEDGEMENTS

This study was carried out in the Department of Health Technology and Informatics, The Hong Kong Polytechnic University during the year 2006-2008. Given this opportunity, I would like to express my sincere thanks to people who helped me during my study. Without their help, I could not have finished my study described in the following sections.

First I would like to give my deepest and most sincere thanks to my supervisor, Prof. Yongping Zheng, for giving me so much help and support during these two years. He has taught me so many things since I began my postgraduate study. Prof. Zheng guided me into the research field, not only by teaching me how to search and learn from the literature, to present ideas and research work, to write academic articles, but also by affecting me with his passion and devotion toward research. I always got plentiful suggestions, feedbacks and ideas by discussing with him about my research work. His working attitude has deeply affected me and pushed me to keep working hard.

I would like to thank Dr. Michael Ying, Dr Patrick Lai, and Dr. Mo Yang for assessing my confirmation report and providing valuable suggestions and comments to my project. Thanks are also given to Mr. Yanping Huang in our research group, who gave me a lot of support during my study, including system setup and suggestion on the experimental design. I learned a lot from him. I would also like to acknowledge Ms. Brenda Cheung of

Medical Lab and Dr. Qing Wang for sharing their knowledge and expertise in histological analysis, and Mr. James Cheung and Mr. Kungchee Chen for their kind help and advice for the use of devices in workshop for specimen preparation and sample fixation device design. Thanks are also given to Ms. Sally Ding for her encouragement and support during my study and her kind help in editing my papers and thesis. I also wish to thank Dr. Mo Yang, Mr. Jinjiang Yu, Mr. Zongbin Liu, and Mr. Baojian Xu for the use of the microscopy system and incubator. I would like to express my thanks to Mr. Jeremy Yang of Materials Research Centre for his assistance in using the SEM system. I would like to thank Prof. Ming Zhang, and Mr. Jia Yu for the use of standard mechanical indentation device. My thanks also go to Dr. Yonghong He and Mr. Peng Li of Graduate School at Shenzhen, Tsinghua University for their help in the design of the OCT system.

I would also like to thank all my fellow colleagues and students who had contributed in my research study. They include Dr. Qinghua Huang, Dr Tracy Lu, Dr. Xin Chen, Dr Yongjin Zhou, Mr. Junfeng He, Mr. Zhengming Huang, Dr. Queeny Yuen, Ms. Jiawei Li, Ms. Jingyi Guo, Mr. Congzhi Wang, Dr Hongbo Xie, and Mr. Louis Lee. Some of them have provided great help in building software system and system setup. Some have given me great suggestion and advice on my project. They have encouraged me with their friendly attitude and helped me a lot all through my study.

I would like to dedicate this thesis to my beloved family and friends. Only with their encouragement and selfless support, I could have concentrated on my research.

Finally, I would like to acknowledge the financial support from The Hong Kong Polytechnic University and Hong Kong Research Grant Council (PolyU5318/05E, PolyU5245/03E).

TABLE OF CONTENTS

LIST OF ABBREVIATIONS

3D	Three-dimensional
A/D	Analog-to-digital
AIB	Apparent integrated backscatter
CT	Computer tomography
CV	Coefficient of variation
EDTA	Ethylenediam-tetra-acetic acid
FCD	Fixed charge density
FEPA	Federation of European Producers of Abrasives
FFT	Fast Fourier Transform
IA	Integrated attenuation
IBS	Integrated backscatter
IRC	Integrated reflection coefficient
MRI	Magnetic resonance imaging
OA	Osteoarthritis
OCT	Optical coherence tomography
ORI	OCT roughness index
PS	Polarization-sensitive
RF	Radio frequency
RI	Refractive index
RMS	Root mean square
ROI	Region of interest
SD	Standard deviation
SEM	Scanning electron microscope
URI	Ultrasound roughness index

LIST OF FIGURES

LIST OF TABLES

CHAPTER 1 INTRODUCTION

1.1 Background of the study

Articular cartilage is a thin complex, biological tissue that covers the bony ends of joints. Structurally, it is mainly composed of 5-10% proteoglycans, 10-20% collagen and 68- 85% water (Mow *et al.*, 2005). Functionally, it provides a cushion and excellent lubrication between two bones of a joint (Benedek, 2006). From the surface to subchondral bone, articular cartilage can be separated into three zones, superficial, middle (transitional), and deep (radial) zones, according to the orientation of collagen fibrils (Mow *et al.*, 2005; Langsjo *et al.*, 1999). The volumetric concentration of collagen fibril increases from the superficial zone to the deeper zones (Langsjo *et al.*, 1999; Patil *et al.*, 2004). The collagen fibrils are known to be responsible for tensile and dynamic properties of cartilage, while proteoglycans establish compressive properties (Armstrong and Mow, 1982; Bader *et al.*, 1992).

Changes in the components of articular cartilage would cause degeneration, which might further lead to osteoarthritis (OA), one of the most common joint diseases among adults (Yelin and Callahan, 1995). Clinically, the diagnostics of OA include radiography (X-ray) (Forman *et al.*, 1983), arthroscopy (Armstrong and Mow, 1982; Dashefsky, 1987), magnetic resonance imaging (MRI) (Burstein and Gray, 2003) and ultrasonography (Grassi and Cervini, 1998; Chao and Kalunian, 2008). However, all these techniques have some limitations. X-ray cannot detect the early stage of the disease, and arthroscopy can only assess the surface condition of articular

cartilage; while most clinically used MRI has limited resolution and is expensive. For the ultrasound assessment, there is still no universal recognized scoring system for OA assessment using greyscale ultrasound alone.

In order to seek for other methods to detect OA at its early stage and at a lower cost, researchers have tried to monitor the changes in the material properties of the articular cartilage, which is associated with the cartilage's degeneration. The propagation of ultrasound wave in articular cartilage has been very systematically investigated and the results of these studies have led to the development of miniaturized probes for potential *in vivo* assessment of cartilage degeneration. Measuring multiple parameters using the same set of samples can provide comprehensive information of articular cartilage. However, most of the studies just measured few parameters due to the focus of the study or the limitation of the available equipment. And the measurement of morphological, mechanical and acoustic properties and the study of the relationships among those properties of articular cartilage using the same set of samples using ultrasound have not been widely reported.

Optical coherence tomography (OCT) has recently attracted researchers' attention for the assessment of articular cartilage due to its characteristics of having miniaturized probe and high resolution and being non-contact. It employs nonionizing optical radiation and an absolute measurement technique developed for high resolution imaging and characterization of optoelectronic components (Podoleanu, 2005; Schmitt, 1999; Huang *et al.*,

1991; Al-Ahalabi *et al.*, 1983). A lot of research has been conducted in order to investigate and assess the ability of OCT in monitoring articular cartilage properties with the purpose of providing an alternative tool for OA detection. However, little has been reported on the basic characteristics of articular cartilage determined using OCT, such as its optical, morphological, and mechanical properties.

1.2 Aim and objectives of the study

The overall aim of this project is to conduct a systematic study on the assessment of articular cartilage using OCT and high frequency ultrasound so as to investigate their feasibility for the early diagnosis of OA. The specific objectives of the study are as follow:

1) To use OCT to assess the refractive index (RI) of articular cartilage under different conditions in order to evaluate the suitability of RI for the detection of OA and as a indicator for different cartilage layers;

2) To employ OCT and high frequency ultrasound to measure the surface roughness of degeneration dependent articular cartilage in order to evaluate the feasibility of surface roughness for the detection of enzyme induced OA;

3) To apply high frequency ultrasound to assess the acoustic properties and thickness of degeneration dependent articular cartilage to comprehensively determine the large set of acoustic parameters and their interrelations; and

4) To use the OCT air jet indentation and the ultrasound water jet indentation systems to assess the mechanical properties of degeneration dependent articular cartilage to determine the feasibility of those novel techniques to detect enzyme induced OA.

1.3 Outline of the dissertation

Following the introduction chapter, the remaining chapters of the thesis are outlined as follows:

In Chapter 2, a review of research and literature related to this study on articular cartilage and current assessment techniques is provided. Articular cartilage structure, degeneration and assessment methods are presented and followed by an introduction of the applications of ultrasound and OCT in articular cartilage assessment. Then some properties of articular cartilage related to this study are discussed, including the optical property (RI), morphological property (surface roughness index), and mechanical properties.

Chapter 3 introduces the methods used in this study. There are three major tests; including RI measurement, roughness and acoustic parameters measurement and indentation tests. In each test, specimen preparation, system setup, measurement procedure, parameters calculation and statistical analysis are introduced in details.

In Chapter 4, the results obtained using the described methods are presented, including the findings of RI, roughness index, acoustic parameters, together with cartilage thickness and stiffness. The images obtained in histological analysis as well as the scanning electron microscope (SEM) test are also presented.

Chapter 5 presents the discussion on the results obtained in the tests. Comparisons are made and limitations of the study are addressed.

Chapter 6 summarizes the findings of this study and the directions for future studies are suggested.

CHAPTER 2 LITERATURE REVIEW

This chapter presents a review of literature on articular cartilage and its assessment methods including OCT and ultrasound. There are three major parts. The first part (Section 2.1) addresses articular cartilage structure, degeneration and assessment methods. The second part (Sections 2.2 and 2.3) presents the applications of ultrasound and OCT in articular cartilage assessment. Then, Sections 2.4 to 2.7 discuss some properties of articular cartilage related to this study.

2.1 Articular Cartilage

2.1.1 Articular cartilage structure

Articular cartilage is a thin complex tissue that covers the bony ends of joints. Functionally, it provides a cushion and excellent lubrication between two bones of a joint (Benedek, 2006). Articular cartilage mainly consists of two distinct phases: liquid phase and solid phase. The liquid phase is composed of interstitial water and mobile ions and constitutes 68-85% of the cartilage wet weight (Mow *et al.*, 2005). The solid phase of articular cartilage is composed of collagen (mainly type II), trapped proteoglycans, other proteins, and the chondrocytes cells (Mow *et al.*, 2005; Saarakkala, 2007; Mow *et al.*, 1980). Collagens and proteoglycans are the two most important macromolecules in solid phase to form the organic matrix. Collagens are proteins which form the fibrillar network of cartilage and constitute 10-20% of the cartilage wet weight. Collagen fibrils are known to

be responsible for tensile and dynamic properties of cartilage (Armstrong and Mow, 1982; Kempson *et al.*, 1973; Bader *et al.*, 1992; Bank *et al.*, 2000). Proteoglycans constitute 5-10% of the wet weight. Each proteoglycan is formed by a core protein and one or more attached glycosaminoglycan chains (Mow *et al.*, 2005). Proteoglycans establish compressive properties in cartilage (Kempson *et al.*, 1973; Bader *et al.*, 1992).

The structure of cartilage tissue is highly organized. Fig 2.1 shows an illustration of articular cartilage zones and distribution of collagen over its full thickness (Mow *et al.*, 2005). The articular cartilage can be divided into superficial, middle (transitional), and deep (radial) zones according to the content of different components.

Superficial zone

The superficial zone represents 10-20% of the total articular cartilage thickness. In this zone, fine collagen fibrils are almost parallel to cartilage surface, and chondrocyte cells are flattened and aligned in parallel to the surface. The content of proteoglycan is the lowest and the content of water and collagen is the highest.

Middle zone

In the middle zone (approximately 40-60% of the articular cartilage thickness), the diameter of collagen fibrils becomes larger and orientation of the fibrils becomes random. The water content, collagen content and cell

density are lower than those in the superficial zone and the content of proteoglycan reaches its maximum in this zone.

Deep zone

The third zone, which comprises approximately 30% of the total thickness, is the deep zone. The collagen fibrils appear to bond together and are oriented approximately perpendicular to the cartilage surface. The water content and cell density are the lowest in this zone (Mow *et al.*, 2005; Mow and Guo, 2002; Patil, 2004; Saarakkala, 2007).

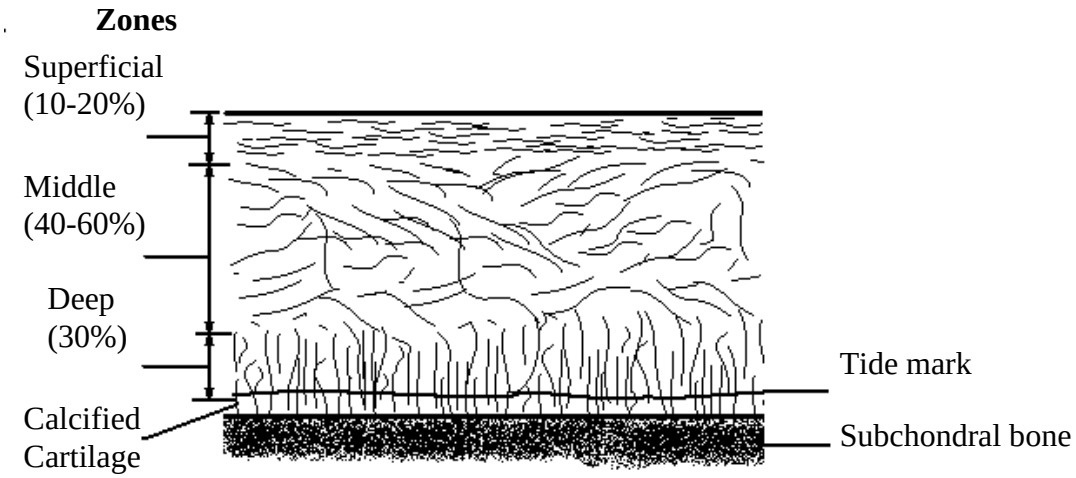

Fig 2.1. Schematic representation of the zonal arrangement of articular cartilage tissue (Mow *et al.*, 2005). The tissue can be divided into superficial, middle, deep zones and calcified cartilage according to the structure and composition. The subchondral bone is located underneath the cartilage tissue.

Because of the inhomogeneous distribution of water, proteoglycan concentration and the orientation of the collagen fibrils, the mechanical properties of articular cartilage vary at different depth (Chen *et al.*, 2001a; 2001b; Schinagl *et al.*, 1997). Since the articular cartilage is structurally

inhomogeneous, measuring the depth dependent properties of articular cartilage is important for the investigation of articular cartilage structure as well as for finding the reason behind its degeneration and for the articular cartilage tissue engineering (Risbud and Sittinger, 2002).

2.1.2 Articular cartilage degeneration

2.1.2.1 Spontaneous cartilage degeneration

OA is caused by the breakdown and eventual loss of the cartilage of one or more joints. It is a common joint disorder and affects millions of elderly individuals all over the world (Lawrence *et al.*, 1966; Rapp *et al.*, 2000; Zhang *et al.*, 2001; Zhang and Jordan, 2008). The most important abnormality associated with OA is cartilage degeneration, which is associated with changes in the properties of the material (Yelin and Callahan, 1995). OA usually appears in the knee, foot, hip, spine and hand joints. It can result in pain, crepitation with motion, progressive restriction of motion, joint effusions and deformity (Buckwalter and Mankin, 1997).

The progression of OA can be divided into three phases: early degeneration, advanced degeneration and late degeneration (Buckwalter and Mankin, 1997; Saarakkala, 2007).

Early degeneration

The early degeneration phase is also known as disruption or alteration of the cartilage matrix. This stage happens either before or with the appearance of

fibrillation. The content of cartilage water increases (Mankin and Thrasher, 1975), and proteoglycan aggregation decreases, while the concentration of type II collagen remains almost constant (Armstrong and Mow, 1982; Bank *et al.*, 2000). Relative minor changes in the collagen network may allow the swelling of the proteoglycan molecules. These changes increase the permeability, lead to the decreasing of cartilage matrix mechanical stiffness and may also increase the chance of cartilage tissue suffering additional mechanical damage.

Advanced degeneration

The advanced phase is also called as the phase of chondrocytic response to tissue damage. This phase begins when tissues damage or change in osmolarity and charge is detected by tissue chondrocytes. The chondrocytes then release mediators into the tissue to stimulate the cartilage repair process. This repair process may last for years and in some cases, the repair response can temporarily reverse the OA course (Buckwalter and Mankin, 1997). Cartilage surface loses its glossy feature in this stage. Surface fibrillation and superficial or deep defects can be observed.

Late degeneration

When the chondrocytic response fails to stabilize or restore the tissue, the late degeneration which is also known as the decline of chondrocytic synthetic response and the progressive loss of tissue begins. In the late degeneration stage, progressive loss of articular cartilage and the decline of

chondrocytic response can occur. The symptoms of OA, such as pain and loss of joint function, appear as a result of cartilage tissue worn out.

2.1.2.2 Experiment-induced cartilage degeneration

The spontaneously degenerated articular cartilage samples are relatively difficult to obtain and the degree of degeneration process is hard to control. Therefore, it is reasonable to use experiment-induced cartilage degeneration models to study OA. In general, there are two typical methods to simulate these pathological changes: enzyme digestion and experimental animal models (Bader and Kempson, 1994; Lyyra *et al.*, 1999; Moskowitz *et al.*, 2007).

Enzyme digestion

Enzyme treatment is a widely accepted method to simulate the degeneration of articular cartilage. Collagenase and trypsin are two frequently used enzymes. Collagenase is responsible for the degradation of the collagen network (Shingleton *et al.*, 1996) while trypsin is effective for the proteoglycan digestion with a slight simultaneous effect on the collagen network (Harris *et al.*, 1972).

The degeneration of collagen fibrils can be investigated by SEM (Saarakkala *et al.*, 2004b) and polarized light microscope (Nieminen *et al.*, 2000; Cherin *et al.*, 2001). The changes of proteoglycan can be quantified by histological analysis using fast green and safranin O staining (Wang, 2007; Wang *et al.*, 2008b; Lyons *et al.*, 2006) and detected by MRI

(Wheaton *et al.*, 2005; Watrin-Pinzano *et al.*, 2005) or high frequency ultrasound (Wang *et al.*, 2008b).

Experimental animal models

Experimental animal models using external operations such as surgical damage, loading, and intra-articular drug injection have also been used to simulate the cartilage degeneration process. Surgical damage models induce OA *in vivo* by surgery such as meniscectomy (Welsing *et al.*, 2008; Song *et al.*, 2006) and transaction of the anterior cruciate ligament (Batiste *et al.*, 2004). Both *in vivo* (Thompson *et al.*, 1991) and *in vitro* (Borrelli et al., 1997) loading can induce cartilage degeneration. Joint immobilization is another method to stimulate OA (Behrens *et al.*, 1989). Intra-articular drug injection is often used to induce acute cartilage damage, using chemical reagents or biological mediators, such as collagenase (Vanderkraan *et al.*, 1990; Kikuchi *et al.*, 1998), papain and mono-iodo-acetic acid (Laurent *et al.*, 2003; Cherin *et al.*, 1998).

2.1.3 Articular cartilage assessment

The measurement of articular cartilage properties is important for investigating the reasons behind the degeneration and exploring the approaches for its diagnosis and treatment. Several techniques have been adopted by researchers to assess articular cartilage *in vitro* or *in vivo*. Radiography (X-ray) (Forman *et al.*, 1983; Swagerty and Hellinger, 2001), arthroscopy (Abdel-Hamid *et al.*, 2006; Venkatesh, 2006), and MRI (Link *et*

al., 2002; Rauscher *et al.*, 2008; Mui *et al.*, 2007) are frequently used clinical diagnostic approaches for OA.

X-ray

A typical sign of advanced or late cartilage degeneration is joint space narrowing. This sign can be observed in X-ray images (Fig 2.2) (Swagerty and Hellinger, 2001). Since the cartilage tissue does not significantly attenuate X-rays because the water content of cartilage tissue can reach to approximately 85% weight, evaluating the status of cartilage tissue only from X-ray images is not applicable. Therefore, routine radiography, is somewhat limited in its sensitivity in detecting early stages of OA (Saarakkala, 2007).

Arthroscopy

Arthroscopy is another OA diagnostics method with a minimal-invasive procedure. An arthroscope is inserted into the joint through a hole; meanwhile, different surgical instruments can be guided into the joint with the assistance of arthroscopy. Arthroscopy method is mainly employed to evaluate articular surface damage (Fig 2.3) (Venkatesh, 2006), and is currently not suitable to examine internal structure and subchondral bone (Saarakkala, 2007).

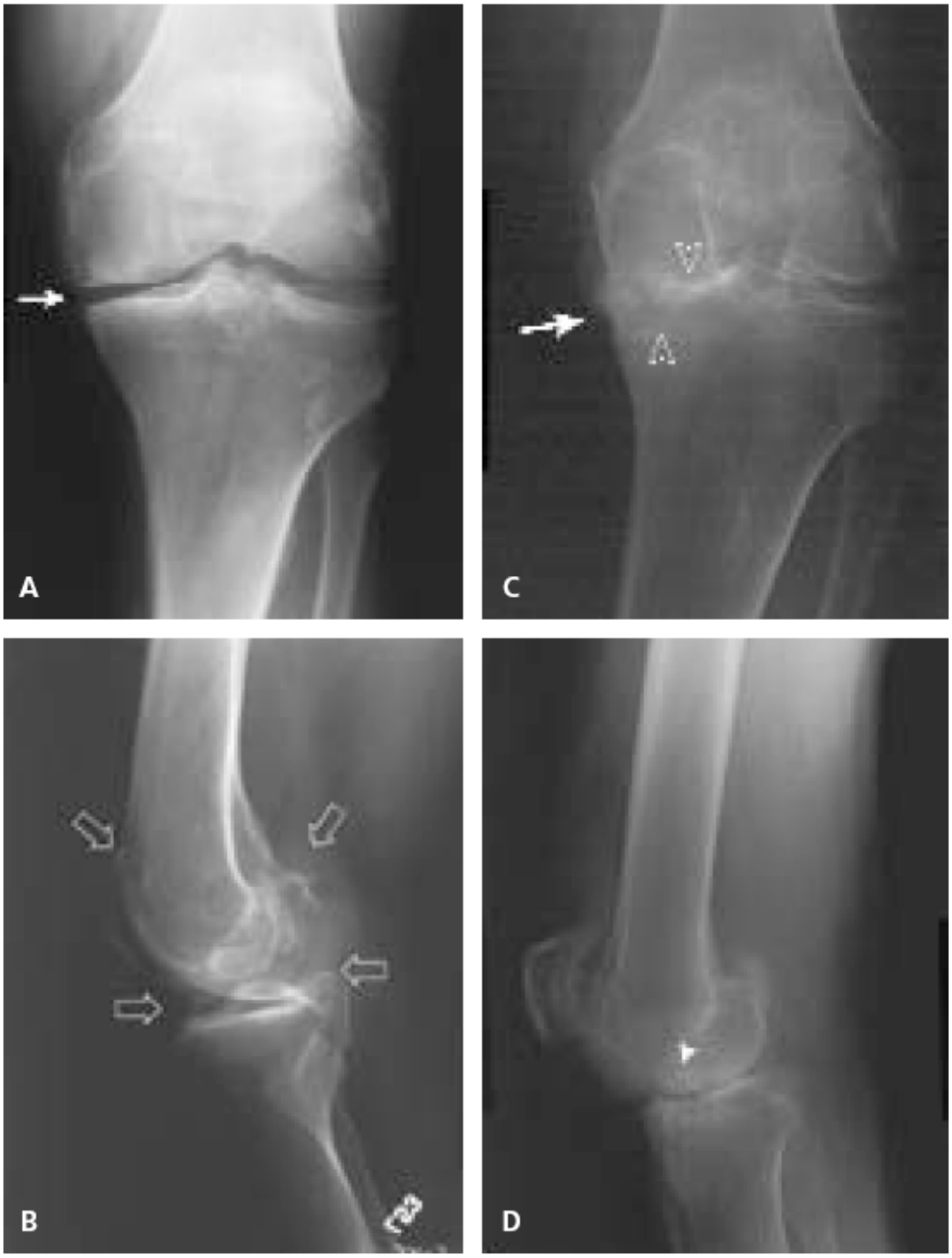

Fig 2.2. Radiographic finding of OA in the knee joints (Swagerty and Hellinger, 2001). (A) Anteroposterior view of the left knee of patient 1. Medial joint space narrowing can be observed (arrow). (B) Lateral view of the left knee of patient 1. Sclerosis with marked osteophyte formation is indicated by the arrows. (C) Patient 2 with medial joint narrowing (white arrow). (D) Subchondral cysts are noted in lateral view of patient 2 (arrowhead).

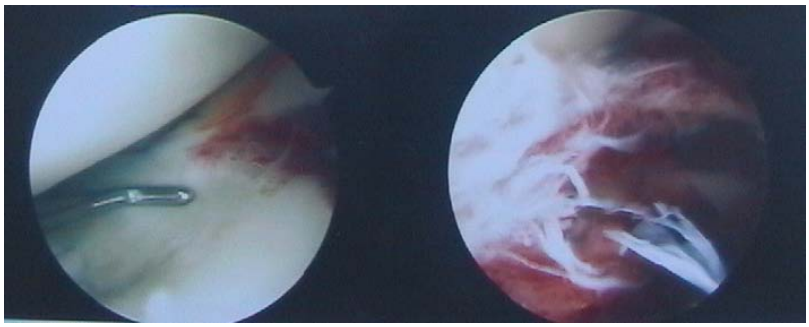

(a) (b)

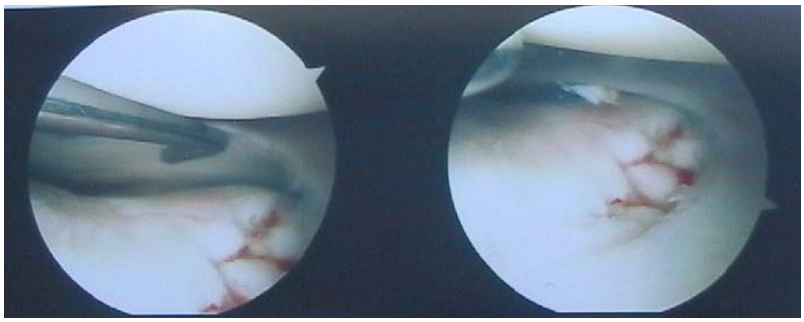

(c) (d)

Fig 2.3. Arthroscopic images before ((a) and (b)), and after ((c) and (d)) fracture reduction of the human knee joint (Venkatesh, 2006).

MRI

MRI is a non-invasive mean of diagnosing knee problems. The high water content of articular cartilage forms the basis for magnetic resonance signal (Peterfy *et al.*, 2007). Thinning and irregularity of cartilage tissue as well as subchondral bone changes can be evaluated by routine MRI (Fig 2.4)(Link *et al.*, 2002). Gadolinium enhanced T1 MRI of cartilage is suggested to be capable of examining proteoglycan concentration and distribution (Bashir *et al.*, 1999). T2 MRI is suggested to sense collagen content, collagen fibrils orientation and collagen integrity (Burstein *et al.*, 2000; Saarakkala, 2007). MRI can be one of the most promising non-invasive methods for OA diagnostics (Burstein and Gray, 2003). The sensitivity of MRI in the early

OA stage, however, is still a challenge (Burstein *et al.*, 2000). The cost of MRI and the relatively unportable nature of MRI machine can also limit its clinical use.

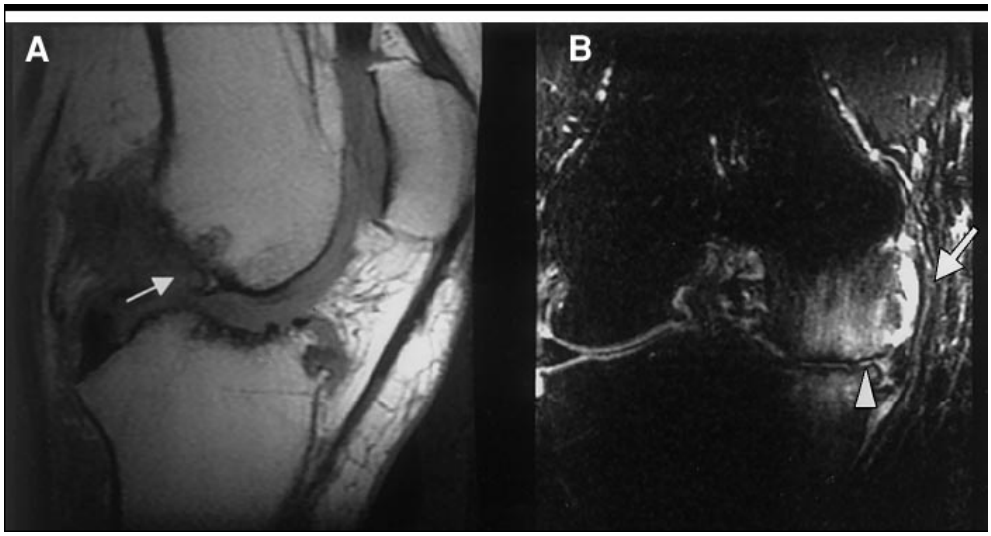

Fig 2.4. MRI images of ligamentous and meniscal lesions in patients with advanced OA (Link *et al.*, 2002). (A) T1 MRI image. The anterior cruciate ligament's absent (arrow indicated) showing a severe degenerative change. (B) T2 MRI image reveals the destruction of medial meniscus (arrowhead indicated) and medial collateral ligament sprain with a tear (arrow indicated).

Other methods of assessing articular cartilage include ultrasonography (Nieminen *et al.*, 2004; Jurvelin *et al.*, 1995; Wang *et al.*, 2008b), computer tomography (CT) (Passariello *et al.*, 1983), OCT (Drexler *et al.*, 2001; Chu *et al.*, 2007), scintigraphy (Thomas *et al.*, 1975), microscope (Myers *et al.*, 1995; Jurvelin *et al.*, 1995; Toyras *et al.*, 1999), needle penetration (Jurvelin *et al.*, 1995; Toyras *et al.*, 1999), stereophotogrammetry (Ateshian *et al.*, 1991), mechanical indentation (Appleyard *et al.*, 2001; Dashefsky, 1987), ultrasound indentation (Zheng *et al.*, 2002; Ling *et al.*, 2007; Laasanen *et al.*, 2002), and electromechanical measurements (Legare *et al.*, 2002).

2.2 Ultrasound assessment of articular cartilage

Ultrasound assessment of articular cartilage has been the subject of many recent investigations. Conventional ultrasonography is a non-invasive technique, and has been widely used for joint evaluations (Lee *et al.*, 2008). Quantitative ultrasound characterization has been recently used for the measurement of changes in thickness (Modest *et al.*, 1989; Barthez *et al.*, 2007), speed of sound (Patil, 2004; Ling *et al.*, 2007), echo pattern and frequency spectrum (Myers *et al.*, 1995; Saied *et al.*, 1997; Brown *et al.*, 2007), attenuation (Toyras *et al.*, 1999), reflection and scattering coefficients (Toyras *et al.*, 1999; Adler *et al.*, 1992; Cherin *et al.*, 1998), mechanical properties obtained using indentation (Cherin *et al.*, 1998; Laasanen *et al.*, 2002) and compression (Zheng *et al.*, 2001; 2002; Yasura *et al.*, 2007), echo reflection (Kuroki *et al.*, 2004; 2006; Kaleva *et al.*, 2008), and swelling effect (Zheng *et al.*, 2004b; 2006a; Wang *et al.*, 2008a; 2008c), The propagation of ultrasound wave in articular cartilage has been very systematically investigated and the results of these studies have led to the development of miniaturized probes for potential *in vivo* assessment of degeneration.

2.2.1 Ultrasonography images of articular cartilage

Ultrasonography is a non-invasive technique which can directly visualize cartilage. It is widely available and relatively inexpensive compared to MRI (Chao and Kalunian, 2008; Lee *et al.*, 2008; Mathiesen *et al.*, 2004). The

reliability of ultrasonography in measuring cartilage thickness and identifying focal chondral defects using animal and *in vitro* models has been demonstrated by previous researchers (Myers *et al.*, 1995; Jurvelin *et al.*, 1995). Lee *et al.* (2008) created the ultrasonographic grading system to assess the degree of OA (Fig 2.5) based on the evaluation of the sharpness of the superficial boundary, and clarity and thickness of the cartilage band.

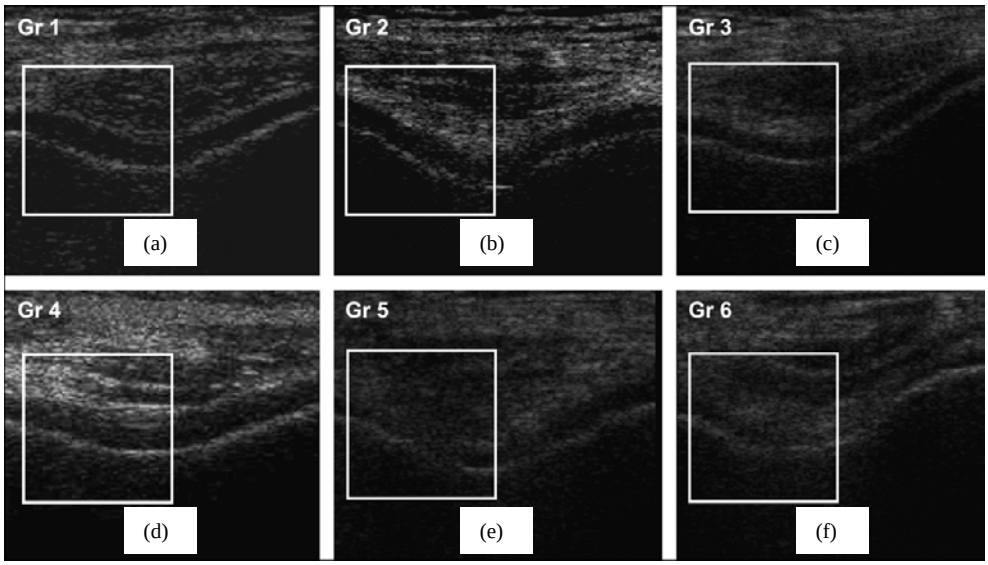

Fig 2.5. Ultrasonographic grading of human medial femoral cartilage (Lee et al., 2008). (a): Grade 1, blurred cartilage boundary or partial lack of the clarity, without obvious thickness change. (b): Grade 2, blurred cartilage boundary and partial lack of the clarity, without obvious thickness change. (c): Grade 3, blurred cartilage boundary and complete lack of the clarity. (d): Grade 4, difficult-defined cartilage boundary and complete-opaque band. (e): Grade 5, significant thickness change. (f): Grade 6, lack of visualized cartilage band. Gr: Grade.

Traditional sonography imaging, however, has its limitations. It can only access part of articulating surfaces. Currently, clinical sonography is usually used on the closed joint where sound signals could pass through the limb (Wagner et al., 2004; Tarhan et al., 2003). And the most commonly used frequency for musculoskeletal system diagnostic sonography is 3-10 MHz

(Kaplan et al., 1990), which is not sufficient enough to view the details of articular cartilage.

2.2.2 Acoustic properties measurement

Acoustic parameters such as attenuation coefficient, reflection coefficient, backscatter coefficient, and speed of sound can provide diagnostic information for articular cartilage (Nieminen *et al.*, 2002; 2007; Pellaumail *et al.*, 2002). Ultrasound has been widely used in assessing the acoustic properties of articular cartilage. Table 2.1 lists a summary of recent studies on the measurement of acoustic properties of articular cartilage.

Attenuation coefficient

Ultrasound attenuation represents ultrasound propagation property in medium. The attenuation coefficient can be a quantitative method to assess internal cartilage network. Attenuation in normal cartilage is considered to be frequency dependent (Senzig *et al.*, 1992; Nieminen *et al.*, 2002; Agemura *et al.*, 1990; Joiner *et al.*, 2001). Agemura *et al.* (1990)'s result showed integrated attenuation (IA) at frequency 100 MHz was 88-105 dB/mm for normal bovine patella articular cartilage. Senzig *et al.* (1992) reported that the IA ranged from 2.8-6.5 dB/mm at the frequency range from 10 to 40MHz. The study of Joiner *et al.* (2001) revealed IA value ranged approximately from 4.2-10.3 MHz dB/mm at the frequency range 20-40 MHz for normal human cartilage. And another study by Nieminen *et al.* (2002) reported an IA value from 9.79 to 11.49 dB/mm at the frequency range 18.8-40.0 MHz.

Backscatter coefficient

Backscatter coefficient has also been used in previous studies to quantitatively assess internal structure of articular cartilage (Pellaumail *et al.*, 2002; Cherin *et al.*, 1998; 2001). These studies showed that the backscatter coefficient of articular cartilage should have no significant relationship with proteoglycan content. Collagen and cell content, however, may affect the backscatter coefficient.

Reflection coefficient

Measuring ultrasound reflection coefficient could be another quantitative method to assess the cartilage condition (Brown *et al.*, 2008; Laasanen *et al.*, 2002; 2005; 2006; Saarakkala *et al.*, 2004b; 2006; Jaffre *et al.*, 2003; Toyras *et al.*, 1999; 2002; Nieminen *et al.*, 2002; Pellaumail *et al.*, 2002; Cherin *et al.*, 1998; 2001; Saied *et al.*, 1997). The reflection from cartilage surface was suggested being a sensitive indicator for the superficial cartilage degradation (Cherin *et al.*, 1998; Jaffre *et al.*, 2003). Surface roughness or superficial collagen network degeneration may affect integrated reflection coefficient (IRC) from cartilage surface (Laasanen *et al.*, 2002; Nieminen *et al.*, 2002). But superficial proteoglycan has no significant effect on the IRC (Laasanen *et al.*, 2002; Pellaumail *et al.*, 2002).

Table 2.1. Recent studies on articular cartilage acoustic properties measurement using ultrasound. 3D: three-dimensional

Authors (Year)	Ultrasound configuration	Sample	Acoustic parameters
(Lu et al., 2009)	A-mode; water jet; 20MHz	Bovine patellar	Reflection
(Brown et al., 2008; 2007)	A-mode; 10MHz	Bovine patellar	Reflection coefficient; frequency profile of reflection
(Kuroki et al., 2008; 2004 Hattori et al., 2005a; 2005b; 2004)	A-mode; 10MHz	Human subject (OA patients); pig and rabbit cartilage	Signal intensities; echo duration; interval between signals of cartilage
(Nieminen et al., 2007)	A-mode; 10.3MHz	Human cadaver knee; bovine knee	Speed of sound
(Laasanen et al., 2006; 2005; Saarakkala et al., 2006; 2004b)	B-mode; 20MHz	Bovine patellar; porcine femoral	Reflection coefficient
(Zheng et al., 2006b; Patil, 2004)	A-mode; 50MHz	Bovine patella	Speed of sound
(Toyras et al., 2003)	A-mode; unconfined compression; 10.5MHz	Bovine knee	Speed of sound
(Jaffre et al., 2003)	3D; 55MHz	Rat patella	Reflection coefficient
(Laasanen et al., 2002)	A-mode; 10.5MHz	Bovine knee	Reflection coefficient
(Nieminen et al., 2002)	A-mode; 29.4MHz	Bovine patella	Attenuation; reflection coefficient
(Toyras et al., 2002; 1999)	A (22MHz), B (20MHz), C, D, F (25-75MHz), M mode;	Bovine patella	Reflection coefficient; speed of sound
(Pellaumail et al., 2002; Cherin et al., 2001; 1998; Saied et al., 1997)	A, B-mode; 50; 55HMz	Rat patella	Reflection, backscatter coefficients
(Suh et al., 2001)	A-mode; 10MHz	Bovine patella	Speed of sound
(Joiner et al., 2001)	A-mode; 30MHz	Human and bovine cartilage	Speed of sound; attenuation coefficient
(Senzig et al., 1992)	A-mode; 25MHz	Bovine femur	Attenuation coefficient
(Agemura et al., 1990)	A-mode; 100MHz	Bovine patella	Attenuation coefficient; speed of sound

Speed of sound

Speed of sound is an important parameter of articular cartilage measurement. Previous studies have investigated the speed of sound in articular cartilage in different cartilage layers and along different directions (Patil *et al.*, 2004),

at different sites and degenerative stage (Toyras *et al.*, 1999; 2002; 2003), under different pressure during mechanical compression (Nieminen *et al.*, 2007), different bathing saline concentration (Zheng *et al.*, 2006b) and temperature (Patil, 2004). It has been reported that tissue composition, i.e. water, proteoglycan, collagen content, has large effect on speed of sound in cartilage (Toyras *et al.*, 2003). Factors such as temperature, medium concentration, pressure applied on the sample can also affect the speed of sound of articular cartilage (Patil, 2004; Patil *et al.*, 2004).

Other ultrasound parameters were also used to investigate the properties of articular cartilage. A novel ultrasound water jet indentation system was used to measured reflected ultrasound echoes, and a significant decrease of echo amplitude was found from trypsin treated bovine articular cartilage samples (Lu *et al.*, 2009). Another group (Kuroki *et al.*, 2008; Hattori *et al.*, 2004; 2005a; 2005b) measured signal intensity and echo duration to assess the surface conditions of articular cartilage. Frequency profile of the reflection from cartilage surface and osteochondral junction had also been studied (Brown *et al.*, 2007).

2.3 OCT assessment of articular cartilage

2.3.1 Background of OCT

OCT has recently attracted researchers' attention for the assessment of articular cartilage due to its characteristics of having miniaturized probe and

high resolution and being non-contact (Podoleanu, 2005; Schmitt, 1999; Huang *et al.*, 1991).

OCT is sometimes analogous to ultrasound except that OCT employs transverse optical and infrared waves while ultrasound uses longitudinal sound waves (Podoleanu, 2005). It is a non-invasive imaging modality which employs nonionizing optical radiation developed for high resolution ranging and characterization of optoelectronic components (Al-Ahalabi *et al.*, 1983; Podoleanu, 2005).

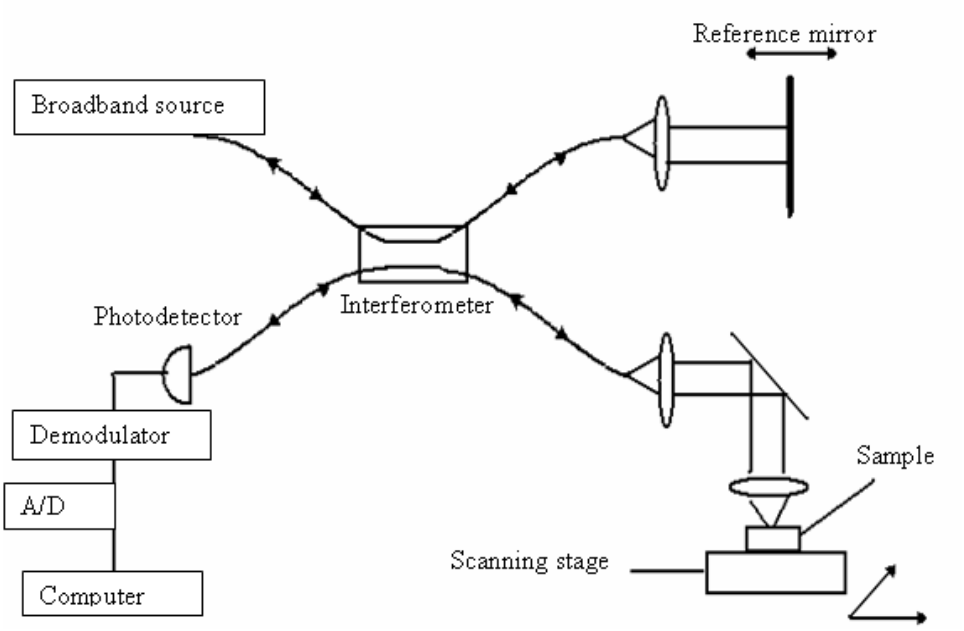

Fig 2.6. A schematic representation of OCT system. A/D: analog-to-digital converter (Tearney *et al.*, 1995).

Most OCT devices use Michelson interferometer (or a variant) to perform low-coherence interferometry. A typical OCT scheme is shown in Fig 2.6 (Tearney *et al.*, 1995; 1997). Light from a broadband source is split into two paths. One path leads to the sample to be imaged, while the second path is a

reference path. Interference is detected by a photodetector at the output of the interferometer only when the optical path lengths of the reference and the sample arm are matched to be within the coherence length of the light (Tomlins and Wang, 2005).

The standard equation for calculating the axial resolution for OCT imaging in free space is equation 2.1 (Brezinski, 2006):

$$l_c = \frac{2\ln 2}{\pi}\frac{\lambda^2}{\Delta\lambda} \qquad (2.1)$$

where l_c is the axial resolution of OCT imaging, λ and $\Delta\lambda$ represent the wavelength and bandwidth of the source, respectively. The wavelength values used for imaging in nontransparent tissue do not vary much (approximately from 1250 to 1350 nm) (Brezinski, 2006). Thus the larger $\Delta\lambda$ value is, the shorter l_c will be and hence the better the OCT axial resolution the imaging will get (Podoleanu, 2005).

2.3.2 Application of OCT in articular cartilage assessment

A number of studies have been conducted to investigate the performance of OCT in monitoring articular cartilage conditions with the aim to provide a tool for the early detection of OA. Table 2.2 lists some of the recent OCT related studies on articular cartilage.

Table 2.2. A summary of the recent studies of application of OCT on articular cartilage measurement. PS: polarization-sensitive.

Authors Year	OCT configuration	Sample	Objectives
(Youn, 2008)	Fiber-based frequency domain 3D OCT; resolution: 8 μm (axial)	Bovine articular cartilage	Demonstrate surface topography and subsurface disruption
(Xie et al., 2008)	GRIN lens rob based spectral domain 3D OCT; resolution: 10 μm (axial, lateral)	Bovine articular cartilage	Show potential for extremely compact OCT endoscopes combined with arthroscope; 3D and surface imaging in the same channel
(Eder et al., 2008)	Fourier domain OCT; resolution: 1 μm (lateral)	Human cartilage	Monitor the healing progress of collagen implant
(Ugryumova and Matcher, 2007)	PS-OCT	Equine articular cartilage	Find reasonable quantitative agreement between the OCT result and histology analysis
(Chu et al., 2007)	Fiber-optic polarized OCT; resolution: 15 μm (axial), 25 μm (lateral)	Human cadaver; human subject	Confirm OCT form birefringence observed in ex vivo detectable during arthroscopic surgery
(Xie et al., 2007)	PS-OCT	Bovine articular cartilage	Map the distribution of normal matrix orientation and articular cartilage birefringence in different regions
(Xie et al., 2006c)	Handhold arthroscopic probe PS-OCT; resolution: 10 μm (axial, lateral)	Bovine femoral-tibial joints	Reveal properties of collagen matrix organization and orientation for studying the degenerative joint disease
(Ugryumova et al., 2006)	PS-OCT	Equine cartilage	Determine the fiber polar angle and true birefringence on sample
(Xie et al., 2006b)	PS-OCT	Bovine femoral-tibial joints	Investigate the polarization sensitivity of articular cartilage by varying the angel of incident illumination
(Mansfield et al., 2006)	PS-OCT	Equine articular cartilage	Spatially map the cartilage birefringence
(Ugryumova and Matcher, 2006)	OCT, PS-OCT	Equine articular cartilage	Spatially map the cartilage birefringence
(Xie et al., 2006a)	OCT, PS-OCT; resolution: 10 μm (axial), 12 μm (lateral)	Bovine femoral-tibial joints; tibial plateaus	Determine the ability of OCT to differentiate various stages of degenerative joint disease as a minimally invasive imaging tool
(Adams et al., 2006)	Handhold probe OCT; resolution: 5 μm (axial), 18 μm (lateral)	Lewis-Wistar rat femoral cartilage	Develop and verify a new technique for monitoring the progression of OA by combing a rat model with the imaging modality OCT
(Davis et al., 2006)	—	Canine femoral articular cartilage	Characterize cartilage, compare the OCT image to corresponding histology results
(Karpie and Chu, 2006)	Handhold probe OCT	Rabbit and in vivo human cartilage	Demonstrate OCT can be used for assessment of cartilage repair

Table 2.2. Continued

Authors Year	OCT configuration	Sample	Objectives
(Li et al., 2005)	Handhold PS-OCT; resolution: 11 μm (axial), 30 μm (lateral)	Human knee joints	Demonstrate the first real-time imaging in vivo of human cartilage in normal and OA knee joints at micrometer resolution
(Ugryumova et al., 2005)	OCT, PS-OCT; resolution: 20 μm (axial, lateral)	Equine fetlock joint	Explore the use of PS-OCT to characterize the regional variability of cartilage birefringence in normal tissue and changes in the vicinity of macroscopic lesions
(Patel et al., 2005)	OCT, PS-OCT; resolution: 12 μm (axial), 30 μm (lateral)	Wistar Hanover rat knee joint	Assess the progression of experimentally induced OA by monitoring articular cartilage thickness, surface abnormalities, and collagen organization
(Xie et al., 2005)	OCT, PS-OCT; resolution: 10 μm (axial), 12 μm (lateral)	Bovine articular cartilage	Assess the microstructure of articular cartilage and differentiate the abnormalities in structure
(Nassif et al., 2004)	PS-OCT	Following knee replace surgery	Demonstrate difference between healthy and diseased cartilage; determine the rate of change
(Chu et al., 2004)	Fiber-optic handheld probe arthroscopic OCT	Human cadaver knees	Determine whether OCT image of human cartilage can be acquired and compare the result with histopathology
(Youn et al., 2004)	Fiber-based dual channel differential phase OCT	Platinum embedded cartilage	Detect surface displacement resulting from an electrokinetic response
(Herz et al., 2003)	Ultrahigh resolution OCT; resolution: 5 μm (axial)	Experimentally induced OA rat knee	Demonstrate the utility of OCT for cartilage integrity assessment
(Pan et al., 2003)	Handhold arthroscopic probe; resolution: 10 μm (axial), 17 μm (lateral)	Hanford minpig hindlimb knee joints	Develop an OCT probe for real-time, in vivo imaging of articular cartilage
(Roberts et al., 2003)	Resolution: 15 μm (axial), 30 μm (lateral)	Male Lewis rat leg knee joint medial/ lateral condyles	Assess early OA, track sequential changes in OA rat knee
(Han et al., 2003a)	Resolution: 13 μm (axial), 10 μm (lateral)	Rabbit knee joints patellar grooves	Evaluate the utility and limitations of OCT for immediate, high resolution structural analysis of rabbit articular repair tissue
(Rogowska et al., 2003)	Resolution: 15 μm (axial), 30 μm (lateral)	Postmortem rabbit knee	Use a new semiautomatic image processing method for detecting the cartilage boundaries in OCT
(Rogowska and Brezinski, 2002)	Resolution: 15 μm (axial), 30 μm (lateral)	Postmortem rabbit knee	Develop new image processing techniques for speckle removal, image enhancement and segmentation of cartilage OCT images
(Li et al., 2001)	OCT, PS-OCT	Normal, OA cartilage	Evaluate the effectiveness of OCT for monitoring articular cartilage
(Drexler et al., 2001)	Resolution: 18 μm (axial), 30 μm (lateral)	Human joints from amputation / resection	Investigate the correlation between changes observed by OCT and the degree of collagen organization in OA cartilage
(Herrmann et al., 1999)	Resolution: 18 μm (axial), 15, 11 or 5 μm (lateral)	Human cadaver / limb resections	Assess OA articular cartilage microstructure

The feasibility of OCT in assessing *in vitro* joint cartilage structural pathologies was tested by obtaining cross-sectional images (Herrmann *et al.*, 1999; Drexler *et al.*, 2001; Roberts *et al.*, 2003; Karpie and Chu, 2006; Xie *et al.*, 2006a, c) and 3D images (Youn, 2008; Xie *et al.*, 2008), and strong correlations between OCT images and the corresponding histological sections were reported, especially by polarization sensitive OCT (Drexler *et al.*, 2001; Xie *et al.*, 2006a, c; Ugryumova *et al.*, 2005; Ugryumova and Matcher, 2007). Animal models were used to monitor the progression of OA (Patel *et al.*, 2005; Adams *et al.*, 2006) and the cartilage repairing after chondrocyte implantation (Han *et al.*, 2003a) using OCT.

The performance of OCT for the cartilage assessment has been verified in human cadaver joint (Chu *et al.*, 2004; 2007). Human studies have also been performed *in vivo* using the endoscope-based OCT (Tearney *et al.*, 1995; Pan *et al.*, 2003) and during the open knee surgery (Li *et al.*, 2005). Youn and his coworkers (Youn *et al.*, 2004) used OCT to monitor the cartilage deformation induced by an electrical field. Image processing techniques have been employed for enhancement and segmentation of cartilage OCT images so as to increase the accuracy of thickness measurement (Rogowska and Brezinski, 2002; Rogowska *et al.*, 2003). However, little has been reported on the basic characteristics of articular cartilage determined using OCT, such as its optical property RI, morphological property surface roughness, and mechanical property stiffness under different conditions.

2.4 Measurement of articular cartilage RI

The RI of a medium is a measure for how much the speed of light (or other waves such as sound) is reduced inside the medium. With the knowledge of the RI in tissue, the propagation of light in tissue can be better understood and better treatment and surgery plan can be made. The RI of human tissue can even have significant diagnostic meaning in some cases. For example, the stratum corneum RI has some relations with tissue hydration. When it comes to the assessment of articular cartilage using RI, the accuracy of the measurement of its thickness could be affected, without a good understanding of how RI changes at different depths of articular cartilage. Thus it is meaningful to investigate the RI of articular cartilage. However, little work has been done to quantify the tissue RI, particularly in articular cartilage (Tearney *et al.*, 1995), using OCT.

Herrmann and coworkers reported an average RI of 1.51 ± 0.009 for human articular cartilage collected from different joints (Herrmann *et al.*, 1999). They found the cartilage thickness measured by OCT using this RI value was consistently smaller than that measured using histology by 7-9%. However in anther study by Rogowska *et al.* (2003), this human cartilage RI value was adopted for the assessment on rabbit and the thickness obtained using OCT was found consistently larger than that obtained using histology by 4-10%. These contradictory results suggested that using a single RI value might not be accurate enough in determining cartilage thickness for cartilages from different species, joints and depths using OCT.

Traditional RI measurement methods include white-light interferometry, prismatic dispersion, and planar reflection for transparent specimens (Bolin *et al.*, 1989; Tearney *et al.*, 1995). The measurement of the RI of transparent tissue was performed *in vivo* using a microscope to focus on the surface of a thin transparent layer (Gahm and Witte, 1986). This method measured the physical thickness of the sample using a high resolution inductive pathfinder. The optical thickness was calculated with the knowledge of the sample stage movement between the two foci and marginal ray analysis. Then the RI of rat mesentery was further calculated (Gahm and Witte, 1986; Tearney *et al.*, 1995). However, this method must be performed on a transparent specimen and cannot be applied for all tissues.

Three methods using OCT to determine the RI of human tissue have been reported (Tearney *et al.*, 1995; Wang *et al.*, 2002b). The first one uses the OCT to measure the optical path length of excised tissue specimens (Tearney *et al.*, 1995). Tissue sample is placed on top of a planar reflecting surface (Fig 2.7). Sample thickness z can be measured by subtracting the outside tissue axial positions of the reflector and the tissue surface in the OCT image. The additional optical path length delay z' can be determined by subtracting the axial position of the outside tissue axial position of the reflector and the through tissue axial position of the imaged reflector in the OCT image. The RI of the tissue sample n can be calculated as follows:

$$n = \frac{z'+z}{z} \qquad (2.2)$$

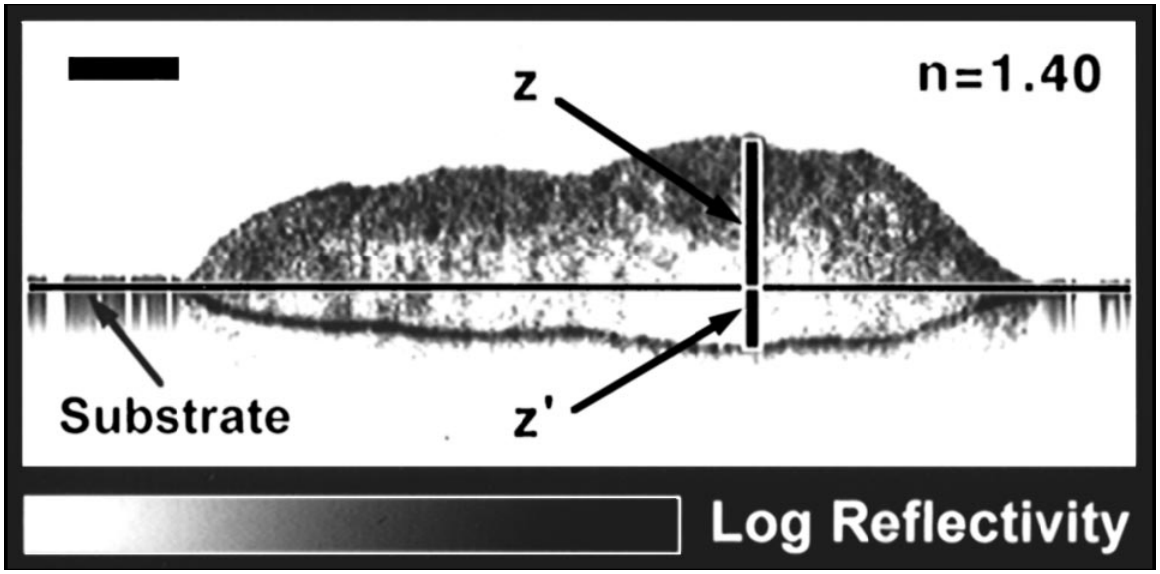

Fig 2.7. OCT image of human dermis placed on an unpolished metal substrate. The two vertical bars represent z, z', from top to bottom. The horizontal bar in the upper left-hand corner represents 500 mm (Tearney *et al.*, 1995).

The second technique is the focus tracking method (Wang *et al.*, 2002b; Tearney *et al.*, 1995). The reference arm path length is first matched to the focus on the surface of the tissue sample (Fig 2.8). Then the sample arm is moved a distance z toward the imaging lens. The focus of the lens is now within the medium. The reference arm is moved a distance of Δz to get the maximum OCT signal. If the sample can be regarded as a single layered medium, the RI of the sample can be determined according to the Snell's law and marginal ray analysis:

$$n^2 = \frac{1}{2}[NA^2 + \sqrt{NA^4 + 4(n_0 - NA^2)(n_0 + \frac{\Delta z}{z})^2}] \qquad (2.3)$$

where n_0 and n are the refractive indices of the surrounding medium and the sample. NA is the numerical aperture of the imaging objective. $NA = \sin\theta$ and θ is the incident angle on the sample surface.

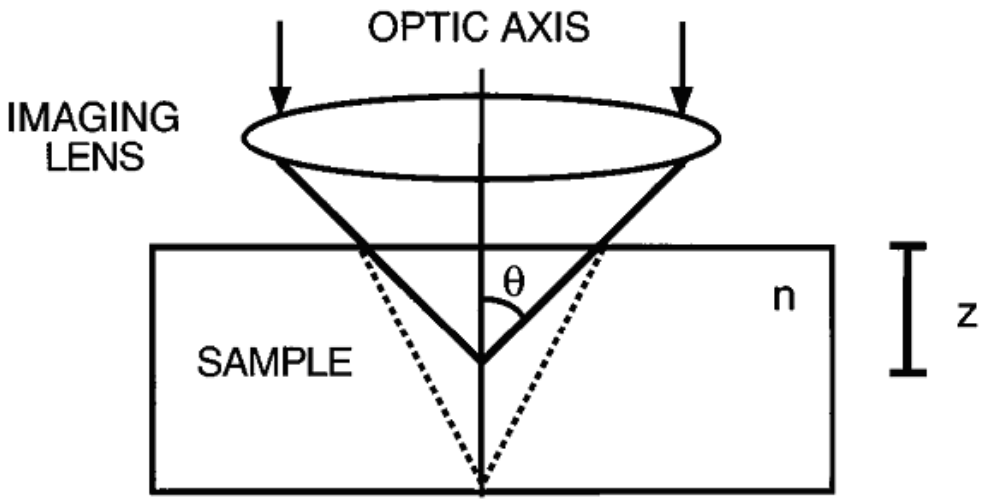

Fig 2.8. OCT focus tracking method geometry (Tearney *et al.*, 1995).

The third technique is called the optical length shifting method (Wang *et al.*, 2002b). A mirror is placed on the sample stage. The optical path lengths of reference arm and sample arm are adjusted to match each other within the coherence length of the light before sample is placed on the sample stage. The axial position of the mirror in the sample arm is Z_0. Then the reference stage is adjusted to axial position Z_2 to match the optical path length again after the tissue specimen is placed on the sample stage (Fig 2.9). The optical path difference is determined by:

$$\Delta Z = Z_2 - Z_0 = (n-1)L \tag{2.4}$$

where L is the sample thickness, which can be calculated by moving the reference mirror from Z_0 to Z_1 to achieve another maximum interference signal. So

$$L = Z_1 - Z_0 \tag{2.5}$$

The RI of sample n can be derived by:

$$n = 1 + \Delta Z / L \tag{2.6}$$

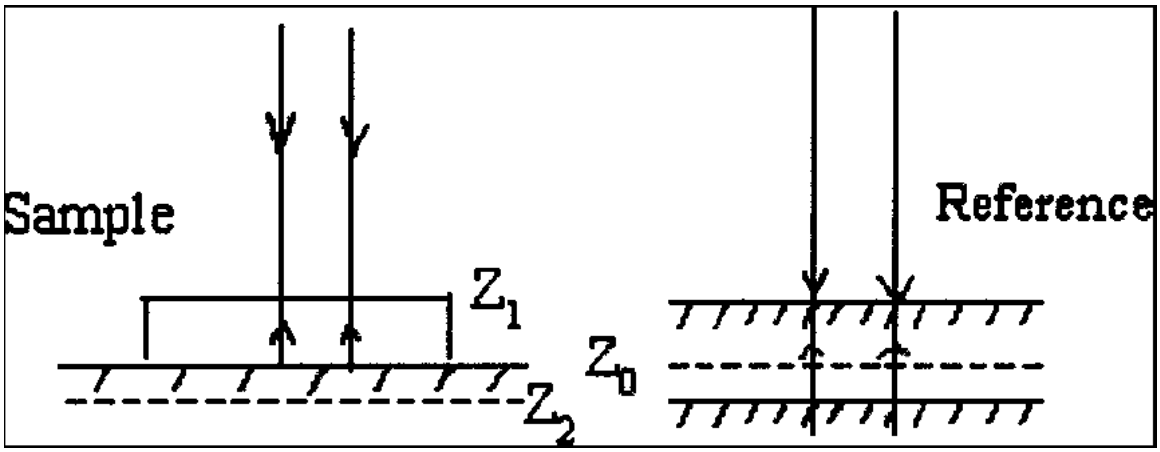

Fig 2.9. Schematic of optical path shifting method (Wang *et al.*, 2002b). Z_0: the axial positions of sample arm mirror (left) and original position of the reference mirror (right) when they match each other within the coherence length of the light. Z_1: the axial position of the first sample interface. Z_2: the axial position of reference mirror when the optical path of both arms match after placing the specimen on the sample stage.

Those above methods, however, require highly stable and precise optical apparatus. And during the measurement, cartilage samples were exposed in the air. Thus the vaporization of the water in the tissue may change the RI value. In the present study, we designed a modified optical length shifting method to measure the RI cartilage and used this method to investigate the depth and degeneration dependences of RI in bovine patellar articular cartilage. Details are discussed later in the Methods Chapter.

2.5 Measurement of inhomogeneous properties of articular cartilage

Articular cartilage is known to be inhomogeneous, anisotropic and depth dependent because of its microstructure (Hunziker, 1992; Jurvelin *et al.*, 2003; Chen *et al.*, 2001a; 2001b; Mow *et al.*, 2005), as described earlier.

Some studies have been conducted by researchers to investigate the inhomogeneous mechanical properties of articular cartilage measured in tension (Guilak *et al.*, 1994; Roth and Mow, 1980), and in compression (Chen *et al.*, 2001a; 2001b) by measuring excised cartilage slides at different depths. Confocal microscope and video microscope were used to measure the mechanical properties of articular cartilage directly (Guilak *et al.*, 1995; Schinagl *et al.*, 1997). A high resolution digital camera and computer-based data acquisition system have been used to investigate the nonuniform strain distribution within cartilage layers during free swelling induced by varying the bathing saline solution concentration (Narmoneva *et al.*, 1999; 2001). It was found that the strain distribution in cartilage was significantly depth dependent. Fibril-reinforced poroviscoelastic cartilage model was employed to analyze indentation modulus in order to better understand the inhomogeneity and anisotropy during *in vivo* tissue characterization (Julkunen *et al.*, 2008). Ultrasound has also been used to directly measure depth dependent articular cartilage properties, such as the compressive strain (Zheng *et al.*, 2002), and transient Poisson's ratio (Fortin *et al.*, 2000). An elastic ultrasound microscope system was extended from elastography technique (Ophir *et al.*, 1991) by Cohn and his colleagues

(Cohn *et al.*, 1997a; 1997b). Articular cartilage deformations were mapped by a newly developed 2D ultrasound elastomicroscopy system (Zheng *et al.*, 2004a). The inhomogeneous swelling effects of articular cartilage were also investigated by ultrasound (Zheng *et al.*, 2006a).

The permeability (Federico and Herzog, 2008) and speed of sound (Patil *et al.*, 2004; Patil, 2004) in different depth of articular cartilage were also investigated. Recently, a number of studies have been conducted to explore the application of OCT in assessing articular cartilage (details have been introduced in Section 2.3). Little research has been done, however, on the depth dependent properties of articular cartilage determined using OCT.

2.6 Measurement of articular cartilage surface roughness

Roughness is a measurement of the small scale variations in the height of a physical surface. The surface roughness of materials can be determined by several techniques. Typically it can be measured by a stylus profilometer (Mattson and Wagberg, 1993; Morrison, 1995). In the stylus profilometer, the stylus is loaded on the surface and then moved across on the surface for a specified distance and specified contact force at a constant velocity to obtain surface height variation of the sample (Poon and Bhushan, 1995). This kind of profilometer can measure small surface variations in vertical stylus displacement as a function of position. This method, however, has very high requirements on apparatus and environment and may induce some damage to the fragile samples as it requires direct contact with the material during the measurement. Also the typical traverse speed of stylus is

relatively low (usually less than 1mm/s)(Morrison, 1995). So it is not quite suitable for biological materials (Cho *et al.*, 1995; Morrison, 1995).

Non-contact optical methods, such as laser profilometry can also be used for the determination of the surface roughness. In optical devices, highly sensitive detectors detect the backscattering of the light from the surface. And the measurement of surface roughness is based on that information. Some studies have proposed methods using the first-order statistics of the intensity of the backscattered light (Ribbens, 1969; Hildebra.Bp *et al.*, 1974). The second-order statistics of the intensity, correlation properties of the speckle pattern, has also been employed to obtain the surface information (Spagnolo and Paoletti, 1996). The optical methods also require very precise apparatus.

With the assumption that the baseline of the measured surface profile is perfectly straight, the average roughness (R_a) and root mean square (RMS) roughness (R_q) can be defined as follows (Saarakkala, 2007):

$$R_a = \frac{1}{L}\int_0^L |\, y(x)\,| dx \tag{2.7}$$

$$R_q = \sqrt{\frac{1}{L}\int_0^L y(x)^2 dx} \tag{2.8}$$

where L is the measurement length on the surface and $y(x)$ is the one-dimensional surface profile. But it also has limitations. When the base surface is not an ideal straight line or plane, this method will not be quite suitable.

In OA, the cartilage surface degenerates, probably through the disruption of the superficial collagen network. So the detection of surface condition would help the early diagnosis of OA.

Ultrasound measurements have a great potential for direct estimation of cartilage surface conditions. One method is to measure the backscattered ultrasound energy amount at different geometrical angles between the ultrasound transducer and cartilage surface (Adler *et al.*, 1992; Chiang *et al.*, 1997). However, this technique provides no direct measure of roughness.

In a recent ultrasound study of articular cartilage, a novel ultrasound parameter ultrasound roughness index (URI) has been introduced to quantify the microtopography of cartilage surface (Saarakkala *et al.*, 2004b). URI is determined from the cartilage surface profile using the line by line distances between the transducer and the cartilage interface as follows:

$$URI = \sqrt{\frac{1}{m}\sum_{i=1}^{m}(d_i - \overline{d})^2} \qquad (2.9)$$

where m is the number of scan lines, d_i is the distance from the transducer to cartilage interface in scan line i and $\overline{d}$ is the mean distance from the transducer to the surface. A high pass filter is used to eliminate the natural articular surface contour before the calculation. However, further studies are required to demonstrate the potentials of this method *in vitro* and *in vivo*.

A few studies have been done to quantitatively determine the cartilage surface roughness. Forster and Fisher (1996) employed a contact stylus

profilometer and a non-contact laser profilometer to assess the bovine articular cartilage surface roughness. The average roughness for normal tissue was 0.8 μm and 1.6 μm measured by stylus and laser profilometer, respectively. In the work of Chiang *et al.*, laser confocal microscopy was used to measure the surface roughness of healthy and osteoarthritic human cartilage (Chiang *et al.*, 1997). The RMS roughness values ranged from 5.4 μm to 99.2 μm. The study conducted by Hu *et al.* employed atomic force microscopy to determine the surface roughness of healthy rabbit articular cartilage (Hu *et al.*, 2001). The average roughness result was 0.16-0.32 μm. Saarakkala *et al.* used ultrasound to measure URI of bovine cartilage in normal, mechanical degraded and enzyme degraded states (Saarakkala *et al.*, 2004b). The average URI results before and after mechanical degradation were 7.7 and 28.8 μm, 7.3 and 18.4 μm, 6.8 and 12.4 μm, 8.5 and 13.1 μm for four different sizes of grinding used emery paper, respectively. The average URI results for enzymatic digestion group were 10.6 and 34.8 μm for before and after collagenase degradation, 7.2 and 9.0 μm before and after trypsin degradation, and 12.3 and 12.4 μm before and after chondroitinase ABC degradation, respectively. However, there is no quantitative technique capable of measuring the surface roughness of articular cartilage *in vivo* right now.

OCT fiber optic systems can be incorporated into catheters or endoscopes, allowing high resolution images of internal organ microstructure (Tearney *et al.*, 1997). OCT laparascopes and hand-held surgical probes have been developed (Boppart *et al.*, 1997). And the ability of OCT to provide detailed

images of subsurface structures in the upper gastrointestinal (GI) tract (Bouma *et al.*, 2000; Jackle *et al.*, 2000) has also been demonstrated. In the case of cartilage, the *in vivo* real-time imaging in human cartilage in normal and osteoarthritic knee joints was also performed using a portable OCT system with a handheld imaging probe during open knee surgery (Li *et al.*, 2005). Since both OCT and high frequency ultrasound have the potential to be employed in *in vivo* measurement using minimally invasive probes, In this study, we proposed a new parameter: OCT Roughness Index (ORI) to quantify the cartilage surface, and URI was used for comparison (details are introduced in Methods Chapter).

2.7 Measurement of articular cartilage mechanical properties

During the joint movement, articular cartilage often experiences loading and unloading repetitively. When a load is applied on the joint, the articular cartilage will deform in order to increase the contact region (Saarakkala, 2007). Therefore, the mechanical properties of articular cartilage play an important part in its daily function. Inferior stiffness is one of the earliest symptoms in cartilage degeneration and stiffness could be used to represent the quality of repaired cartilage. Thus the assessment of articular cartilage stiffness would help the detection of early OA. As mentioned before, the collagen network is mainly responsible for tensile and dynamic properties of cartilage while proteoglycans establish compressive properties in cartilage.

Traditional techniques for measuring the mechanical properties include unconfined compression, confined compression and indentation (Mow and Guo, 2002). In unconfined compression test, cartilage tissue is compressed between two smooth metallic plates. In confined compression, cartilage sample is placed on a chamber and compressed with a porous filter (Fig 2.10 (a) and (b))(Mow and Guo, 2002). In both unconfined and confined compression, the cartilage tissue has to be taken from the joint and thus these two tests are *in vitro*. In the indentation test, cartilage is often compressed with a cylindrical plan-ended or spherical-ended indenter (Fig 2.10 (c))(Mow and Guo, 2002). Indentation can be performed when the cartilage is attached to the bone. Therefore indentation tests can be conducted *in vivo*. In this study, the mechanical properties of articular cartilage were measured by indentation tests.

Using indentation data, the Young's modulus and shear modulus can be derived from the following equations (Hayes *et al.*, 1972):

Young's modulus: $$E = \frac{(1-\nu^2)\pi a}{2\kappa h}\frac{\sigma}{\varepsilon} \quad (2.10)$$

Shear modulus: $$\mu = \frac{(1-\nu)\pi a}{4\kappa h}\frac{\sigma}{\varepsilon} \quad (2.11)$$

Poisson's ratio: $$\nu = \frac{\varepsilon_l}{\varepsilon_a} \quad (2.12)$$

Stress: $$\sigma = \frac{dF}{dA} \quad (2.13)$$

Strain: $$\varepsilon = \frac{L'-L}{L} \quad (2.14)$$

where F is the reaction force, A is the area of the surface in which the force is acting, L is the initial thickness and L' is the thickness after compression, ε_l and ε_a are lateral and axial strains, a is the indenter radius, h is the cartilage thickness, κ is the theoretical scaling factor due to the finite and variable cartilage thickness (Hayes *et al.*, 1972).

Giving the assumption that articular cartilage is an elastic material with a fixed rigid underlying surface, the Young's modulus E in cartilage indentation test using a cylindrical indenter can be determined by the following equation (Hayes *et al.*, 1972):

$$E = \frac{\left(1-v^2\right)}{2a\kappa\left(v, a/h\right)} \cdot \frac{F}{d} \tag{2.15}$$

where d is the deformation, $\kappa\left(v, a/h\right)$ is the theoretical correction factor for the finite articular cartilage thickness h.

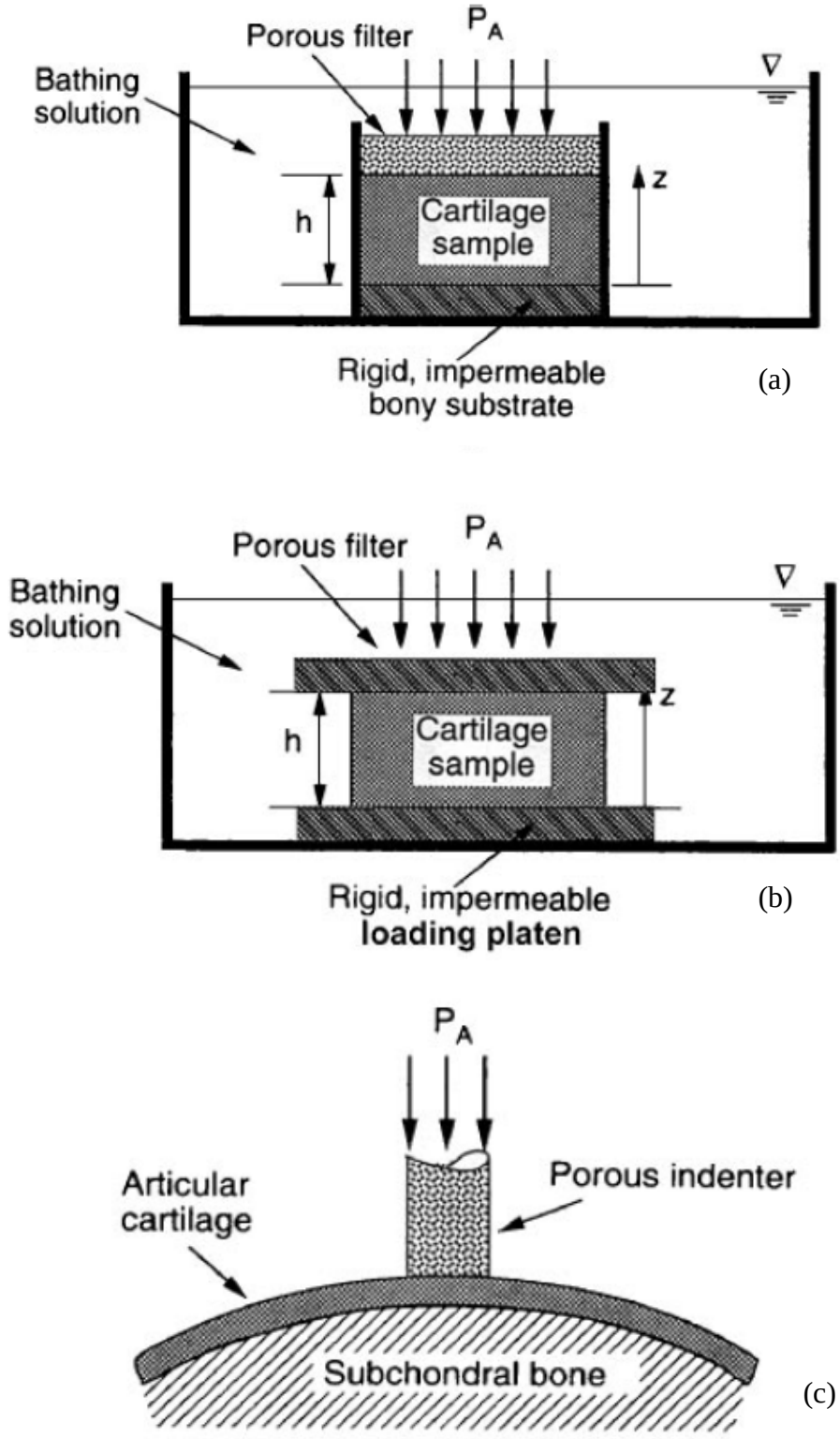

Fig 2.10. Schematic representations of (a) confined compression, (b) unconfined compression, and (c) indentation tests (Mow and Guo, 2002).

Several indentation devices have been developed to assess biomechanical properties of the soft tissues (Hayes *et al.*, 1972; Han *et al.*, 2003b). The traditional indentation devices measured the tissue surface displacement according to the displacement of the indenter (Bader and Bowker, 1983; Fergusonpell *et al.*, 1994; Zheng and Mak, 1996). Tissue thickness was not monitored in those studies. So not only the tissue material properties but also some geometric effects will affect the stiffness result (Zheng and Mak, 1996; Zhang *et al.*, 1997).

Ultrasound indentation systems have been developed to measure both the displacement of tissue surface and the thickness of the soft tissue layer. With this approach and some theoretical models, the geometric effects could be separated from the indentation data (Zheng and Mak, 1996). Ultrasound indentation typically operates in the frequency range between 2 and 10 MHz and its resolution is not sufficient to assess the mechanical properties of soft tissue with fine structures. High frequency focused ultrasound transducer may improve the resolution, but it could not be used for traditional contact indentation test because of the concave-face (Zheng *et al.*, 2002; Lu *et al.*, 2007).

Mechanical and ultrasound indentations are not commonly employed for imaging the elastic modulus distribution for a region of tissue, due to their relatively low spatial resolution (typically larger than 2 mm) and long time of measurement, since the region needs to be measured point by point (Lu, 2006; Vannah *et al.*, 1999; Appleyard *et al.*, 2001). Nanoindentation has

been developed for material surface mechanical properties assessment (Pethica *et al.*, 1983). However, nanoindentation can only provide the surface information but not the inside tissue.

Recently a new ultrasound water indentation system was introduced, using a water beam as the indenter as well as the medium for ultrasound propagation (Lu *et al.*, 2005; 2007; 2009). Since this water jet indentation system does not require a rigid compressor to compress the tissue, the attenuation caused by the compressor and the strong echoes reflected from its surfaces can be avoided (Lu *et al.*, 2007). High frequency ultrasound (20 MHz) was utilized to measure the indentation deformation at a microscopic level.

Since OCT has the advantages of high resolution, free of transmit medium and the possibility of developing small diameter catheter probes, a novel indentation system utilizing the air jet to indent the specimen combined with OCT for the measurement of tissue deformation was developed earlier by our group (Huang *et al.*, 2009). The schematic of the OCT-based air jet indentation system is shown in Fig 2.11 (Huang *et al.*, 2009). A fiber-based OCT was modified to allow an installation of an air jet bubbler. A pipeline with stable air pressure was connected to the system to provide air jet for the indentation and a proportioning valve was used to adjust the pressure of the air jet continuously. OCT air jet indentation system could achieve non-contact indentation and could even get quantification of thickness and distance.

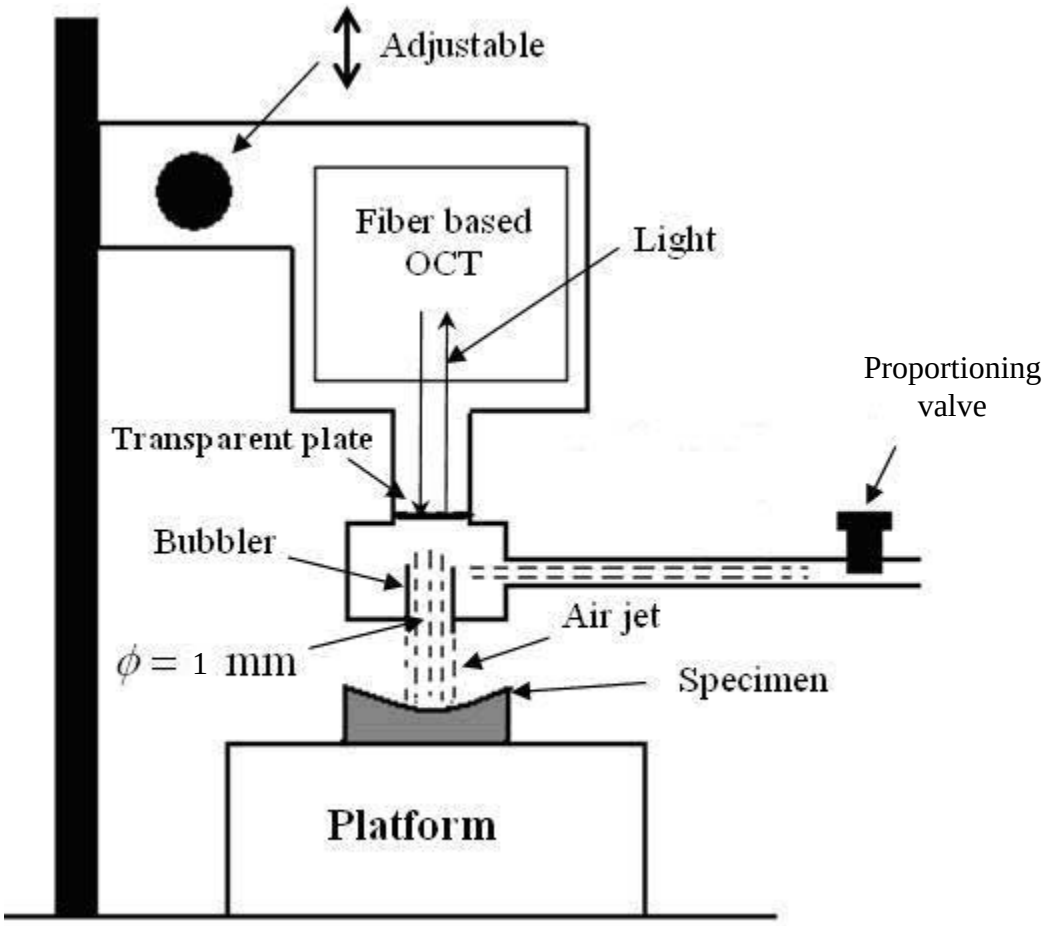

Fig 2.11. Schematic representation of the OCT-based air jet indentation system (Huang *et al.*, 2009).

Previous studies have been conducted to measure the articular cartilage mechanical properties. Table 2.3 lists Young's modulus and Poisson's ratio results of some studies on human or bovine cartilage.

Table 2.3. A summary of results of average Young's modulus and Poisson's ratio of human and bovine articular cartilage.

Authors Year	Test	Sample	E (Mpa)	ν
(Lu et al., 2009)	Indentation	Bovine patella	1.59 (normal)	
			0.47 (digested)	
(Kiviranta et al., 2008)	Unconfined compression	Human patella	0.21-0.70	
(Park et al., 2008)	Unconfined compression	Bovine femoral	0.38-0.49 (normal)	
			0.19-0.23 (digeste)	
(Nissi et al., 2007)	Unconfined compression	Human patella	0.19-0.96	
		Bovine patella	0.32-0.97	
(Julkunen et al., 2007)	Unconfined compression	Bovine	0.19	
(Demarteau et al., 2006)	Confined compression	Human femoral	1.57-1.64	0.14
		Bovine	0.27-0.28	0.13-0.14
(Kiviranta et al., 2006)	Unconfined compression	Bovine patella	0.48	0.20
(Verteramo and Seedhom, 2004)	Unconfined compression	Bovine humeral	0.18-0.35	0.017-0.065
(Jin and Lewis, 2004)	Indentation	Bovine patella	0.45	0.463
(Park et al., 2004)	Unconfined comression	Bovine femoral	0.49	
(Jurvelin et al., 2003)	Confined compression	Human patella	0.58	0.16-0.18
(Korhonen et al., 2002)	Unconfined compression	Bovine patellar	0.78-0.80	
	Confined compression	Bovine patellar	0.81	
	Indentation	Bovine patellar	1.15	
(Fortin et al., 2000)	Unconfined compression	Bovine humeral	0.62-0.69	
(Athanasiou et al., 1991)	Indentation	Human patellar		0.00
		Bovine patellar		0.25

In this study, we used both OCT air jet indentation and ultrasound water jet indentation systems to measure the mechanical properties of articular cartilage (details are introduced in the following chapter).

2.8 Summary

In this chapter, background of this study has been introduced. A lot of studies have been conducted using various methods for the assessment of articular cartilage. However, little has been reported on the basic characteristics of articular cartilage measured using OCT, such as its RI, roughness index and mechanical properties. And to the best of our knowledge, the relationships among the optical, acoustic, morphological and mechanical properties of the same set of articular cartilage samples have not been systematically analyzed. The assessment of those properties of articular cartilage could help determine the cartilage degeneration state and therefore may help diagnose OA in the early stage. Thus it is necessary and meaningful to do fundamental studies on cartilage properties in large sample size using both OCT and high frequency ultrasound systems. These properties were assessed and their relationships were determined in this study. Details about experiment design are introduced in the next chapter.

CHAPTER 3 METHODS

In this chapter, the methods applied in this study including specimen preparation, system setup, measurement procedure, parameters calculation and statistical analysis are introduced.

The major tests in this study are RI measurement, roughness measurement, acoustic parameters measurement, and indentation tests. Those tests were designed to assess the optical, morphological, acoustic, and mechanical properties of articular cartilage, respectively. The main experiments (Fig 3.1) are summarized as follows:

1) Depth and degeneration dependence of articular cartilage RI using OCT;
2) Surface roughness measurement of emery paper and articular cartilage using OCT;
3) Surface roughness measurement of emery paper and articular cartilage using 55 MHz high frequency ultrasound (Vevo);
4) Thickness measurement of articular cartilage using 55 MHz high frequency ultrasound;
5) Acoustic parameters extraction of articular cartilage using 55 MHz high frequency ultrasound;
6) OCT air jet indentation tests on articular cartilage;
7) Ultrasound water jet (20 MHz) indentation tests on articular cartilage;
8) Mechanical indentation tests on articular cartilage;
9) Histological analysis of articular cartilage;
10) SEM test on articular cartilage surface;

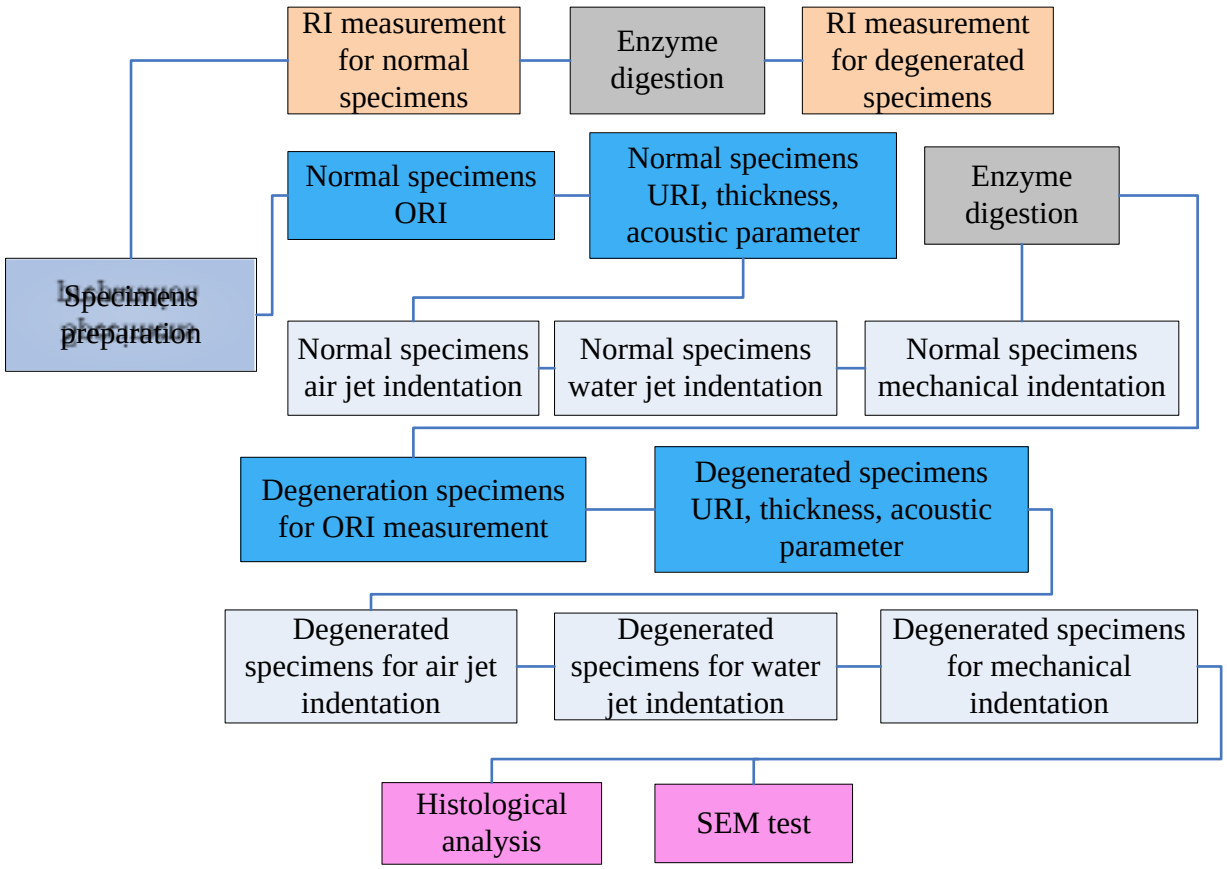

Fig 3.1. Block diagram of the measurement procedure.

Table 3.1. The main expected outcome of the study.

Main experiments	Main expected outcomes
RI measurement for normal and degenerated samples	RI value is different for different cartilage layers or different degenerated state
ORI measurement for normal and degenerated samples	Demonstrate the possibility of using ORI as an indicator to differentiate normal and enzyme degenerated samples
URI measurement for normal and degenerated samples	URI result consistent with ORI result and previous studies
Acoustic properties measurement	Find relationship between acoustic properties and degeneration state
Thickness measurement	Measure cartilage thickness result for different degenerate groups and as a parameter for the later stiffness calculation
OCT air jet indentation test	Demonstrate the feasibility of using OCT air jet to measure the mechanical properties of articular cartilage
Ultrasound water jet indentation test	Stiffness result measurement by ultrasound water jet consistent with stiffness result measured by OCT air jet

3.1 Measurement of articular cartilage RI

3.1.1 Specimen preparation

Fresh mature bovine patellae without obvious lesions were obtained from a local market within 6 h of sacrifice and then stored at -20°C until further preparation. Previous studies have showed that cryopreservation storage, freezing and thawing of articular cartilage samples would not affect the mechanical and acoustic properties (Kiefer *et al.*, 1989; Agemura *et al.*, 1990). Then each patella was cut into four quadrants using a bend saw machine (Fig 3.2)(Patil, 2004). The four quadrants were named as medial upper, medial lower, lateral upper and lateral lower. Cylindrical cartilage-bone plugs with a diameter of 6.35 mm and thickness of approximately 1.5 mm (n=18) were prepared from patella using a metal punch (Zheng *et al.*, 2001; Zheng *et al.*, 2002).

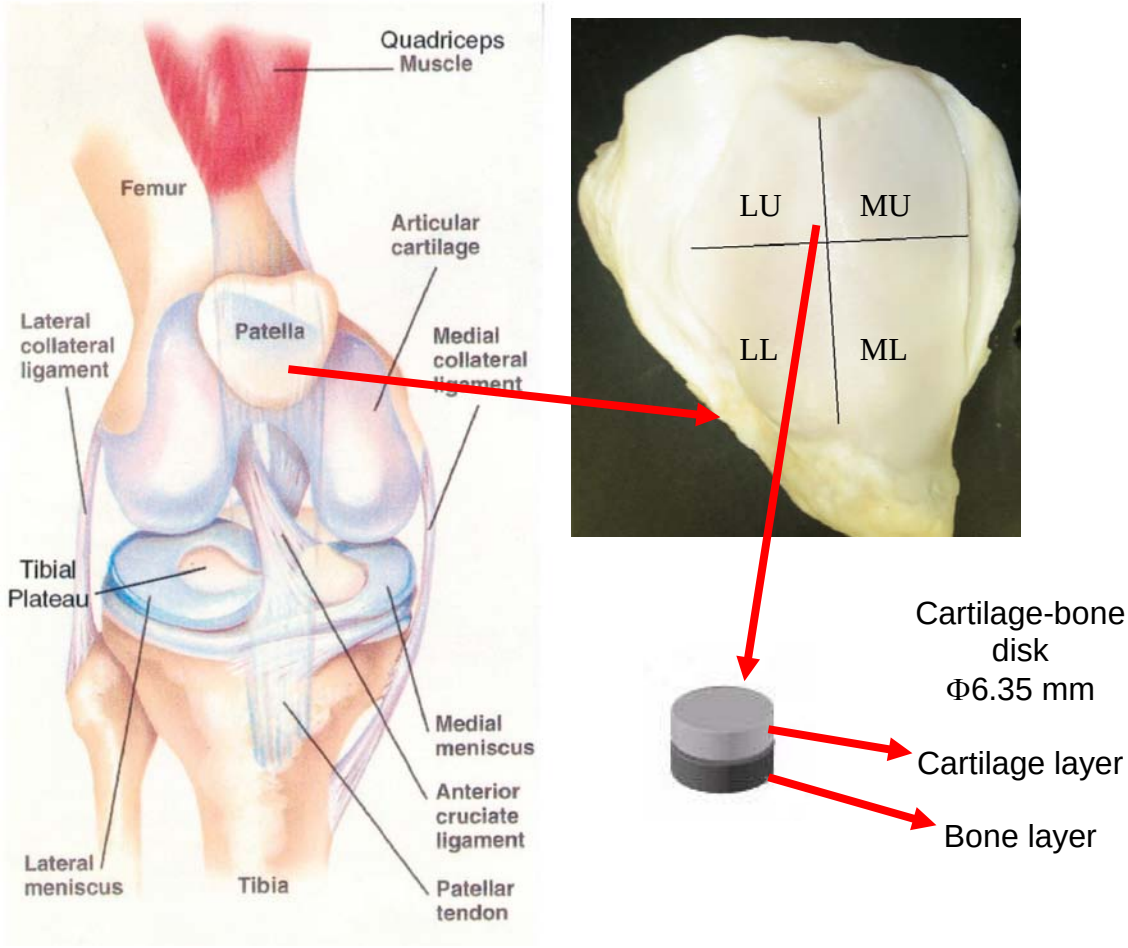

(a) (b)

Fig 3.2. Schematic representation of articular cartilage-bone disks preparation. (a) A total joint perspective (Burstein *et al.*, 2000). (b) Picture of a typical bovine patella. MU: medial upper, ML: medial lower, LU: lateral upper and LL: lateral lower parts of the patella. Cylindrical cartilage-bone plugs were prepared from the patella using a metal punch.

In the study of RI, total patellae number was 18. Cartilage-bone plugs were prepared from the lateral upper region of patella. Then bone was removed from the plugs by surgical blade and then each disk was cut into two equal halves along the diametric direction. One half was prepared for future trypsin digestion while the other half was for collagenase digestion. Both the halves were then further horizontally cut into three different slices using a thin surgical blade manually. Each slice had an approximately equal

thickness of about 0.5 mm. Since the thickness of the whole cartilage layer varies for different cartilage samples. The thickness of the top, middle and deep layers may not be consistent for different samples. For the RI calculation, the optical path length for different cartilage layer was not assumed to be the same, but measured according to the individual cross-sectional image for each specimen. So the inconsistent of the thickness for different specimen may not affect the calculation of RI.The three slices from the cartilage surface to the bone approximately covered superficial-middle layer, middle layer, and deep layer, respectively (Clark, 1990; Mow *et al.*, 2005). In this study, these slices were called top, middle and deep layers.

3.1.2 System setup

A schematic representation of the OCT system used in the study was showed earlier in Fig 2.6. A picture of the system used in our lab is showed in Fig 3.3. This OCT system (Developed by Lab of Optical Imaging and Sensing, Graduate School at Shenzhen, Tsinghua University, China) used a 1310 nm superluminescent diode with a bandwidth of 50 nm, corresponding to an axial resolution of 15 μm. The signal-to-noise ratio of the system was about 90 dB. The OCT probe, which included optical fiber and focusing lens, could be translated vertically in one dimension.

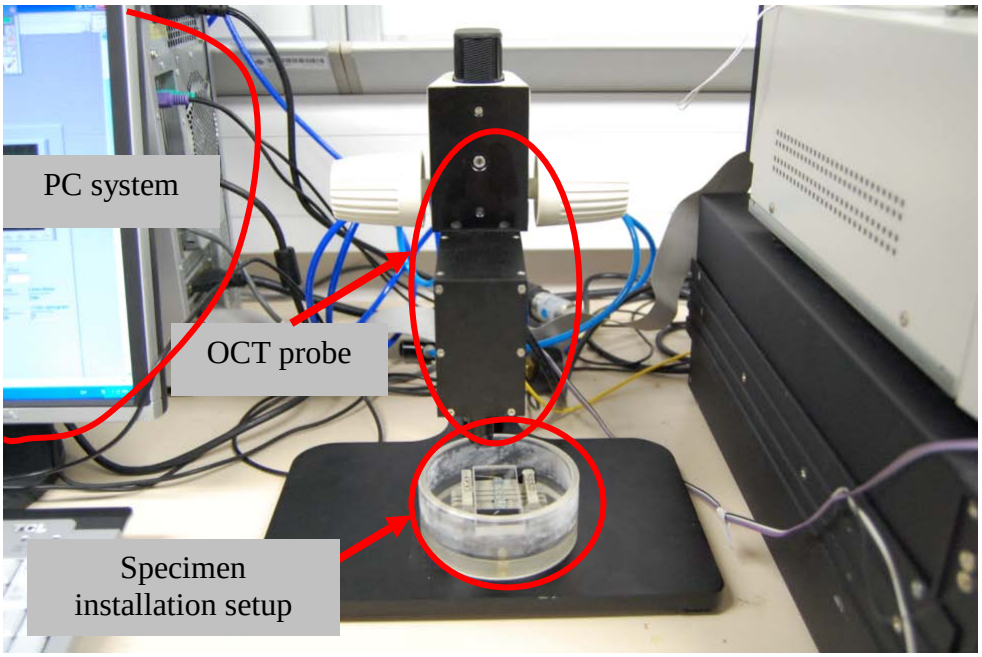

Fig 3.3. The OCT system used in the experiment.

The articular cartilage specimen was installed on a pair of plastic plates and secured by elastic threads to prevent its potential movement during the test (Fig 3.4 (a)). Three pairs of this arrangement were contained in a physiological saline bath that could be translated in two horizontal directions. The distance between the neighboring pairs of plates was 2 mm. A piece of transparent glass was installed parallel to the container base about 0.5 mm above the specimens to provide a marker in the cross-sectional images for further calculation. This specimen arrangement was modified based on a previous study on speed of sound in articular cartilage (Patil, 2004). Fig 3.4 (b) shows an enlarged version of the specimen installation setup to elaborate how the OCT signals were obtained from different interfaces, which would be later used for calculation of RI.

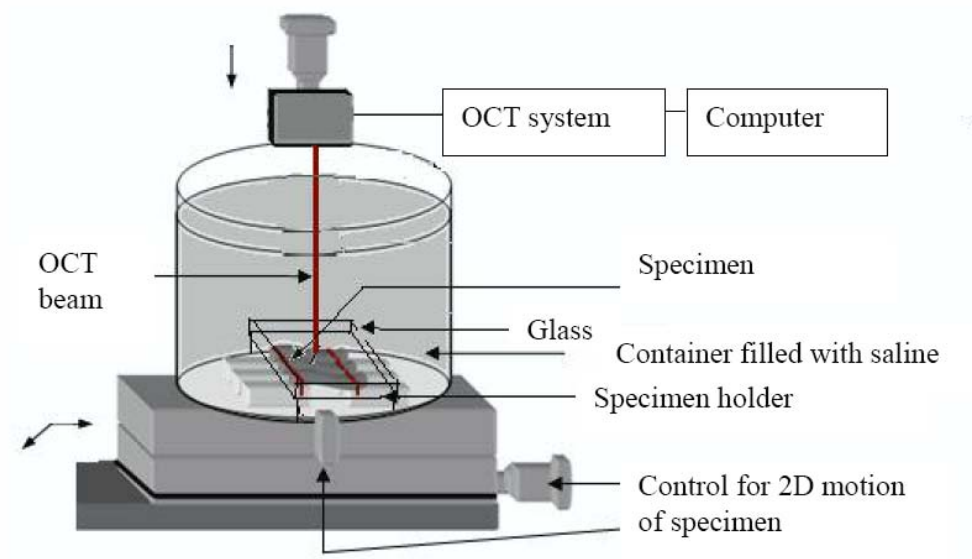

(a)

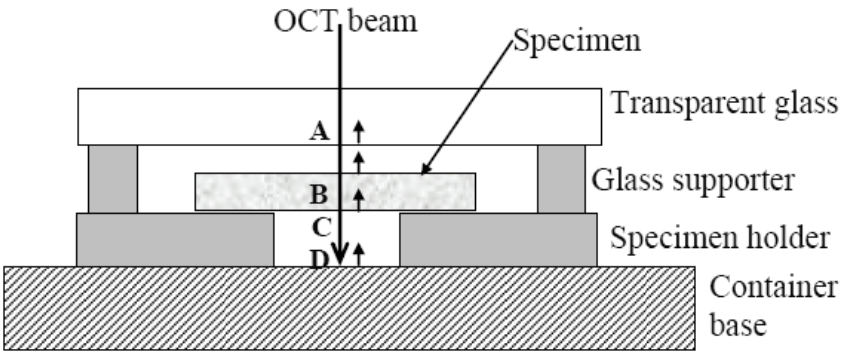

(b)

Fig 3.4. (a) Experimental setup for the measurement of the RI of articular cartilage. The specimen base can be moved horizontally in two dimensions to locate different measurement points. The OCT signals were digitized, displayed in real-time, and stored in PC for further off-line analysis. (b) The enlarged figure showing how the specimen was placed in relation to the transparent glass covering it, the specimen holder supporting it, and the bottom of the container. A, B, C, D are labeled according to the descriptions in Fig 3.6. The arrows indicate the strong OCT signal scattering occurred at the interfaces.

The received OCT signals were digitized by a data acquisition card (PCI-6251, National Instruments, Austin, Texas, USA) and analyzed with the Labview software (v8.0, National Instruments, Austin, Texas, USA). Each

cross-sectional image was composed of 100 lines of depth scans covering a width of approximately 0.67 mm, and each depth scan was sampled with 10000 data points along the vertical direction. In scattering tissues the imaging depth of this system was about 1 to 2 mm.

3.1.3 Measurement procedure

3.1.3.1 Normal specimen measurement

The three slices of articular cartilage were fixed in order on the three pairs of plates in the container using a thin rubber band (Fig 3.4). Initial cross-sectional images were recorded by OCT along different directions of the specimen to see whether the cartilage surface was parallel to the container base, thus the cartilage surface could be adjusted to be perpendicular to the OCT beam. The specimens were tested at room temperature (24.5±1°C) and humidity (62±5%) using the following procedures, with the top layer scanned first, followed by the middle and deep layers. The OCT beam was first located approximately 1 mm away from the edge of the first specimen (the top layer) and the OCT signals reflected from the bottom of the container and the lower surface of the glass plate were collected. Then the specimen platform was moved horizontally perpendicular to the OCT beam at 0.5mm interval, and a total of 2 sites without specimen were measured and the corresponding OCT signals were recorded. Then the platform was further moved to let the OCT scan beam pass through the first specimen, where 6 different sites with an interval of 0.5 mm in the direction of platform moving were scanned and each site was scanned for 10 times (Fig

3.5). After the OCT beam passed the first specimen region, 2 different sites with an interval of 0.5 mm were also sampled between the first and second slices. These signals from different regions without specimen helped provide a better reference optical path with the consideration of the potential inconsistency of the distance from the lower surface of the glass plate to the bottom of the container along the scanning path. A similar procedure was applied to the middle and deep zone slices, and OCT signals were collected correspondingly. All the normal specimens (n=18×2×3) from both halves were scanned.

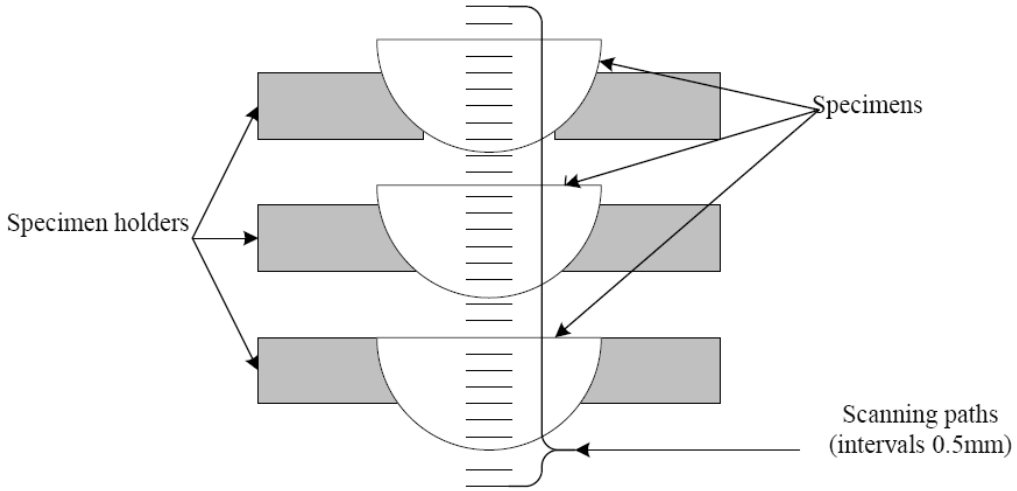

Fig 3.5. The Schematic representation of OCT scanning paths on specimens, gaps and beyond.

3.1.3.2 Enzyme digestion and degenerated specimen measurement

After all the normal specimens (n=18×2×3) from both halves were scanned, the three layers from one half disk (n=18×3) were digested with trypsin and those from the other half (n=18×3) were treated with collagenase to observe the digestion effect on articular cartilage. Enzyme treatment is a widely

accepted method to simulate the degeneration of articular cartilage. As mentioned earlier, trypsin is effective for the proteoglycans digestion with a slight simultaneous effect on the collagen network (Harris *et al.*, 1972) while collagenase is responsible for the degradation of the collagen network (Shingleton *et al.*, 1996).

For the trypsin degeneration group, the three layers (n=18×3) were placed in order in a plastic multi-well array (24 Well Plate, Arraycote, Nunc, Roskilde, Denmark) containing 0.25% trypsin-ethylenediamine-tetra-acetic acid (EDTA) (GIBCO, Invitrogen Corporation, Carlsbad, California, USA) at room temperature for 5 h (Zheng *et al.*, 2004b). Histology study using safranin-O staining conducted a in previous study confirmed that most proteoglycans in full thickness cartilage were depleted after 4 h trypsin digestion (Lu *et al.*, 2009). The slices in the collagenase degeneration group (n=18×3) were put into the other multi-well array which contained 30 U/ml collagenase solutions (GIBCO, Invitrogen Corporation, Carlsbad, California, USA) and kept in an incubator (Incucell-V111, Nunc, Denmark) at 37°C for 5 h (Saarakkala, 2007). According to the literature, such collagenase digestion would cause a significant damage to the collagen in articular cartilage. After the digestion, the specimens were submerged in the physiological saline solution for 1 h and then scanned again using a similar procedure as introduced above.

3.1.4 Parameters calculation

Reflected OCT signals were collected in real-time and analyzed off-line by a custom-designed Labview program. Fig 3.6 (a) and (b) shows the typical cross-sectional images collected without and with the specimen installed between the glass plate and the container base. In order to reduce noise, every 40 points among the 10000 data points (overlap length was set to be 20 points) were performed using Short Time Fast Fourier Transform (ST-FFT) and further filtered by a band-pass filter using Labview program. The amplitude of these signals was then added to represent the intensity value of one pixel in the image. So each image was composed of 500×100 pixels.

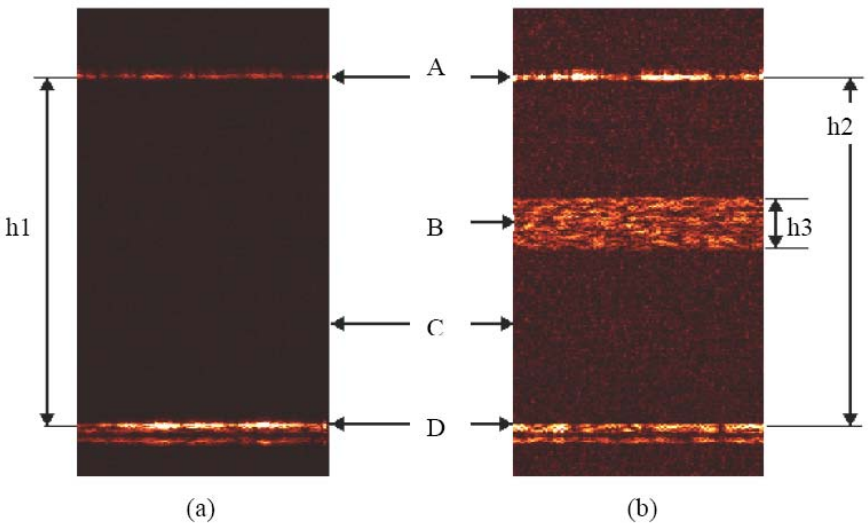

Fig 3.6. Typical images collected without (a) and with (b) the specimen installed between the glass plate and the container base. A: lower surface of the glass plate; B: articular cartilage slice; C: physiological saline bath; D: bottom of the container base; h_1, h_2: the optical path lengths from the lower surface of the glass plate to the bottom of the container without and with the presence of the specimen; h_3: the optical path length from the upper to the lower surfaces of the specimen.

In this study, we modified the optical length shifting method (Wang *et al.*, 2002b) to calculate the RI of cartilage. In OCT system, only when the optical path length of the sample and the reference arm match, will the observed interference signal reach the maximum. Thus the distances measured in the images represent the corresponding optical path lengths. By using the optical path lengths of the two reference interfaces, i.e. from the lower surface of the glass plate to the container base without and with the specimen installed between them and the average thickness of the specimen, as indicated in Fig 3.6, the RI of articular cartilage can be calculated as follows with the knowledge that the physical distance between the lower surface of the glass plate and the container base would not change:

$$\frac{h_1}{n_s} = \frac{h_2 - h_3}{n_s} + \frac{h_3}{n_c} \tag{3.1}$$

$$n_c = \frac{h_3}{h_1 + h_3 - h_2} \cdot n_s \tag{3.2}$$

where n_s and n_c are the RI of physiological saline and articular cartilage, while h_1 and h_2 represent the optical path lengths from the lower surface of the glass plate to the bottom of the container without and with the specimen, and h_3 the optical path length from the upper to the lower surfaces of the specimen, respectively. To measure the optical path lengths, further image processing approach was adopted to reduce the speckle effect. The pixel intensity values in the image were added along the horizontal direction to obtain a signal with 500 data points. Fig 3.7 shows the result from Fig 3.6 after this procedure. The intensity value of container base is on the left and that of the lower surface of the reference glass on the right. Therefore, as

demonstrated in Fig 3.7, h_1 and h_2 were calculated by the difference between the positions of intensity value peaks of the container base and glass lower surface, and h_3 was calculated by the distance between the $1/\sqrt{2}$ of the max intensity of two specimen surfaces. An RI value of 1.334 for the physiological saline (Levin *et al.*, 2004) was used as the standard value for the calculation of RI of articular cartilage.

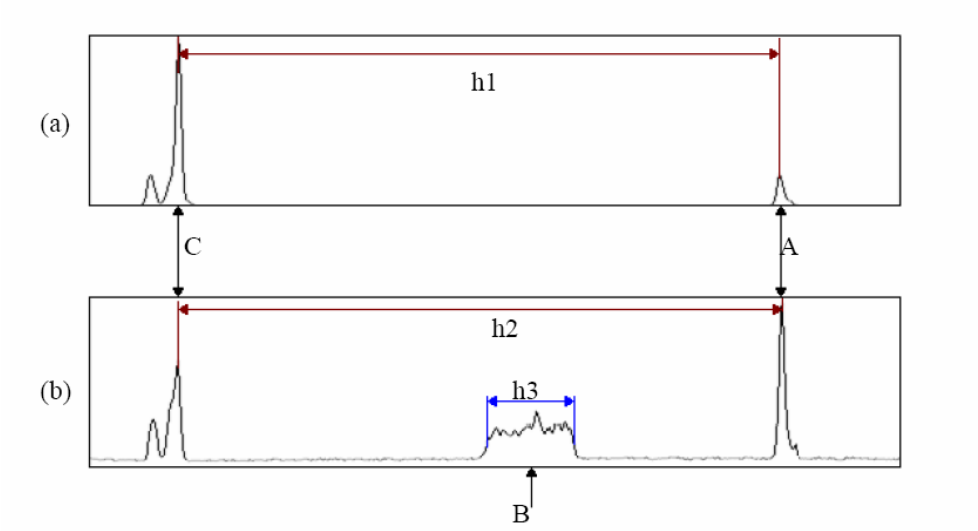

Fig 3.7. The profiles of the intensity along the depth direction corresponding to Fig 3.6, (a) without and (b) with the presence of the specimen. A: the lower surface of glass plate; B: articular cartilage slice; C: container base; h_1, h_2: the optical path lengths from the lower surface of the glass plate to the bottom of the container without and with the presence of the specimen; h_3: the optical path length from the upper surface to the lower surface of the specimen.

3.1.5 Statistical analysis

To test the reproducibility of the study, the coefficient of variation (CV) was calculated as an indicator (Giraudeau *et al.*, 2003). If the random variations of the n repeated measurements on a subject j are normally distributed,

the reproducibility or CV could be expressed as follows (Gluer *et al.*, 1995; Fournier *et al.*, 2001):

$$CV_j = \frac{SD_j}{\bar{x}_j} \times 100\% \qquad (3.3)$$

where SD_j is the standard deviation (SD) and $\bar{x}_j$ the mean of all the n measurements on subject j. The global reproducibility of the measurement (CV) is defined using the following equation (Gluer *et al.*, 1995):

$$CV = \sqrt{\frac{1}{m}\sum_{j=1}^{m} SD_j^2} \Big/ \sum_{j=1}^{m} \frac{\bar{x}_j}{m} \qquad (3.4)$$

where m is the total subjects number.

Based on equations 3.3 and 3.4, for each of the tests among the different layers 3 (normal, trypsin digested, and collagenase digested) ×3 (top, middle, and deep layers), CV was calculated. For the normal test, specimen number m was 36 (18×2), while for the trypsin and collagenase digestions, each test had a sample size of 18 (m =18).

Two-factor repeated measure ANOVA (SPSS v15.0, SPSS Inc, Chicago, IL, USA) was used to test the significance of the differences in RI for the three different zones of articular cartilage before and after the enzyme degeneration. $p<0.05$ was used to indicate significant difference for all the statistical analyses.

3.2 Measurement of articular cartilage surface roughness

3.2.1 Sample preparation

The first part of sample preparation for surface roughness assessment was similar to that in RI measurement. The patellae obtained from local market were cut into four quadrants using a bend saw machine and cylindrical cartilage-bone plugs with a diameter of 6.35 mm and thickness of approximately 1.8 mm were prepared from each patella using a metal punch. The total patellae number was 20 and cartilage-bone plugs were prepared from the medial upper region. From each patella, two disks were harvested (n=20×2), for later trypsin digestion and collagenase digestion, respectively. Another nine normal cartilage disks were reserved for future histological and SEM analysis.

Prepared specimens were labeled and wrapped by physiological saline soaked gauze, and stored at -20°C until testing. In the test day, the specimen was removed from the refrigerator, immersed into the physiological saline solution, and thawed for one hour at room temperature to achieve equilibrium (Wang, 2007).

3.2.2 System setup

In this study, surface roughness of articular cartilage was assessed using both OCT and ultrasound. The same OCT system as for RI measurement was employed to test the articular cartilage surface roughness. A high frequency ultrasound system (Vevo 770, Visualsonics, Inc., Toronto, CA)

was used for ultrasound surface roughness measurement as well as the acoustic properties and cartilage thickness investigation.

The schematic experimental design for sample fixation is showed in Fig 3.8. The specimen was secured at the bottom of the container surrounded by rubber gel. The container was filled with physiological saline during the whole process of the experiment to simulate *in vivo* environment.

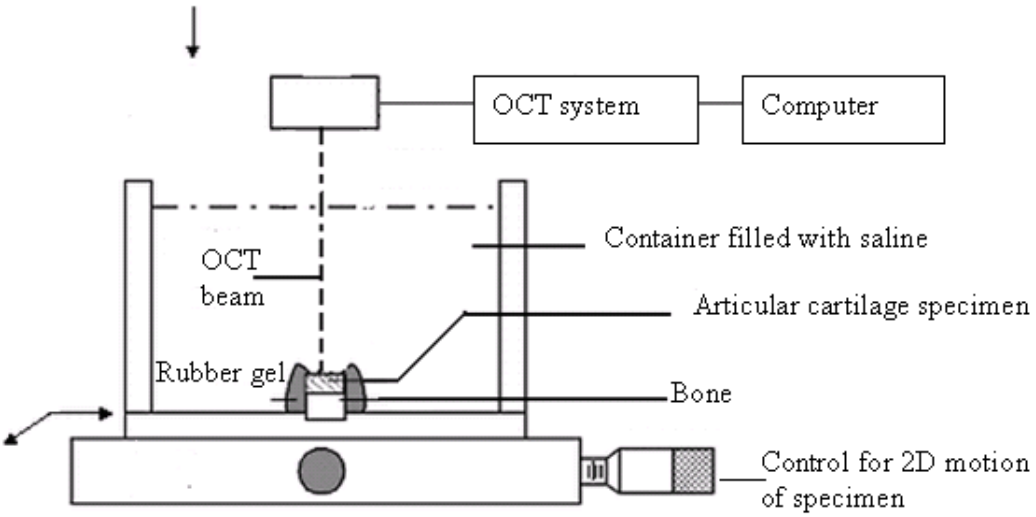

Fig 3.8. Schematic diagram of the OCT measurement system used for assessment of surface roughness index.

For ORI measurement, the received OCT signals were digitized by the data acquisition card and analyzed by a custom-designed Matlab (Matlab 6.5, The Mathworks, Inc., Natick, MA, USA) program. Each original scan data set was composed of 100 lines of depth scans covering a width of about 1 mm in this study, and each depth scan sampled 10000 data points along the

vertical direction. Calibration using two surfaces of a standard microscope slide was carried out. Equivalences of 0.51 μm per point in air, 0.38 μm per point in saline for each A-line were obtained as a result.

For URI measurement, B-mode image was obtained using a 55 MHz scanhead (RMV 708, Visualsonics, Inc., Toronto, CA). The region of interest (ROI) of radio frequency (RF) signal can be chosen in the control software (Fig 3.9). In this study the ROI of RF data was set to be 1 mm in width and approximately 2 mm in depth containing 100 lines of raw RF data. The RF signals were collected from the RF output and digitized at a sampling frequency of 420 MHz by the Vevo system. Each data point equivalent to 1.83 μm in the axial direction in saline was obtained with the information of the sampling frequency and the reference speed of sound in saline (1540 m/s (Jago and Whittingham, 1992)). The received digital signals were also analyzed by a custom-designed Matlab program.

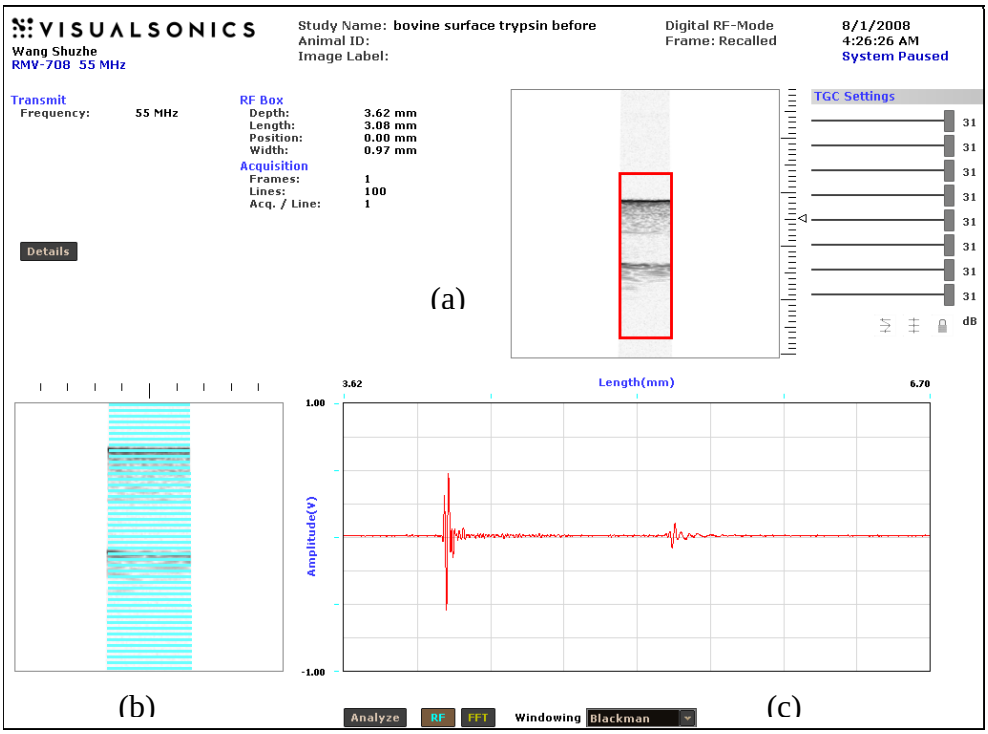

Fig 3.9. Software interface of the Vevo high frequency ultrasound system. (a) B-mode image of articular cartilage; (b) chosen RF region; (c) RF signal of one typical line.

3.2.3 Measurement procedures

3.2.3.1 ORI measurement of glass and emery papers

A piece of glass with smooth surface was tested in this study to see whether the scanning process itself would introduce any system noise to the result of ORI or URI. The glass was placed at the bottom of the container and fixed by rubber gel (Fig 3.8), and the container was filled with physiological saline, similar as the condition in cartilage specimen test. A cross-sectional OCT image with the scan width of 1 mm was collected with the information of reflected signals from the upper surface of glass. The glass was scanned along four different directions with an interval of 45°. Along each direction

reflected signals from three different parallel scan lines with the interval of 0.5 mm were collected. Each site was scanned for 10 times.

Nine different emery papers with Federation of European Producers of Abrasives (FEPA) standard particle sizes (Silicon carbide waterproof abrasive paper, KMCA, Korea) were used in this study for both OCT and ultrasound systems. The emery papers and corresponding particle sizes are showed in Table 3.1.

Table 3.2. Emery papers and average particle sizes used in ORI and URI tests.

Emery paper	P60	P120	P180	P280	P320	P1000	P1200	P1500	P2000
Particle size (μm)	269	125	82	52.2	46.2	18.3	15.3	12.6	10.3

The emery paper was fixed at the bottom of the container by rubber gel (Fig 3.8), and the container was filled with physiological saline, similar to the condition in cartilage specimen test. A scanning process similar to the one used in glass surface testing was carried out. A cross-sectional OCT image with the scan width of 1 mm was collected with the information of reflected signals from the emery paper surface. Each emery paper was scanned along four different directions with an interval of 45°. In each direction reflected signals from three different parallel scan lines with an interval of 0.5 mm were collected. Each site was also scanned for 10 times.

3.2.3.2 URI measurement of glass and emery papers

Similar to the ORI measurement, the glass as well as the emery paper was fixed at the bottom of the container by rubber gel (Fig 3.8), and the container was filled with physiological saline. The RF ultrasound signal with the scan width of 1 mm was collected together with the information of ultrasound echoes from the surface. Each sample was scanned along four different directions with an interval of 45°. And in each direction reflected signals from three different parallel scan lines with an interval of 0.5 mm were collected.

3.2.3.3 ORI measurement of normal specimen

Six articular cartilage samples aside from the main set of specimens were included in the reproducibility test. Then the roughness of articular cartilage specimen (n=20×2) was measured using OCT and ultrasound before and after the enzyme degeneration.

The articular cartilage bone disk was fixed at the bottom of the container by rubber gel (Fig 3.8), and the container was filled with physiological saline during the whole process of measurement. Initial OCT cross-sectional images were recorded along different directions of the specimen so that adjustment could be conducted to make sure that the cartilage surface was parallel to the container base. All the roughness tests were carried out at room temperature (24.5±1°C) and humidity (62±5%). The OCT beam was first located at the centre of the specimen disk. A cross-sectional OCT

image with a scan width of 1 mm was collected with the information of reflected signals from the cartilage surface. Then the specimen platform was moved horizontally perpendicular to the OCT beam at 0.5 mm interval, and another cross-sectional image was collected. A total of three sites in this scanning direction were obtained. After finishing scanning in one direction, the sample was carefully rotated 45° clockwise in the horizontal plane. Following the similar procedure, another three sites were scanned in this new direction. Images from a total of four directions (sites number in one cartilage sample: 4×3) with an interval of 45° were obtained in order to assess the surface roughness of cartilage sample. Each site was scanned 10 times and data of each scan was recorded for further off-line analysis.

3.2.3.4 URI measurement of normal specimen

After being scanned using OCT system, the samples were then scanned by the Vevo high frequency ultrasound system following the similar procedure. Each specimen was scanned in four directions with an interval of 45° and totally 12 sites were tested. RF signals from 100 scan lines, corresponding to a width of 1 mm were collected and saved by the program (Fig 3.9). The corresponding ultrasound echoes from the saline-cartilage interface and cartilage-bone interface were recorded in the RF data format for the further analysis.

3.2.3.5 Enzyme digestion and measurement of degenerated specimen

All the normal specimens (n=20×2) were scanned by both OCT and ultrasound, and then employed for indentation tests, which is presented in Section 3.3. After that, the normal specimens were divided into two groups: trypsin (n=20) and collagenase (n=20) treatment groups. Each group contained the cartilage-bone disks from 20 different patellae. For the trypsin treatment group, the specimens were placed in order in a plastic multi-well array (24 well plate, Arraycote, Nunc, Roskilde, Denmark) containing 0.25% trypsin-EDTA (GIBCO, Invitrogen Corporation, Carlsbad, California, USA) in an incubator (Incucell-V111, Nunc, Denmark) at 37 °C for 4 h (Lu *et al.*, 2009). For the collagenase treatment group, the samples were placed in another plastic multi-well array containing 30 U/ml collagenase solutions (GIBCO, Invitrogen Corporation, Carlsbad, California, USA) and kept in the incubator at 37 °C for 24 h (Hattori *et al.*, 2005a).

After the digestion treatment, the specimens were submerged in the physiological saline solution for 1 h and then scanned again using a similar procedure as for the normal samples introduced above by both the OCT and ultrasound systems.

3.2.4 Parameters calculation

3.2.4.1 ORI calculation

Reflected OCT signals with the information from cartilage surface were collected by a custom-designed Labview program. Fig 3.10 (a) shows a

typical cross-sectional image collected from cartilage surface. Arrows indicate the saline-cartilage interface. Hilbert transform was applied to the original optical signal to obtain the signal envelope. The position of saline-cartilage interface was determined by the location of maximum value of the envelope in each line. The profile of this interface was calculated by a custom-designed Matlab program. The interface profile of the image in Fig 3.10 (a) is shown in Fig 3.10 (b). Assuming that the roughness was rather in the high frequency range, a three-order Butterworth high pass filter with cutoff frequency equivalent to 0.05 times cyclic change in 1 mm was applied to eliminate the cartilage contour before the calculation of ORI (Saarakkala *et al.*, 2004b)(Fig 3.10 (c)).

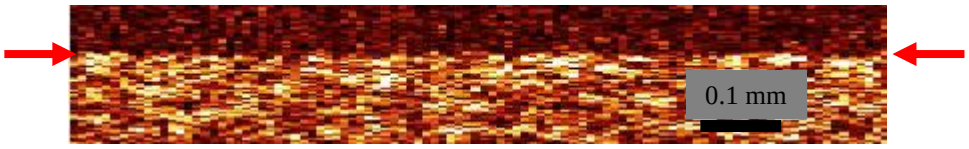

(a)

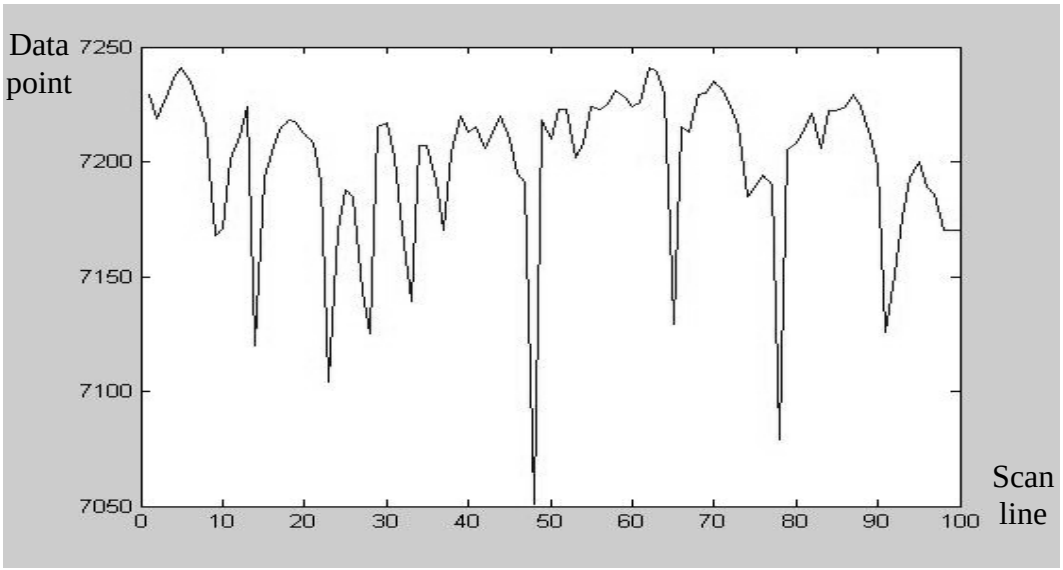

(b)

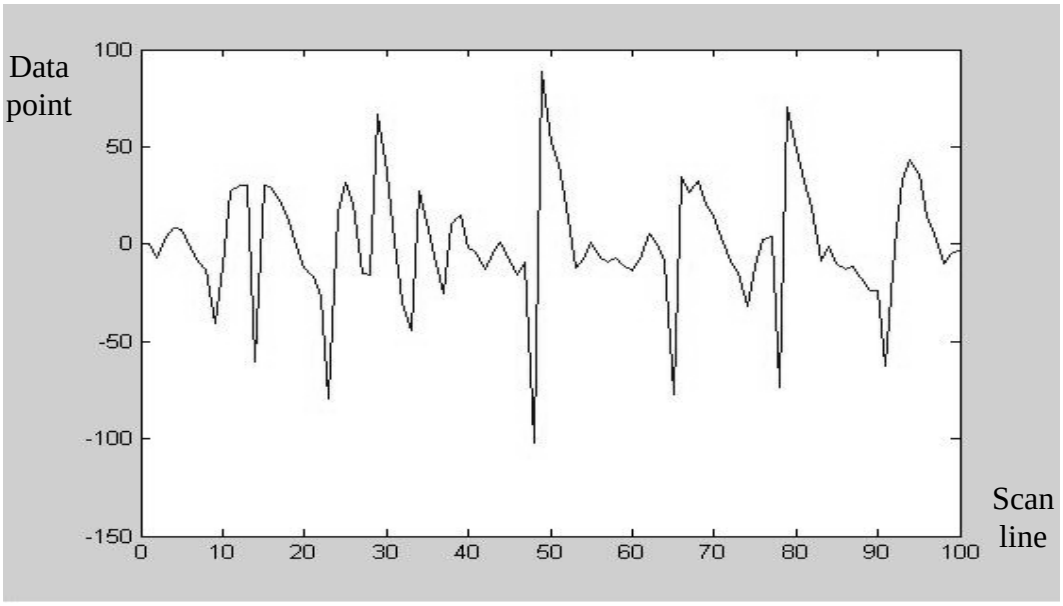

(c)

Fig 3.10. (a) Cross-sectional OCT image of one typical cartilage sample. Arrows indicate the saline-cartilage interface. (b), (c) Saline-cartilage interface profile of the sample in (a) before and after the high pass filter, plotted by the Matlab program.

In this study, a new parameter ORI was introduced (equation 3.5) following the principle of URI parameter (Saarakkala *et al.*, 2004b).

$$ORI = \sqrt{\frac{1}{m}\sum_{i=1}^{m}(d_i - \overline{d})^2} \tag{3.5}$$

where m is the number of scan lines, d_i is the distance from optical source to cartilage interface in scan line i and $\overline{d}$ is the mean distance from the optical source to the surface. The distances from optical source to the position of the first data point in each scan line were considered to be the same. If this distance is d_0, equation 3.5 can be rewritten as:

$$ORI = \sqrt{\frac{1}{m}\sum_{i=1}^{m}[(d_0 + d_i') - (d_0 + \overline{d}')]^2} \tag{3.6}$$

where d_i' is the distance from the position of the first data point to the saline-cartilage interface in line i, and $\overline{d}'$ is the mean distance from the position of first data point to the saline-cartilage interface. Equation 3.6 can be further revised as:

$$ORI = \sqrt{\frac{1}{m}\sum_{i=1}^{m}(d_i' - \overline{d}')^2} \tag{3.7}$$

The distance d_i' and $\overline{d}'$ can be calculated with the information of the number of data points between the first point to the point of maximum value of the envelope in each line and the equivalences of 0.38 μm per point in saline, which was calibrated by using two surfaces of a standard microscope slide with known thickness.

3.2.4.2 URI calculation

Similar to the ORI calculation, ultrasound echoes with the information from cartilage surface were collected by the software of the Vevo system. Fig 3.11 (a) shows a typical B-mode image collected from the cartilage surface. Arrows indicate the saline-cartilage interface. Hilbert transform was applied to the RF signal to obtain amplitude signal in order to obtain the signal envelope. The position of saline-cartilage interface was determined by the location of maximum value of the envelope in each RF line. The profile of this interface was calculated by a custom-designed Matlab program. The interface profile of the image in Fig 3.11 (a) is shown in Fig 3.11 (b). Assuming that the roughness was rather in the high frequency range, a three-order Butterworth high pass filter with cutoff frequency equivalent to 0.05 times cyclic change in 1 mm was also applied to eliminate the cartilage contour before the calculation of URI (Saarakkala *et al.*, 2004b)(Fig 3.11 (c)).

(a)

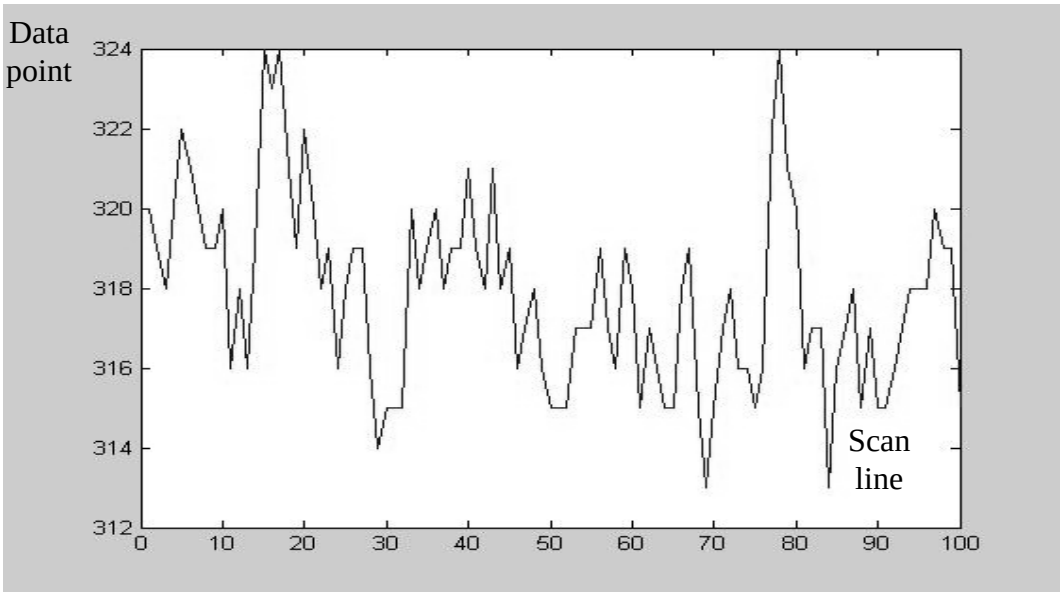

(b)

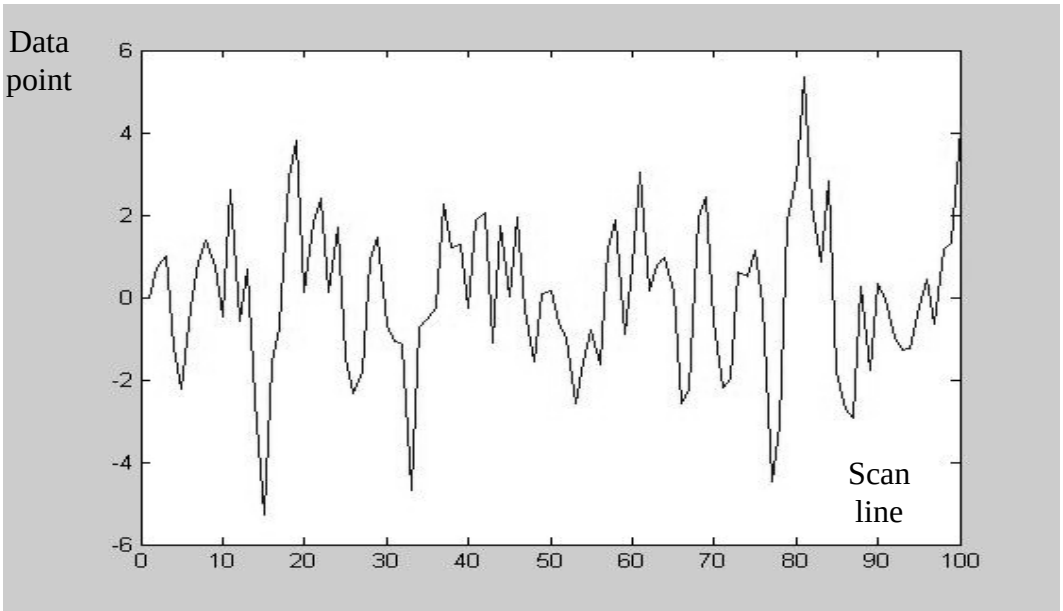

(c)

Fig 3.11. (a) Cross-sectional B-mode image of one typical cartilage sample obtained by the Vevo system. Arrows indicate the saline-cartilage interface. (b), (c) Saline-cartilage interface profile of the sample in (a) before and after the high pass filter plotted by the Matlab program.

The equation for calculating URI (equation 2.9) has been introduced in the Literature Review Chapter.

$$URI = \sqrt{\frac{1}{m}\sum_{i=1}^{m}(d_i - \bar{d})^2} \qquad (2.9)$$

where m is the number of scan lines, d_i is the distance from the transducer to cartilage interface in scan line i and $\bar{d}$ is the mean distance from the transducer to the surface. Distances between the transducer and cartilage surface can be calculated by multiplying the ultrasound flight time by the speed of sound in physiological saline (1540 m/s (Jago and Whittingham, 1992)) and then dividing the result by 2, since ultrasound travels double the distance from the transducer to the cartilage surface. The ultrasound flight time can be determined with the information of location of maximum value of the Hilbert enveloped RF signal and the sampling rate of the A/D converter (420 MHz).

3.2.4.3 Calculation of acoustic parameters

Ultrasonic measurement can provide an effective method to assess the tissue characteristics. In this study, acoustic parameters were analyzed by custom-designed Matlab programs (Huang, 2004).

Before the scanning of cartilage specimen, reference signals from a steel plate in physiological saline at different axial distances z were collected to compensate the system dependent effects (Fournier *et al.*, 2003). During the URI test, the ultrasonic signals of the specimen were recorded under small and large amplification gains to study the interface echo and backscattering

inside the tissue, respectively. A substitution method and a multi-narrowband algorithm were used in this study (Fink and Cardoso, 1984; Lizzi *et al.*, 1983; Huisman and Thijssen, 1996; Roberjot *et al.*, 1996). The ultrasonic signal backscattered from ROI was gated using a Hamming window with a length of 100 points, and Fourier transformed using FFT (1024 points) and squared to get the power spectral density. Reference signals from the steel plate were also processed in a similar way to obtain reference spectra. The power spectrum of cartilage tissue in each scan was averaged among the 100 independent RF lines. The calibrated power spectra could be calculated by the following equation:

$$\langle S_{cal}(f,z)\rangle = \frac{\langle S_C(f,z)\rangle}{S_R(f,z)} \qquad (3.8)$$

where z represents the axial distance of the window centre, $S(f,z)$ is the power spectrum at z. The subscript "cal" represents the calibrated power spectrum, "C" for cartilage tissue and "R" for reference spectrum. "$\langle ... \rangle$" stands for the spatial averaging over the 100 independent lines for each B-mode scan.

Integrated Attenuation (IA)

Attenuation coefficient was calculated by a regression of the power spectra with respect to the corresponding penetration depth in cartilage (Huang, 2004). The saline-cartilage and cartilage-bone interfaces were detected in the program automatically based on the sudden change of signal intensity. The central part of the signals was selected by excluding saturated signals between these two interfaces, with the purpose to avoid adding noise

frequency components to the power spectra. The selected central part of the signals was then divided into narrow bands with a width of 52 points (approximately 0.09 mm) and an overlap of 26 points (Fig 3.12). Each segment of signal was gated by a Hamming window with a length of 100 points and then zero-padded to 1024 points. FFT was applied to obtain power spectrum. The power spectra from the 100 lines were averaged and divided by the power spectra of reference signals.

If the cartilage was assumed to be ultrasonically homogeneous (Agemura *et al.*, 1990), the calibrated power spectrum could be written as:

$$\langle S_{cal}(f,z)\rangle = B(f)\cdot 10^{-2a(f)\cdot 2z/20} \qquad (3.9)$$

where $B(f)$ is the backscatter transfer function, $a(f)$ is the frequency dependent attenuation in unit of dB/mm and $2z$ is the total propagation distance. The relationship between the calibrated spectrum and the propagation distance could be more easily observed after performing logarithm transform on both side of equation 3.9:

$$10\lg\langle S_{cal}(f.z)\rangle = 10\lg B(f) - a(f)\cdot 2z \qquad (3.10)$$

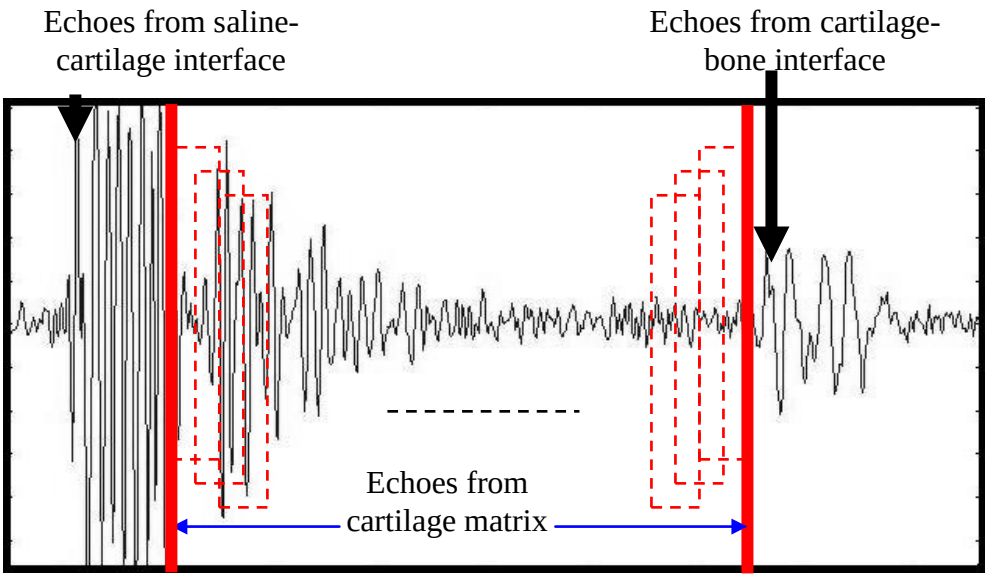

Fig 3.12. One typical line of RF signal using a large amplification gain. Echoes from saline-cartilage and cartilage-bone interfaces were indicated by vertical arrows. Unsaturated echoes from cartilage tissue (horizontal arrows) were detected by Matlab software. The echoes from cartilage matrix were further divided into several narrow bands with a depth of 52 points and 50% overlap.

In this study, the -6 dB frequency ranged from 18 to 55 MHz. If a linear frequency dependence of attenuation was assumed in cartilage tissue (Senzig *et al.*, 1992), equation 3.10 could be revised as:

$$a(f) = \beta \cdot f + a_0 \qquad (3.11)$$

where β is the attenuation slope in unit of dB/mm/MHz. IA (unit: dB/mm) could be defined as:

$$IA = \frac{1}{f_2 - f_1} \int_{f_1}^{f_2} a(f) df \qquad (3.12)$$

where f_1=18 MHz and f_2=55 MHz according to the -6 dB bandwidth of the transducer.

Integrated backscatter (IBS)

Backscatter coefficient reflects the acoustic energy backscattered from the cartilage internal structure (Pellaumail *et al.*, 2002). The signals collected under the large amplification gain between the two interfaces (saline-cartilage interface and cartilage-bone interface) were chosen to calculate the backscatter coefficient. This signal section was windowed by Hamming window, averaged among 100 lines, and divided by the spectra of reflection signals from the plane steel plate of the same length. The calibrated spectra were then logarithmically transformed to obtain the backscatter spectra $B(f)$ of the cartilage matrix. IBS (unit: dB) was defined similarly to that of IA from 18 MHz to 55 MHz as follows:

$$IBS = \frac{1}{f_2 - f_1}\int_{f_1}^{f_2} B(f)df \qquad (3.13)$$

where f_1=18 MHz and f_2=55 MHz, according to the -6 dB bandwidth of the transducer, are the lower and upper limits of the frequency range used, respectively. This backscatter coefficient was only related to the middle part of the tissue excluding the top superficial zone and the calcified cartilage zone.

Integrated reflection coefficient (IRC) and apparent integrated backscatter (AIB)

When ultrasound wave travels through the saline solution and cartilage, portion of the sound is reflected at the saline-cartilage interface and the rest travels through the cartilage. The reflection coefficient can represent the surface condition of cartilage (Nieminen *et al.*, 2002; Toyras *et al.*, 1999;

2002). IRC was used to investigate the surface property of cartilage in this study. During the signals collection, B-mode scan was conducted with the ultrasound beam perpendicular to the cartilage surface to reduce the possible errors induced by the oblique incidence.

The backscatter coefficient can also be used to represent the property at subchondral bone interface (Jaffre *et al.*, 2003). It was defined as AIB in this study.

Fig 3.13 shows one typical RF signal collected under the small amplification gain. The echoes from the saline-cartilage and cartilage-bone interfaces were detected by the Matlab program based on the sudden change of signal intensity. A Hamming window with a width of 100 points was used to gate the signals for both groups of echoes. Similar to the calculation of IA and IBS, the calibrated spectra were logarithmically transformed to obtain the reflection spectra $R(f)$ of cartilage surface and backscatter spectra $B(f)$ from the cartilage-bone interface. IRC and AIB can be calculated in similar equations:

$$IRC = \frac{1}{f_2 - f_1}\int_{f_1}^{f_2} R(f)df \tag{3.14}$$

$$AIB = \frac{1}{f_2 - f_1}\int_{f_1}^{f_2} B(f)df \tag{3.15}$$

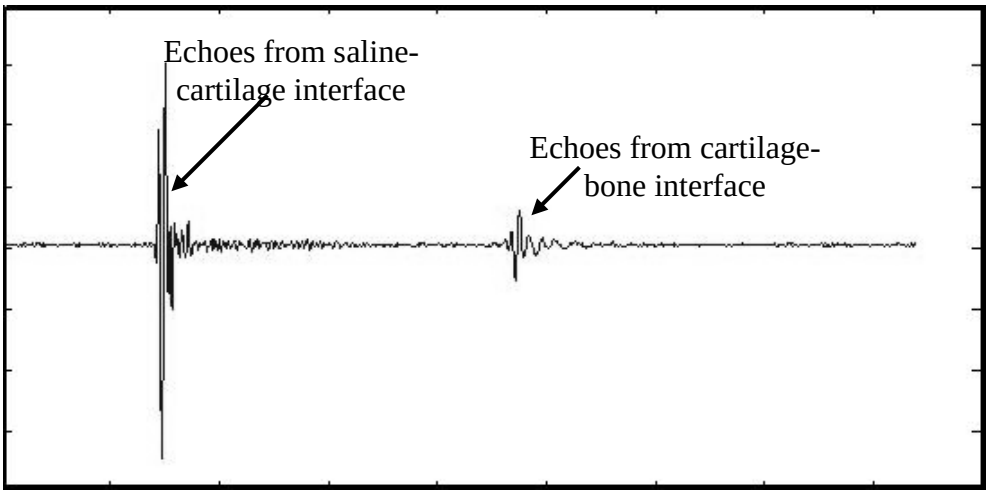

Fig 3.13. One typical line of RF signal collected under the small amplification gain. Echoes from saline-cartilage and cartilage-bone interfaces (indicated by arrows) were detected by the Matlab program based on the sudden change of signal intensity.

3.2.4.4 Cartilage thickness calculation

Articular cartilage thickness in this study was determined by the RF ultrasound signals collected in B-mode image. Since every B-mode image contains 100 RF lines, the 50th line in each scan was used for thickness calculation. Fig 3.14 (a) shows a typical RF line collected in B-mode scan during the measurement. The two echoes were reflected from saline-cartilage and cartilage-bone interfaces, respectively. Hilbert transform was applied to the RF signal to obtain the signal envelope (Fig 3.14 (b)). The cartilage thickness was calculated by multiplying the ultrasound flight time between the two interfaces by the speed of sound in articular cartilage. In this study, the speed of ultrasound was assumed to be 1610 m/s in normal articular cartilage and be 1595 m/s and 1580 m/s after trypsin and collagenase treatments, respectively (Laasanen *et al.*, 2002). The ultrasound flight time could be determined with the information of data points number

between peak locations of the Hilbert enveloped RF signal and sampling rate of the A/D converter (420 MHz).

3.2.5 Statistical analysis

To test the reproducibility of the study, CV was calculated as an indicator, as introduced earlier. Specimen number m used for the reproducibility test for surface roughness, acoustic parameters and cartilage thickness was 6.

Paired-samples t test was used to test the significance of the differences in those parameters before and after degeneration. Pearson's analysis was applied to analyze the relationships between different measures. $p<0.05$ was used to indicate significant difference for all the statistical analyses. All the statistical analysis was carried out using SPSS (SPSS v15.0, SPSS Inc, Chicago, IL, USA).

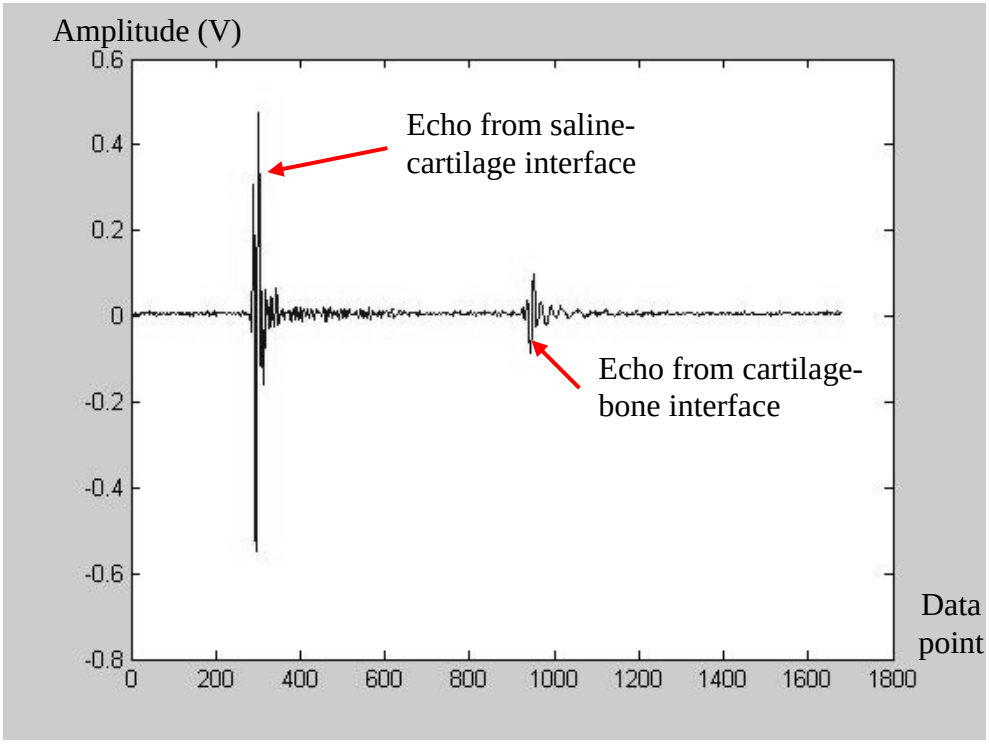

(a)

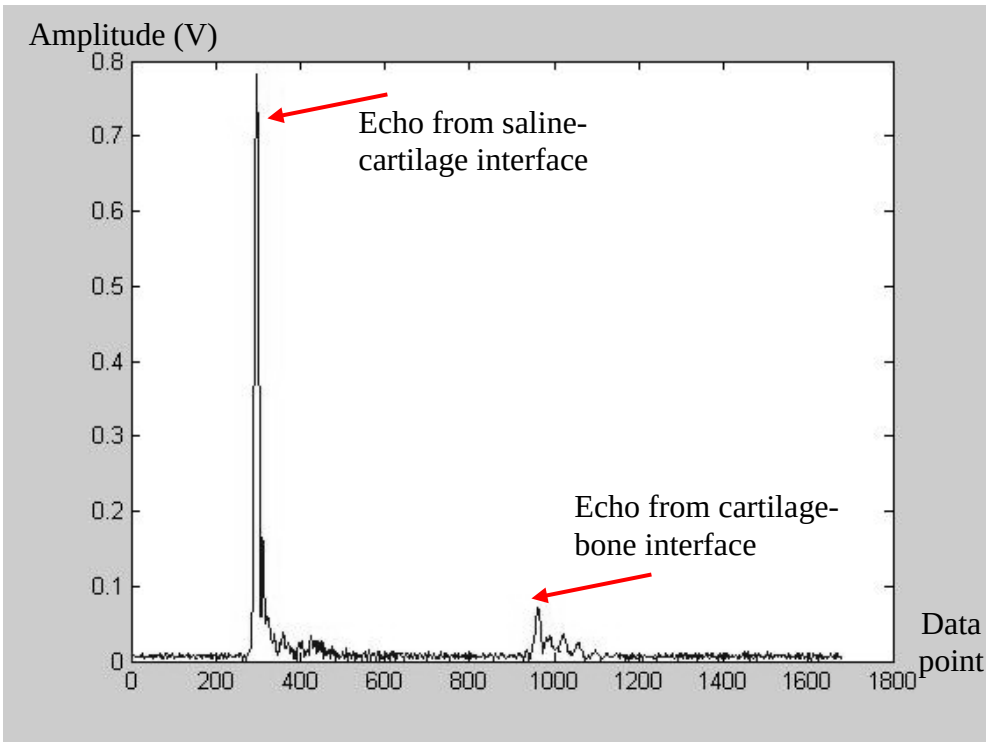

(b)

Fig 3.14. Typical RF lines collected in B-mode scan before (a) and after (b) Hilbert transform. Arrows indicated the echoes from saline-cartilage interface and cartilage-bone interface, respectively.

3.3 Indentation tests

3.3.1 Sample preparation

The samples used for the indentation tests were the same ones used in the surface roughness measurement. So that the relationship between the morphological and mechanical properties of articular cartilage cab be investigated.

3.3.2 System setup

3.3.2.1 OCT air jet indentation

The novel OCT air jet indentation system which has been introduced in Chapter 2 was firstly used for the indentation test (Fig 2.11, Fig 3.15) (Huang *et al.*, 2009). The fiber-based OCT probe was modified to allow the installation of an air jet bubbler. The OCT probe was fixed and the laser beam focuses vertically around 5 mm under the lower surface of the bubbler. A transparent plate was installed at the top of the bubbler to seal the pressurized air from the OCT components but let the laser beam pass through. A pipeline with maximally constant air pressure was connected to the system. In order to control and measure the pressure within the pipe, an electronic proportioning valve (ITV 1030-311L-Q, SMC Networks, Inc., Irvine, CA, USA) with a measure range of 5 bar (0.5 MPa) was installed before the bubbler to the pipeline. A tube with orifice diameter of 1 mm was installed at the tip of bubbler to guide the air jet and make the jet more uniform. The relationship of proportioning valve output and the actual force

applied on sample surface was calibrated by placing an electronic scale (TP-1000, Lantescale, Shenzhen, China) in the position of sample during indentation.

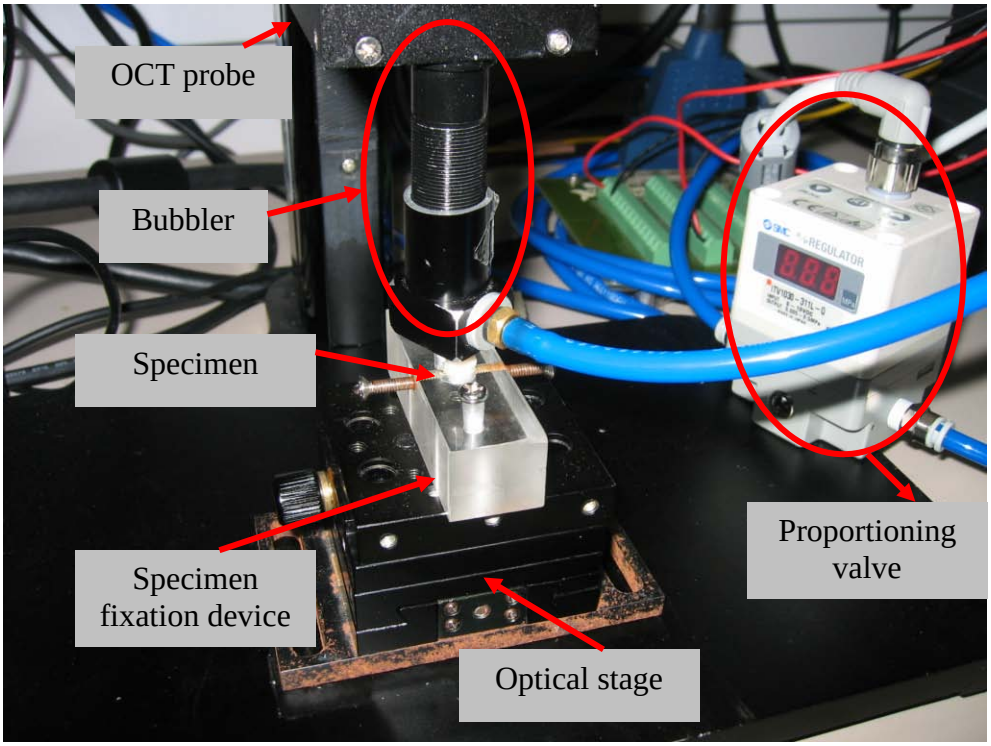

Fig 3.15. A picture of the OCT air jet system.

In order to fix the underlying bone layer of cartilage specimen during the indentation test, a special specimen fixation device was made (Fig 3.16). A hole with a diameter of 7.5 mm and a depth of 4 mm was drilled in the middle of one piece of plexiglass block in order to hold the cartilage-bone disk. And a screw thread tunnel parallel to the upper surface of plexiglass block with a diameter of 3 mm was further drilled across the plexiglass through the hole so that a pair of screws could be used to fix the bone layer of cartilage-bone disk from both sides. Another two holes perpendicular to the block upper surface were also drilled through so that another pair of screws could be used to fix this specimen fixation device to the optical stage.

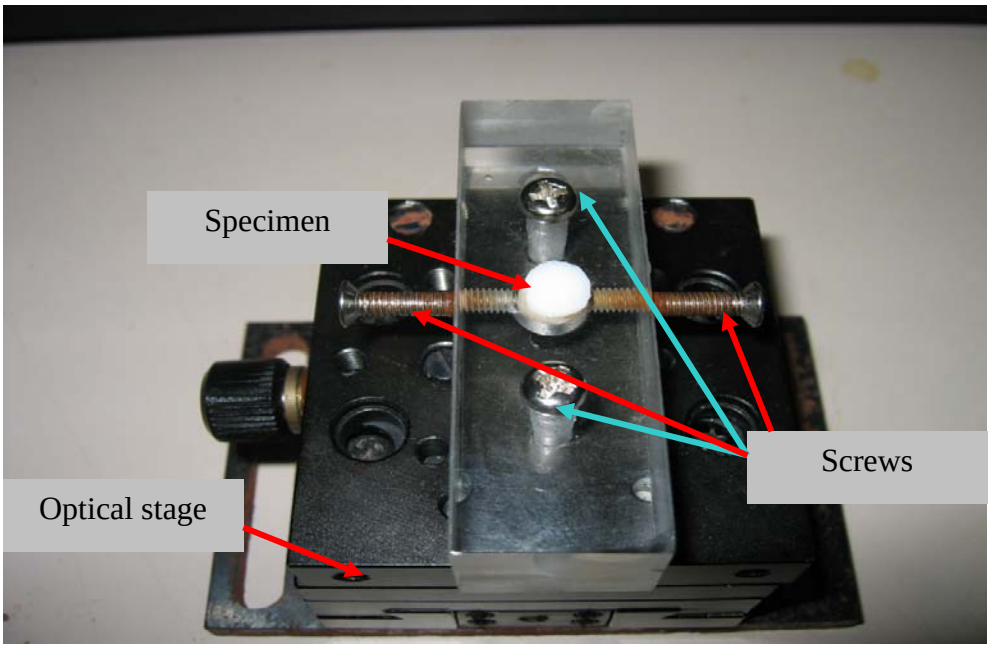

Fig 3.16. Picture of the custom-designed device for fixing cartilage specimens.

A PC was used to control the operation of the OCT air jet system. A data acquisition card (DAQ, PCI-6251, National Instruments, Austin, TX, USA) was employed to control the main OCT unit and collect the optical signals. Another DAQ card (PCI-6024E, National Instruments, Austin, TX, USA) was used to control the proportioning value as well as collect the signal from the pressure sensor in the valve. A custom-designed Microsoft VC++ program was developed for signal synchronization, signal control, data collection, and data analysis (Fig 3.17, Fig 3.18). During the indentation, signals from the OCT and pressure sensor on the proportioning valve were synchronized, sampled, displayed in real-time and saved for later off-line data processing by the program.

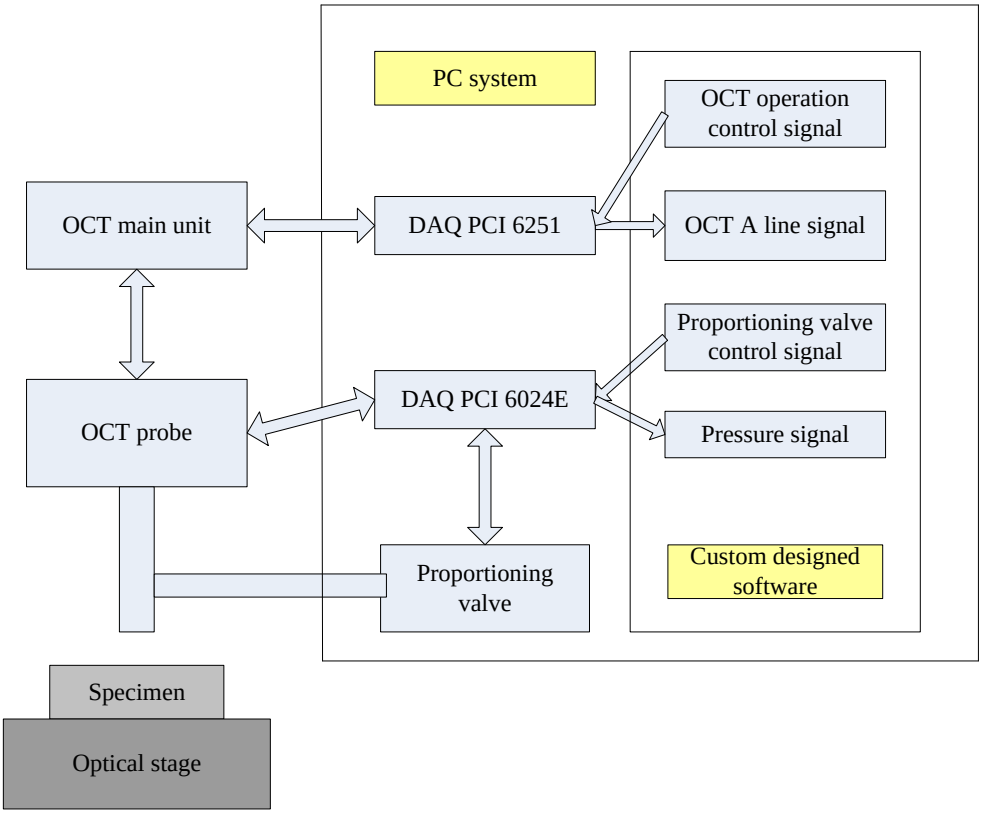

Fig 3.17. The diagram of the OCT air jet and data collection modules in the indentation system (Huang *et al.*, 2009).

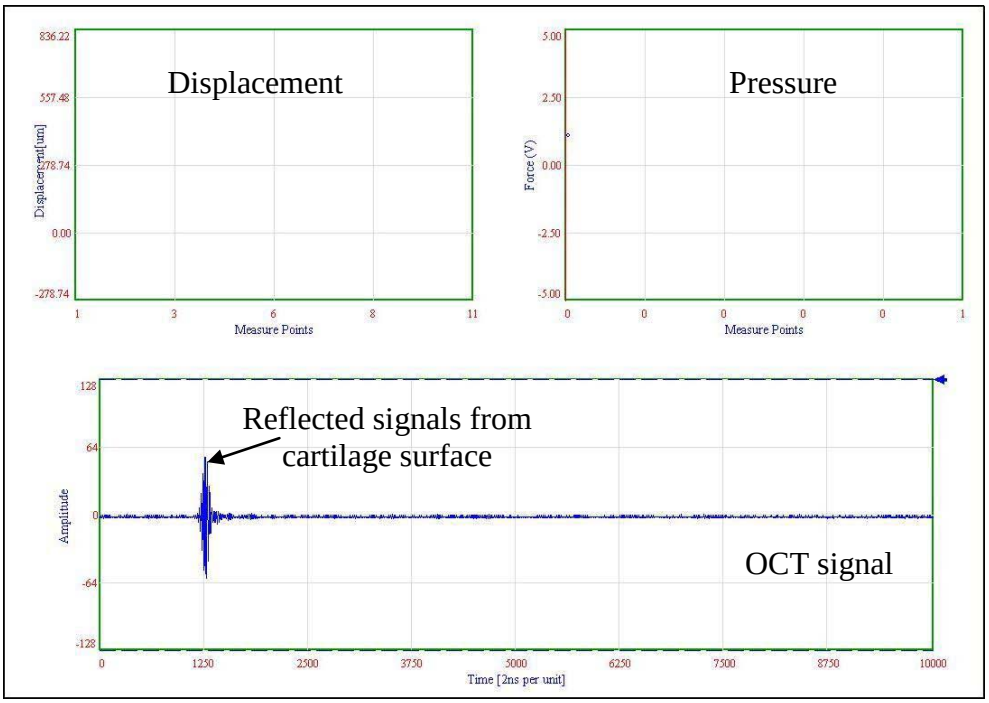

(a)

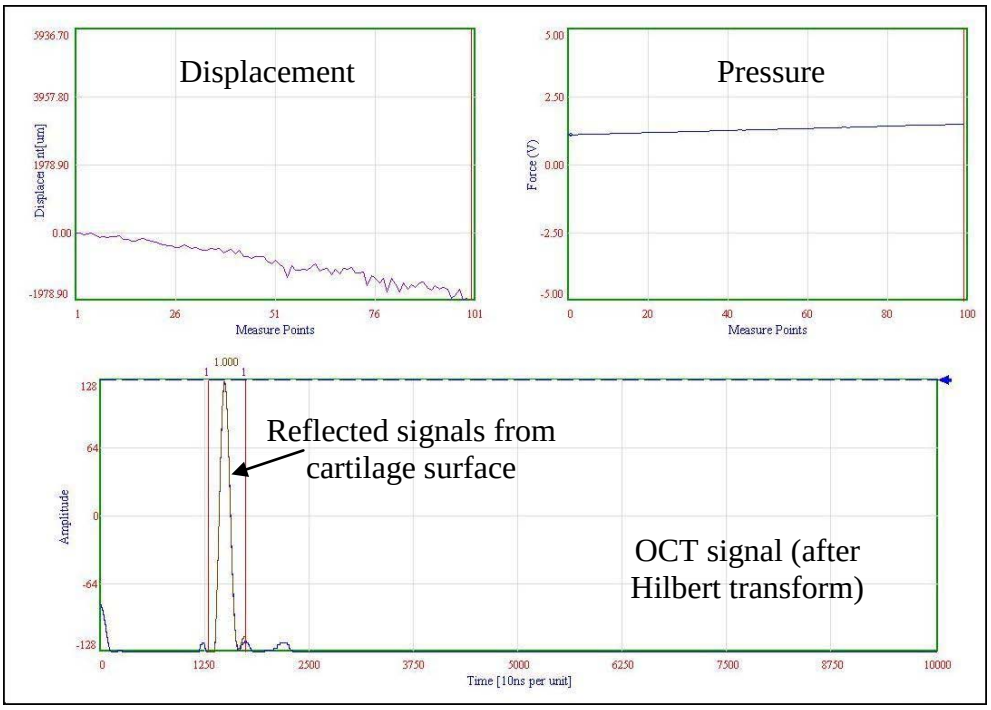

(b)

Fig 3.18. The software interface of the OCT air jet indentation system. (a) OCT signal before indentation. (b) OCT signal tracking (after using Hilbert transform to obtain the signal envelope). Tracking results for surface displacement and pressure measured are also shown in the interface. Reflected signals from cartilage surface are indicated with arrows. The vertical lines in the OCT signal window in (b) were used for tracking the movement of the signal during the air jet compression.

In this study, A-scan signal was acquired by continuously monitoring the OCT signal at a single location. Surface deformation of the specimen could be tracked according to the signal. The pressure control signal was sent from PC at approximately 16 Hz, and the digitized A-scan signal and signal from pressure sensor were acquired at a synchronized rate. Totally 7500 effective digital data points were obtained in each single A-scan. Calibration using two surfaces of a standard microscope slide was carried out. An equivalence of 0.43 μm per point in air for each A-line was obtained as a result. During the indentation, the displacement of sample surface was tracked by applying a cross-correlation algorithm to a pre-selected ROI (Lu *et al.*, 2005; 2007; Huang *et al.*, 2009). This algorithm was used to seek the most similar part by comparing every A–scan frame to the pre-selected ROI, which was the air-specimen interface in this study. Hilbert transform was applied to the original optical signal before tracking to obtain the signal envelope in order to reduce the effect of signal phase change during the indentation.

3.3.2.2 Ultrasound water jet indentation

A non-contact ultrasound water jet indentation developed earlier in our lab was also employed for the indentation test (Lu *et al.*, 2005; 2007)(Fig 3.19). A bubbler was used to eject the water jet by controlling the water flow. The diameter of the water ejecting nozzle was 1.94 mm. A 20 MHz focused ultrasound transducer (GE Panametrics, Inc, OH, USA) was fixed with bubbler. When the bubbler was filled with water the focused ultrasound

beam could propagate through the bubbler. The transducer was fixed to a 3D translating device (Parker Hammifin Corporation, Irvine, CA, USA) so that the position of transducer could be adjusted with a spatial resolution of 1 μm. Before indentation, the distances from the specimen surface to the nozzle outlet and the surface of transducer were adjusted by the 3D translating device to be approximately 5.0 mm and 19.5 mm to focus the ultrasound beam at the specimen surface and obtain the maximal water-cartilage surface interface echoes. The sample fixation device was similar to the one used in OCT air jet indentation test.

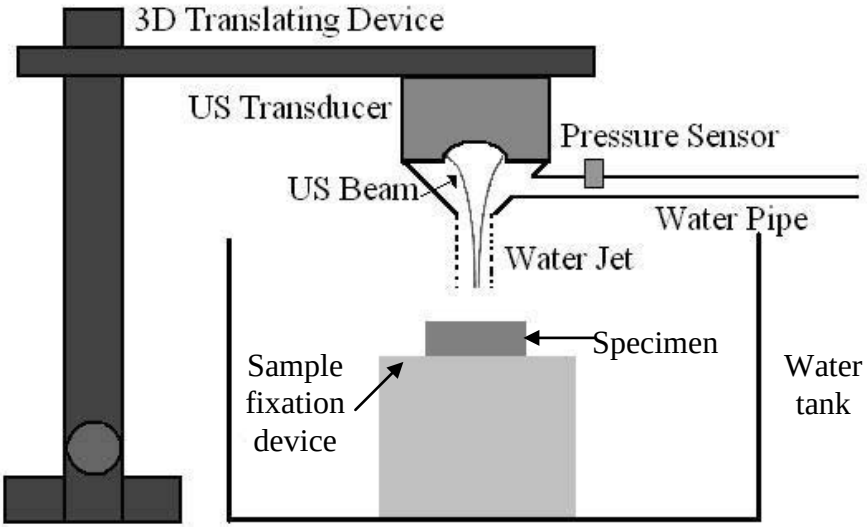

Fig 3.19. Schematic figure of non-contact ultrasound indentation system using water jet. The water jet was used as the indenter and focused high frequency ultrasound (20MHz) was applied to monitor the deformation of cartilage.

A pressure sensor (EPB-C12. Entran Devices, Inc., Fairfield, NJ, USA) was employed to measure the water pressure within the water pipe. The relationship between the overall force applied on the position of specimen and the water pressure sensor was determined using a load cell before the

study (ELFS-T3 mol/L, Entran Devices, INC., Farifield, NJ, USA). A custom-designed Microsoft VC++ program was developed to control the 3D translating device, and to collect, display and process the ultrasound signals and value of pressure sensor in real-time as well as to save the data for off-line process (Fig 3.20). The acquisitions of RF ultrasound signal and pressure data were synchronized. Cross-correlation algorithm was used to track the ultrasound echoes reflected from the water-cartilage interface and cartilage-bone interface in this study, similar to the one used in OCT air jet indentation system. Thus, the change of articular cartilage thickness could be monitored during the indentation process.

3.3.3 Measurement procedure

The same set of specimens as in the surface roughness measurement was used for the indentation test. Six articular cartilage samples aside from the main set of specimens were included in the reproducibility test. Then the articular cartilage specimen (n=20×2) was measured using OCT air jet and ultrasound water jet before and after the enzyme degeneration.

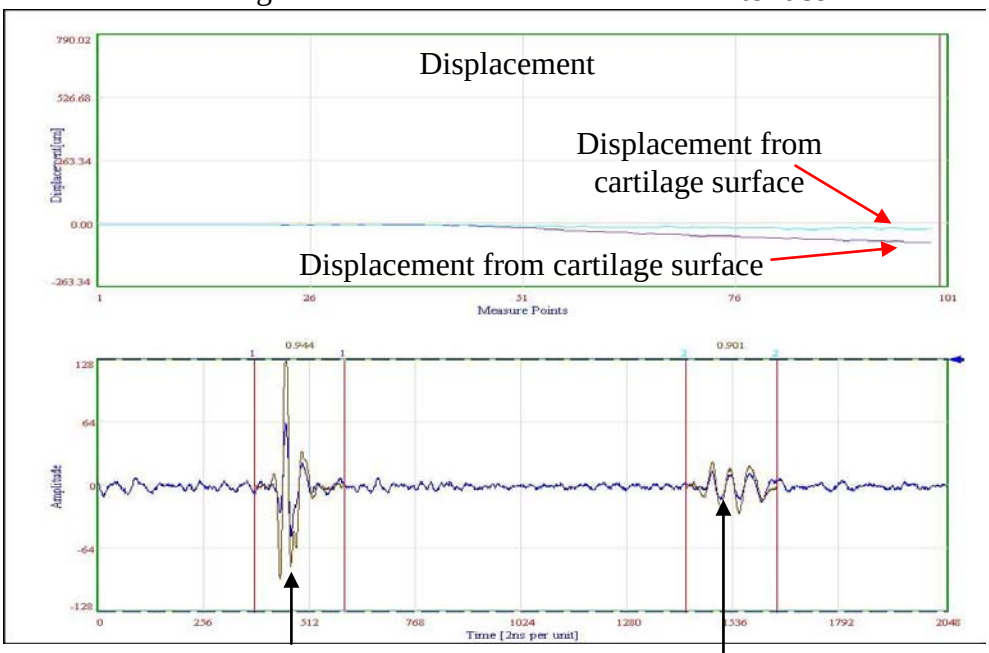

Fig 3.20. Software interfaces of the ultrasound water jet indentation system. (a) Ultrasound echoes before indentation. (b) Ultrasound saline-cartilage and cartilage-bone interfaces tracking result. Displacements of those interfaces during the indentation are indicated by arrows in upper part of (b). Echoes from those two interfaces are indicated with vertical arrows in lower part of (b). The vertical lines in the ultrasound signal window in (b) were used for tracking the movement of the echoes.

3.3.3.1 OCT air jet indentation test on normal specimen

Before the air jet indentation, specimen was fixed in the special device described before. The air jet was exerted at the center of the surface. A-scan signals were obtained and fine adjustment of the surface was made to obtain the maximal reflection signal amplitude so as to make sure the optical beam perpendicular to the cartilage surface. The boundary condition criterion could fulfill the one proposed earlier (Galbraith and Bryant, 1989).

For the indentation test, the specimen was preloaded with a force of 0.04 N for 3 seconds and then it was indented with the linearly increased pressure controlled by the software to approximately 0.1 N within 6 seconds. The stiffness of cartilage was determined by calculating the slope of pressure applied on the cartilage to the local strain induced in the loading phase (Lu *et al.*, 2009). Previous studies showed that instantaneously induced deformation of a biphasic tissue such as articular cartilage can be simplified using an equivalent incompressible single phase elastic material model (Hayes *et al.*, 1972; Mak *et al.*, 1987). In this study, the strain of each indentation was within 10% and only the data within 3% was adopted to obtain a load-indentation curve fitted by a linear regression in order to obtain stiffness.

After each indentation, the cartilage sample was immersed in physiological saline for at least half an hour before the next indentation (Bae *et al.*, 2006). The indentation test was performed on each specimen three times and the mean value of stiffness was calculated.

3.3.3.2 Ultrasound water jet indentation test on normal specimen

Similar to air jet indentation measurement, the specimen was fixed in the special device. The water jet was exerted at the center of the surface with less than 1 kPa. A-scan signals were obtained and fine adjustment of the surface was made to obtain the maximal echo amplitude so as to make sure the ultrasound beam perpendicular to the cartilage surface.

After the examining site was determined, the specimen was first scanned using the water jet with the pressure less than 1 kPa for approximately 15 minutes, allowing the cartilage swelling caused by the change of the concentration of solution from 0.15 M/L physiological saline to approximately 0 M/L reaching equilibration (Lu *et al.*, 2009). The specimen was then preloaded with a pressure of 20 kPa (a preload of 0.04 N) for 3 seconds, and then indented with the manually controlled pressure increased to approximately 180 kPa within around 6 seconds. The stiffness of cartilage was determined similarly by calculating the slope of pressure applied on the cartilage to the local strain induced in the loading phase.

After each indentation, cartilage sample was immersed in physiological saline for at least half an hour before the next indentation for cartilage recovery. The indentation test was performed on each specimen three times and the mean value of stiffness was calculated.

3.3.3.3 Enzyme digestion and degenerated specimen measurements

The enzyme digestion process had been introduced in Section 3.2, 3.5. The same set of specimens was used to investigate the surface roughness, acoustic and stiffness properties changes before and after digestion.

The stiffness of specimens after enzyme treatment was also measured using both OCT air jet and ultrasound water jet following the similar protocols as mentioned above.

3.3.4 Parameters calculation

3.3.4.1 Calculation for OCT air jet

The air jet indentation used in this study was assumed to be similar with mechanical indentation, hypothesizing that the air pressure measured in the pipe was linearly proportional to the force induced on the specimen. In order to test this hypothesis, relationship between the output of pressure sensor in proportioning valve and the force applied on the specimen surface measured by an electronic scale was established. The result of linearity was positive, which is shown in the result section.

The stiffness of cartilage was determined by:

$$S = \frac{F/A}{\Delta L/L_0} \tag{3.16}$$

where F/A is the pressure induced on the cartilage surface and $\Delta L/L_0$ is the averaged deformation of the cartilage layer (called strain level, ΔL is

the change of the cartilage layer and L_0 is the initial thickness of cartilage. L_0 is obtained by the cartilage thickness measurement carried out using high frequency ultrasound in this study. Different thickness values before and after the enzyme degeneration were used for the stiffness calculation). This parameter was calculated by a linear regression of the pressure-strain curve of the indentation in the loading phase.

The stiffness correlated well with Young's modulus (Lu *et al.*, 2005; Lu, 2006). In this study, the stiffness was calculated as an indicator of cartilage mechanical properties. Only the data within the deformation less than 3% were used for calculation.

3.3.4.2 Calculation for ultrasound water jet

Similar to the calculation for OCT air jet, the relationship between the output of pressure sensor and the force applied on the specimen surface was earlier investigated (Lu *et al.*, 2005). In this study, the relationship was also measured by a load cell and weights. The output of load cell when applying different weights on its surface was first recorded. Then load cell was placed in the position of specimen and its output and the output of pressure sensor were synchronized and recorded during the indentation. The result of this relationship study is shown later in the result section.

The calculation of stiffness in water jet indentation is similar to that in OCT air jet indentation test. The radius of the indenter was 0.97 mm in water jet

indentation system. Only the data with the deformation less than 3% were used for calculation.

3.3.5 Statistical analysis

To test the reproducibility of the study, CV was calculated as an indicator, as introduced earlier. CV was calculated for stiffness in both OCT air jet and ultrasound water jet system. Specimen number *m* used for reproducibility test was 6. Paired-samples t test was used to test the significance of the differences in those parameters before and after degeneration. The Pearson analysis was employed to assess the linear relationship. Curve estimation was also applied to assess the relationships between properties. $p<0.05$ was used to indicate a significant difference for all the statistical analyses. The statistical analysis was carried out using SPSS.

3.4 Reference methods

3.4.1 Mechanical indentation test

For the purpose of comparison, indentation tests with a rigid steel indenter with a diameter of 2 mm were performed using a standard mechanical testing machine (Instron 5569, Norwood, MA, USA) on specimens before and after enzyme treatment. The maximum indentation depth was within 10% of the initial cartilage thickness and only the data within 3% deformation were employed for the calculation. The indentation speed was

set to be 2 mm/min, which was similar to the indentation speed used for the air jet and water jet tests.

With the assumptions of a linear elasticity in cartilage (Hayes *et al.*, 1972; Mak *et al.*, 1987), a constant Poisson's ratio and a small aspect ratio (indenter radius/initial thickness a/h, was around 0.6 in mechanical indentation system), equation 2.15 can be simplified as:

$$E = \frac{(1-v^2)}{2a} \cdot \frac{F}{d} \tag{3.17}$$

where E is the Young's modulus of the cartilage, v is the Poisson's ratio, a represents the radius of the indenter, F represents the indentation force and d is the deformation, with the scaling factor related to v and a/h approaching to one in equation 2.15 (Hayes *et al.*, 1972). The Poisson's ratio of cartilage was regarded as 0.45 for articular cartilage, assuming that the tissue was nearly incompressible. The radius of the mechanical indenter was 1 mm. The stiffness and Young's modulus in standard mechanical indentation could thus be calculated accordingly.

The Young's modulus is a material property and is therefore one of the most important and wildly assessed properties in engineering design. The stiffness was defined in previous study by calculating the slope of pressure applied on the cartilage to the local strain induced in the loading phase. The calculation of the stiffness takes the pressure applied on the specimen surface, the initial cartilage thickness and the deformation of the cartilage layer during the indentation into account. The Young's modulus for

different cartilage samples was differentiated by the force applied on the specimen surface and the cartilage deformation.

3.4.2 Histological analysis

After the whole roughness and indentation tests, seven normal cartilage samples and seven samples from each enzyme digested group were selected for histological evaluation, following the protocol of a previous study (Wang, 2007).

The safranin O staining contra-stained with fast green and conventional light microscopy imaging were employed in the histological analysis. The specimens were first labeled and immersed in 10% formalin buffered to pH 7 for 8 hours at room temperature (24.5±1°C) for preservation. The 10% EDTA solution and ultrasound fast decalcificater (Guo *et al.*, 2005) were used to decalcify the bone tissue in specimens. The EDTA solution was renewed every 24 hours until the attached bone tissue could be easily cut by a scalpel. After the decalcification process was finished, the specimens were infiltrated in Hypercenter XP tissue processor (Leica ASP300, Leica Microsystems, Nussloch, Germany), and embedded into paraffin using Thermolyne Histo Center II (Shiraimatsu Co. Ltd., Osaka, Japan). Then paraffin sections were cut perpendicularly to the cartilage surface with the thickness of 4 μm using a rotary microtome (Leica RM-2135, Leica Microsystems, Nussloch, Germany).

The paraffin sections were stained by the following procedures: First immersed in xylene for approximately 15 minutes to clear the wax. Then, sections were taken into water through a descending series of ethanol (100%, 95% and 70%). After deparaffinization, the sections were stained with safranin O (SiGMA, CAT No. F7258, USA) and contra-stained with fast green (SiGMA, CAT NO). After that, the sections were taken into xylene through an increasing series of ethanol (70%, 95% and 100%).

After mounting with DPX (MLS Lab, the Hong Kong Polytechnic University) and covered by cover glass (FCGT20, Shanghai, China), the sections were observed using light microscope imaging system (model FN-S2N, Nikon, Japan) at a magnification of ×4. The proteoglycan content corresponded to the region stained by safranin O in the histological image (Leung *et al.*, 1999).

3.4.3 SEM analysis

An SEM analysis was performed to view the superficial structure of articular cartilage. After the whole roughness and indentation tests, two normal cartilage samples and two digested samples from each enzyme treatment group were selected for SEM evaluation.

The samples were first fixed in 10% formalin buffered to pH 7 for 8 hours at room temperature (24.5±1°C) and then dehydrated in an ascending series of ethanol solutions (70%, 95% and 100%). After dehydration the samples were anchored on sample holds, coated by sputtering with a gold layer and

then inserted in SEM system (Model JSM-6490, JEOL Ltd., Tokyo, Japan). SEM images of articular cartilage surface were then obtained at a magnification of ×100.

3.5 Summary

In this chapter, details of sample preparation, system setup and measurement procedures have been introduced in each test. Methods for parameter calculation and data analysis have also been explained. Results of the study are presented in the next chapter.

CHAPTER 4 RESULTS

In this chapter, the main findings in this study are presented, including the results of RI, roughness index, acoustic parameters, cartilage thickness and stiffness. Images obtained from histological analysis and SEM test are also showed.

4.1. RI measurement

In the reproducibility test, it was found that the RI measured at different sites for the same specimen had a mean CV of 1.90±0.44%, which demonstrated that the current test is highly repeatable (Fournier *et al.*, 2001; Romano, 2005).

The refractive indices calculated in this study are listed in Table 4.1 and shown in Fig 4.1. The RI of the top, middle and deep layers of the normal samples was 1.361±0.032, 1.338±0.036 and 1.371±0.041 (mean ± SD), while the values of the three layers for the trypsin and collagenase digested groups were 1.357±0.036, 1.331±0.030 and 1.392±0.037; and 1.361±0.032, 1.336±0.048 and 1.376±0.043, respectively. Repeated measures ANOVA showed that the differences in the RI at different depths for all the three groups were all significant ($p<0.05$). For all the specimens, the RI was statistically significantly lower for the middle layer, with that of the deep zone being the highest. However, statistical analysis revealed that there were no significant effects of trypsin and collagenase treatments on the RI for all the three layers of the specimens ($p>0.05$). The overall mean RI values

obtained by averaging the data of the three layers were 1.358± 0.022, 1.360±0.023 and 1.360±0.020 for normal, trypsin-digested, and collagenase treated articular cartilage samples, respectively.

Table 4.1. The mean refractive indices of articular cartilage in different regions before and after enzyme digestion. The means and SDs for each group were calculated from the results of samples in normal (n=36) or trypsin or collagenase digested group (n=18). The overall mean was calculated by averaging the data of the three regions for the specimens (n=36 for normal specimens, n=18 for trypsin or collagenase digested specimens). * Statistically significant difference ($p<0.05$, Two-factor Repeated measures ANOVA) compared to corresponding middle zone.

Regions	Normal cartilage (mean ± SD)	Trypsin digested cartilage (mean ± SD)	Collagenase digested cartilage (mean ± SD)	
Top	1.361±0.032	1.357±0.036	1.361±0.032	*
Middle	1.338±0.036	1.331±0.030	1.336±0.048	*
Deep	1.371±0.041	1.392±0.037	1.376±0.043	
Overall Mean	1.358±0.022	1.360±0.023	1.360±0.020	

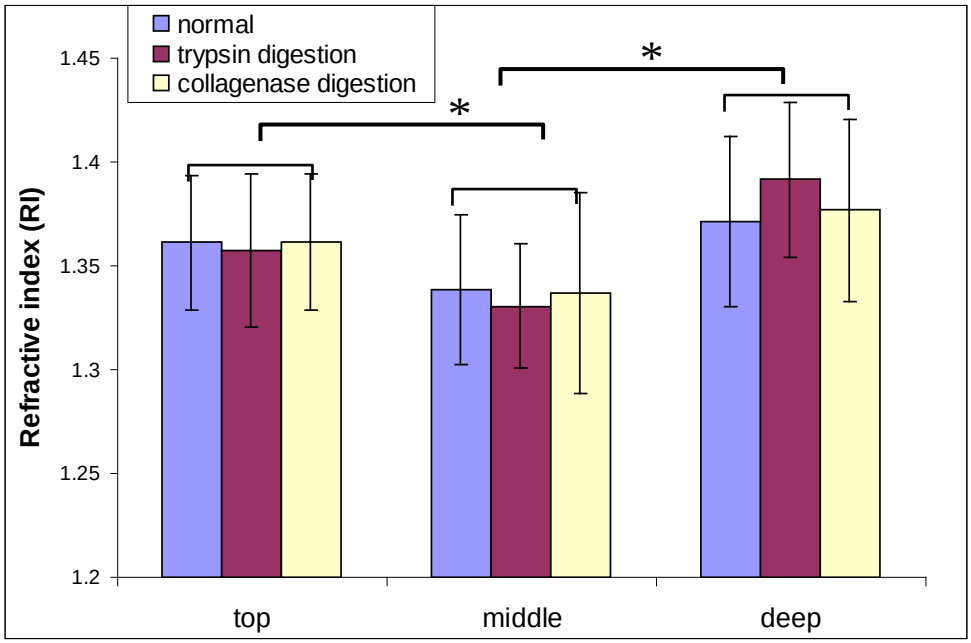

Fig 4.1. Depth dependent RI of articular cartilage before and after digestion. The error bars represent the SD values for the specimens (n=36 for normal group, n=18 for trypsin or collagenase digested group). * Statistically significant difference ($p<0.05$, Two-factor Repeated measures ANOVA) compared to corresponding middle zone.

4.2 Roughness measurement

4.2.1 Reproducibility test

In the reproducibility test for ORI and URI, it was found that the roughness indices measured at three different times for the six specimens had a CV value of 11.1% and 18.1%, respectively, indicating that the tests for ORI and URI measurement is repeatable (Saarakkala *et al.*, 2004b).

4.2.2 Glass and emery paper measurement

The ORI result of glass surface was 0.68±0.07 μm. And the URI result of glass surface was 0.55 ±0.08 μm.

Nine FEPA standard emery papers with different particle sizes were employed for ORI and URI measurement. The results of emery paper roughness index are listed in Table 4.2 and demonstrated in Fig 4.2.

The results showed that the roughness index decreased as the particle size of the emery paper decreased for both measurements. The relationships between the roughness index and grit size was also examined for both ORI and URI measurements (Fig 4.3 (a)). Pearson's analysis suggested the relationships were linear for both measurements ($p<0.05$) with $R^2=0.95$ for both correlations between ORI and grit size and between URI and grit size. Furthermore, the relationship between URI and ORI results for emery paper measurement was also analyzed. A linear relationship ($p<0.05$) with $R^2=0.89$ was also found (Fig 4.3 (b)). The results showed that the measurements of ORI and URI agreed very well.

Table 4.2. The mean roughness indices of different emery papers measured by OCT and ultrasound. The means and SDs for each paper were calculated from the results of the 12 measurements on one sample.

Emery paper	Particle size (μm)	ORI (μm) (mean ± SD)	URI (μm) (mean ± SD)
P60	269	73.7±13.2	74.9±31.1
P120	125	43.6±9.5	30.3±11.9
P180	82	39.2±12.9	26.6±8.9
P280	52.2	20.1±5.3	25.6±10.8
P320	46.2	19.1±5.8	24.9±15.0
P1000	18.3	9.1±5.2	16.6±4.9
P1200	15.3	6.7±1.9	11.7±3.8
P1500	12.6	5.0±1.6	7.1±1.2
P2000	10.3	5.0±1.2	6.7±1.1

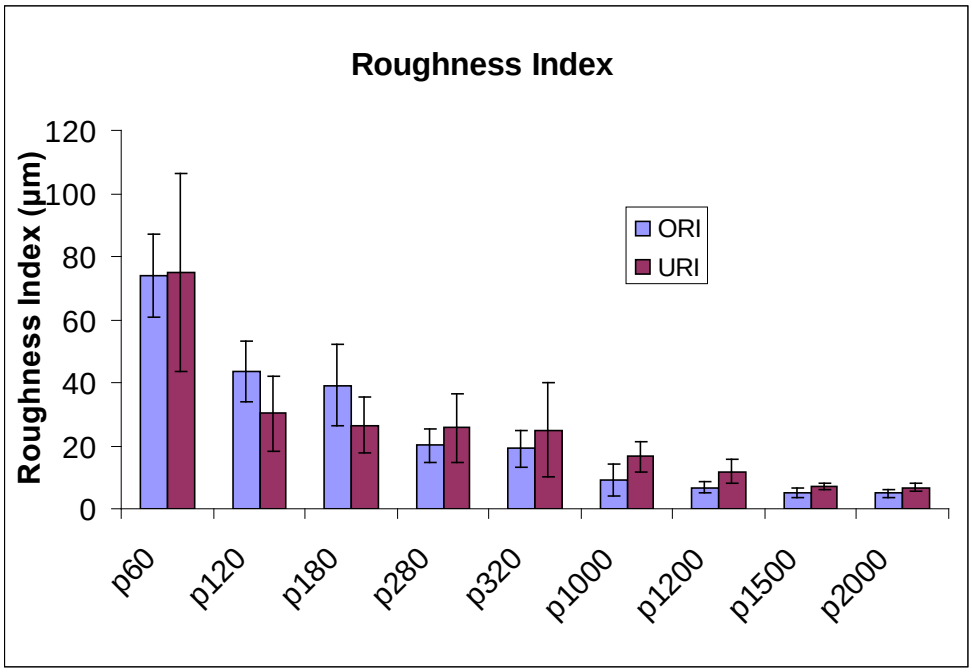

Fig 4.2. The mean roughness indices of different emery papers measured by OCT and ultrasound. The error bars represent the SD values of 12 measurements on each sample.

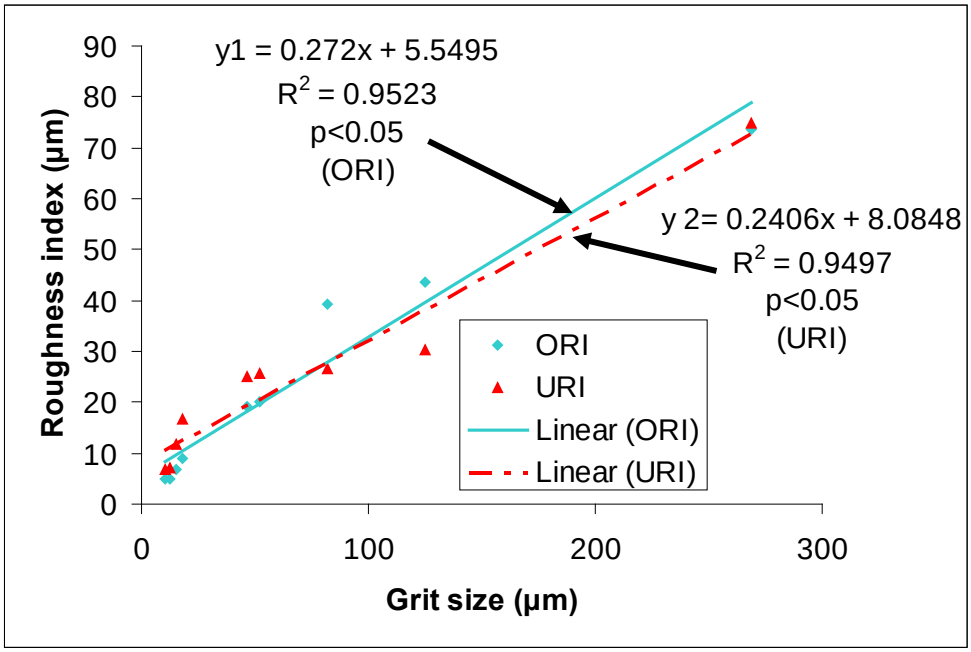

(a)

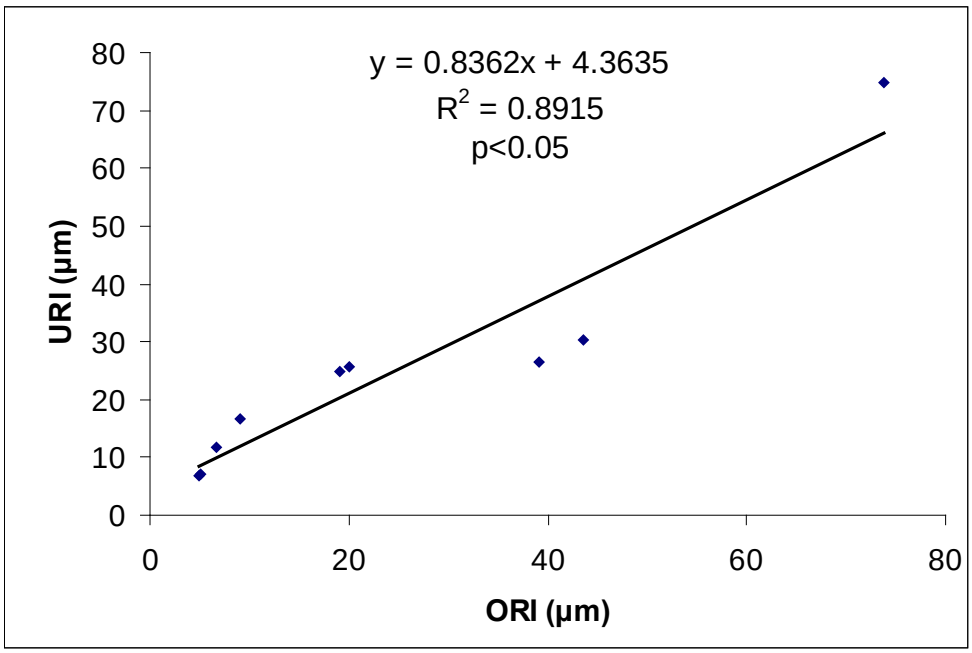

(b)

Fig 4.3. Correlations between (a) roughness index and grit size of emery paper; and (b) URI and ORI results of different emery paper. Linear relationships were found ($p<0.05$, Pearson's analysis).

4.2.3 Articular cartilage measurement

The Articular cartilage surface was examined by both OCT and ultrasound before and after enzyme treatment. The overall mean ORI and URI results for normal specimens were 8.8±1.4 μm (mean±SD), and 6.0±1.5 μm, respectively. The mean and SD of ORI and URI results of each group are listed in Table 4.3 and shown in Fig 4.4 and Fig 4.5. Significant differences of roughness index were found in collagenase digestion group using both OCT and ultrasound ($p<0.05$). The ORI increased by 368% after collagenase digestion, while the URI increased by 602%. There was no significant difference in trypsin group before and after treatment measured by either OCT or ultrasound ($p>0.05$).

Table 4.3. Mean ± SD values of ORI and URI before and after enzyme degradation. * Statistically significant difference ($p<0.05$, Paired-samples t test) before and after treatment.

		ORI (μm) (mean± SD)	URI (μm) (mean ± SD)
Collagenase (n=20)	before	8.5±1.4 ┐*	6.0±1.4 ┐*
	after	39.8±30.9 ┘	42.1±35.6 ┘
Trypsin (n=20)	before	9.2±1.4	5.9±1.7
	after	8.3±2.3	5.4±1.7

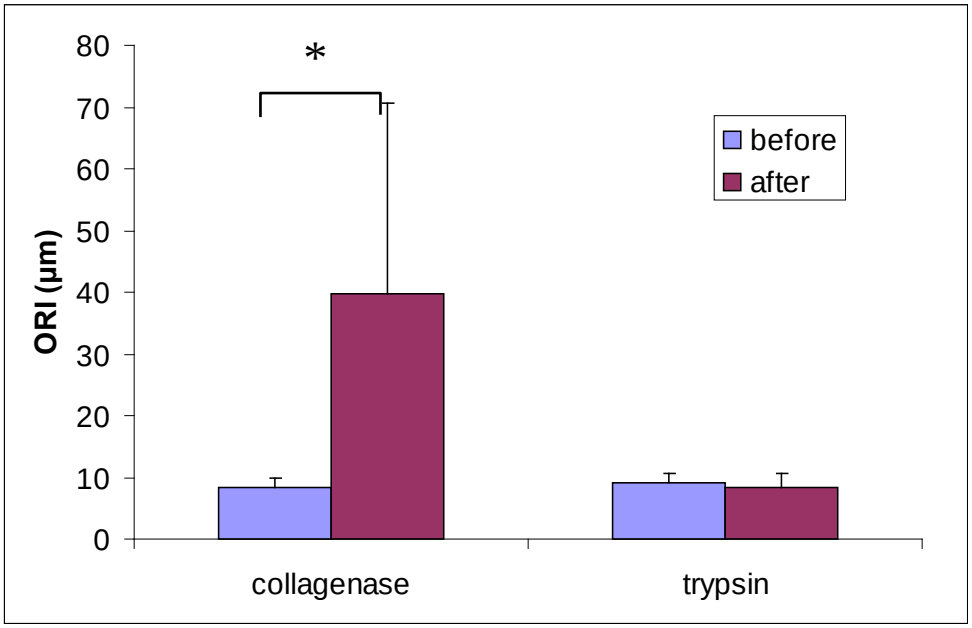

Fig 4.4. ORI results of collagenase digestion and trypsin digestion groups before and after treatment. The error bars represent the SD values for specimens in the same group (n=20). * Statistically significant difference ($p<0.05$, Paired-samples t test) before and after treatment.

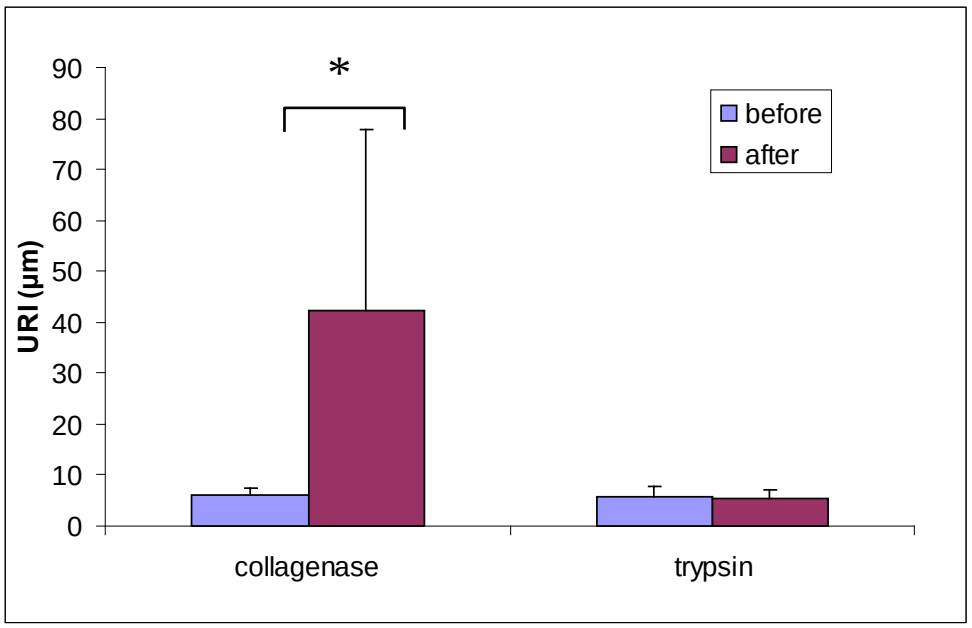

Fig 4.5. URI results of collagenase digestion and trypsin digestion groups before and after treatment. The error bars represent the SD values for specimens in the same group (n=20). * Statistically significant difference ($p<0.05$, Paired-samples t test) before and after treatment.

The relationship between the URI and ORI results of articular cartilage was also investigated (Fig 4.6). Pearson' analysis suggested a linear correlation between the results of URI and ORI measurements on articular cartilage (R^2 =0.74, p<0.05), indicating that these two measurements were comparable.

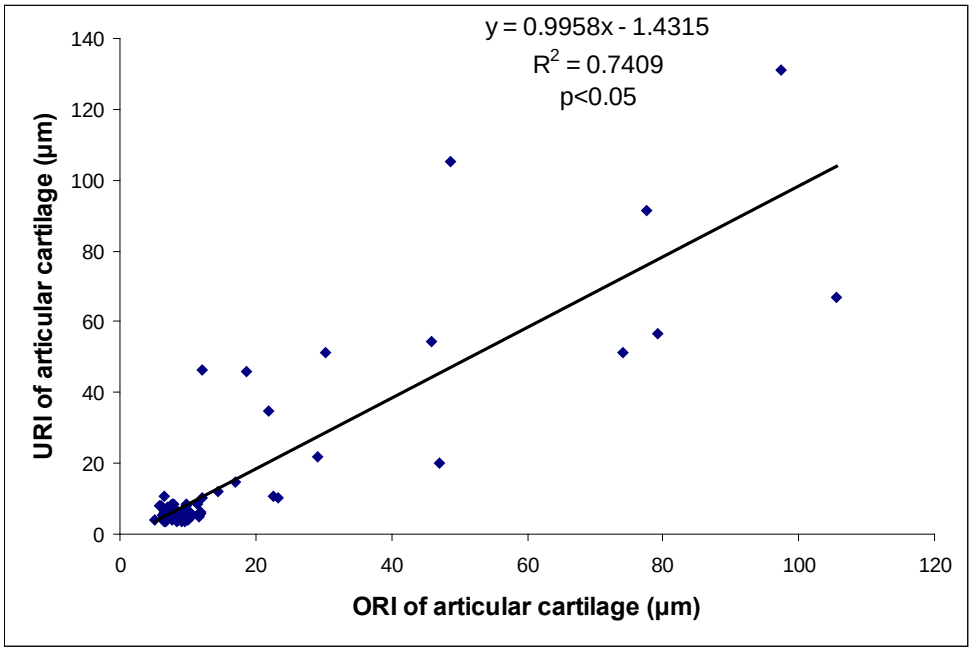

Fig 4.6. Correlations between URI and ORI results of all articular cartilage specimens (n=20×2, both before and after treatments). A linear correlation was noted (p<0.05, Pearson's analysis).

4.3 Measurement of acoustic parameters

As mentioned before, IA and IBS were used to evaluate the attenuation and backscatter coefficient of signals collected under the large amplification gain, while IRC and AIB were used to assess the reflection and backscatter coefficient of signals collected under the small amplification gain. The reproducibility tests measured in six specimens showed the CV value was

20.6% and 2.7% for IA and IBS, and 15.9% and 3.6% for IRC and AIB, respectively. The reproducibility results indicated that the acoustic parameters measurement tests are repeatable (Saarakkala *et al.*, 2004a; Toyras *et al.*, 1999). The results for those acoustic parameters measurements are listed in Tables 4.4 and 4.5 and demonstrated in Figs 4.7 and 4.8.

The IA increased 1.8 dB/mm after trypsin digestion, but decreased 0.1 dB/mm after collagenase digestion. The difference before and after treatment was not significant ($p>0.05$). IBS values increased approximately 2 dB after treatment in both groups. Those increases were found to be significant ($p<0.05$) (Table 4.4, Fig 4.7).

Table 4.4. IA and IBS results from signals of articular cartilage specimens collected under the large amplification gain. * Statistically significant difference ($p<0.05$, Paired-samples t test) before and after treatment.

		IA (dB/mm) (mean±SD)	IBS (dB) (mean ± SD)	
Collagenase (n=20)	before	6.4±4.1	-53.1±2.7	*
	after	6.3±4.8	-50.1±3.2	
Trypsin (n=20)	before	7.9±3.6	-52.7±2.0	*
	after	9.7±4.9	-51.2±2.4	

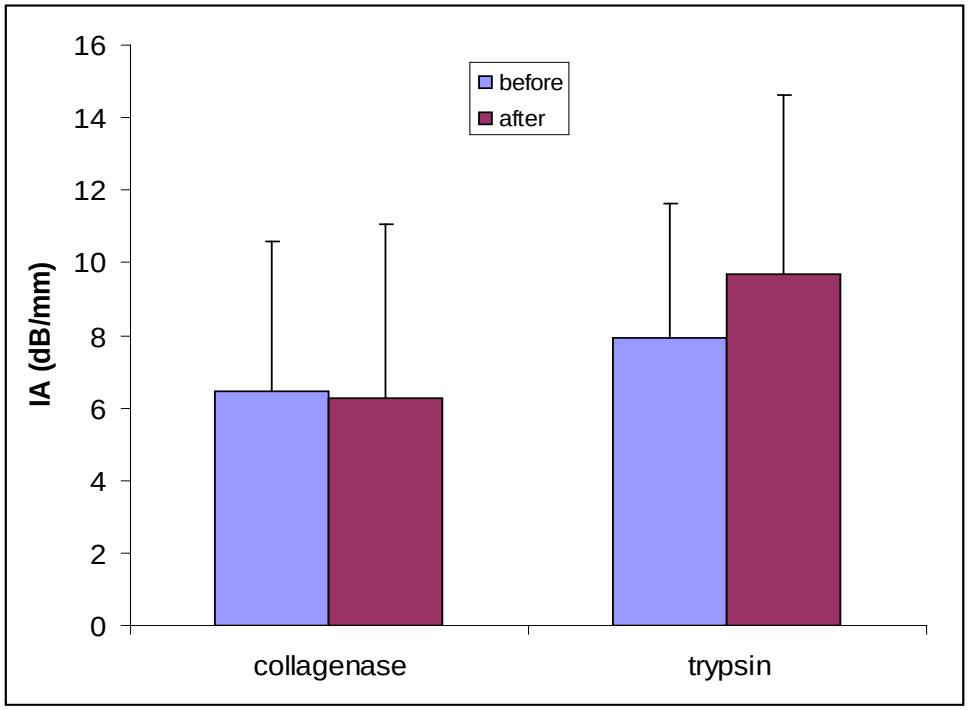

(a)

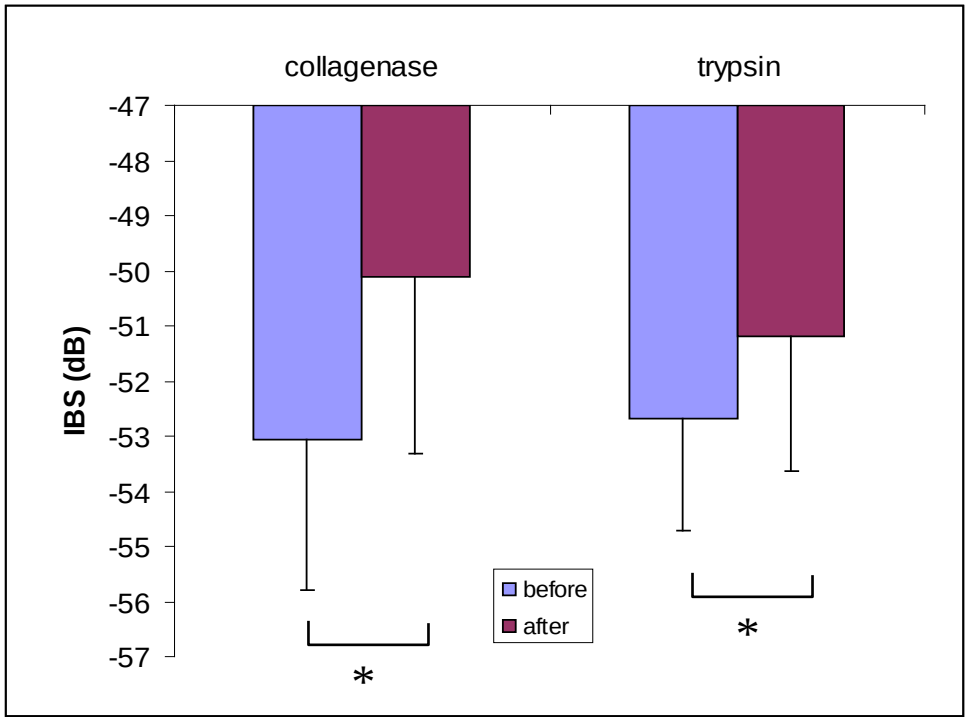

(b)

Fig 4.7. Results of (a) IA and (b) IBS from signals of articular cartilage specimens collected under the large amplification gain. The error bars represent the SD values for specimens in the same group (n=20). * Indicates statistically significant difference ($p<0.05$, Paired-samples t test) before and after treatment.

The IRC increased insignificantly (3 dB, $p>0.05$) after trypsin digestion, but decreased significantly (8.3 dB, $p<0.05$) after the collagenase digestion. The AIB decreased but not significantly ($p>0.05$) after the collagenase treatment, while decreased significantly (2.4 dB, $p<0.05$) in the trypsin digestion group (Table 4.5, Fig 4.8).

Table 4.5. IRC and AIB results extracted from the signals of articular cartilage specimens collected under the small amplification gain. * Statistically significant difference ($p<0.05$, Paired-samples t test) before and after treatment.

		IRC(dB) (mean± SD)	AIB (dB) (mean ± SD)
Collagenase (n=20)	before	-17.7±4.3 *	-44.6±4.6
	after	-26.0±6.8 *	-49.4±14.0
Trypsin (n=20)	before	-17.6±4.6	-42.2±5.9 *
	after	-14.6±3.8	-44.6±5.0 *

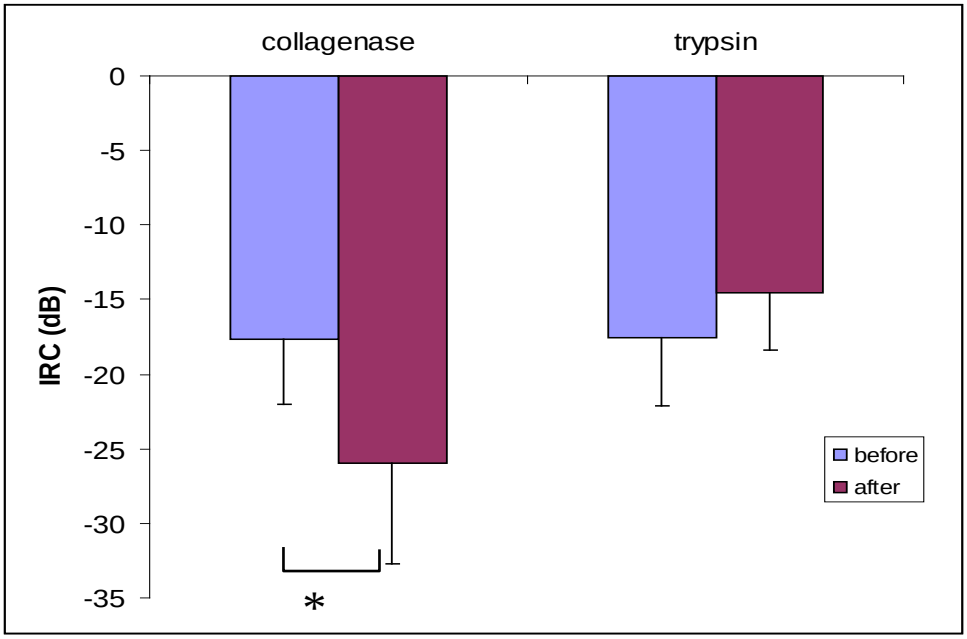

(a)

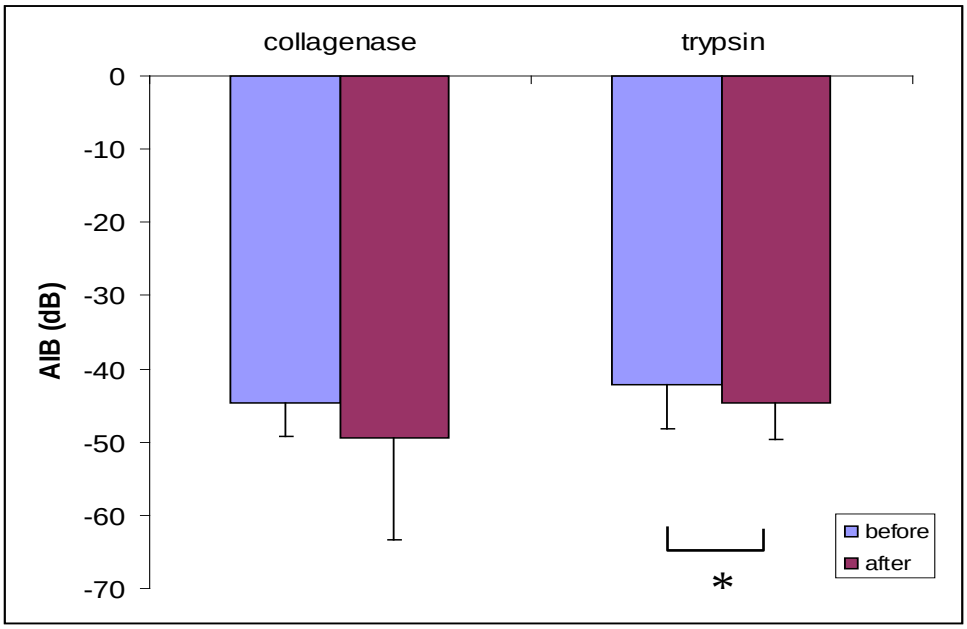

(b)

Fig 4.8. Results of (a) IRC and (b) AIB from signals of articular cartilage specimens collected under the small amplification gain. The error bars represent the SD values for specimens in the same group (n=20). * Indicates statistically significant difference ($p<0.05$, Paired-samples t test) before and after treatment.

Since IRC can represent the surface condition of cartilage (Nieminen *et al.*, 2002; Toyras *et al.*, 1999; 2002), the relationship between IRC and URI was

also investigated in this study (Fig 4.9). A linear relationship was found (R^2 =0.49, p<0.05, Pearson's analysis)(Fig 4.9 (a)). Logarithmic relationship was also used to estimate the curve in order to find better fitted relationship model. Curve estimation showed significant logarithmic relationship between IRC and URI result (R^2 =0.71, p<0.05, Curve estimation)(Fig 4.9 (a)). The results suggested that when URI increased, the IRC value decreased. Since for normal and trypsin digested samples, the URI value was relatively small, an enlarged figure for data points with URI value smaller than 15 μm was also plotted (Fig 4.9 (b)). Significant linear relationship was also found among those data points (R^2 =0.56, p<0.05, Pearson' analysis).

4.4. Thickness measurement

The cartilage thickness was measured using 55 MHz Vevo system before and after treatment. The reproducibility measured in six specimens showed a CV of 3.7% for thickness measurement, demonstrating the test had a good repeatability (Romano, 2005). The overall mean thickness of normal cartilage samples was 1.77±0.27 mm. The results of cartilage thickness of both groups are listed in Table 4.6 and shown in Fig 4.10. The cartilage thickness decreased significantly by 9.8% from 1.83±0.23 mm to 1.65± 0.27 mm (p<0.05) after collagenase digestion. However, no significant change was observed in trypsin digestion group (p>0.05).

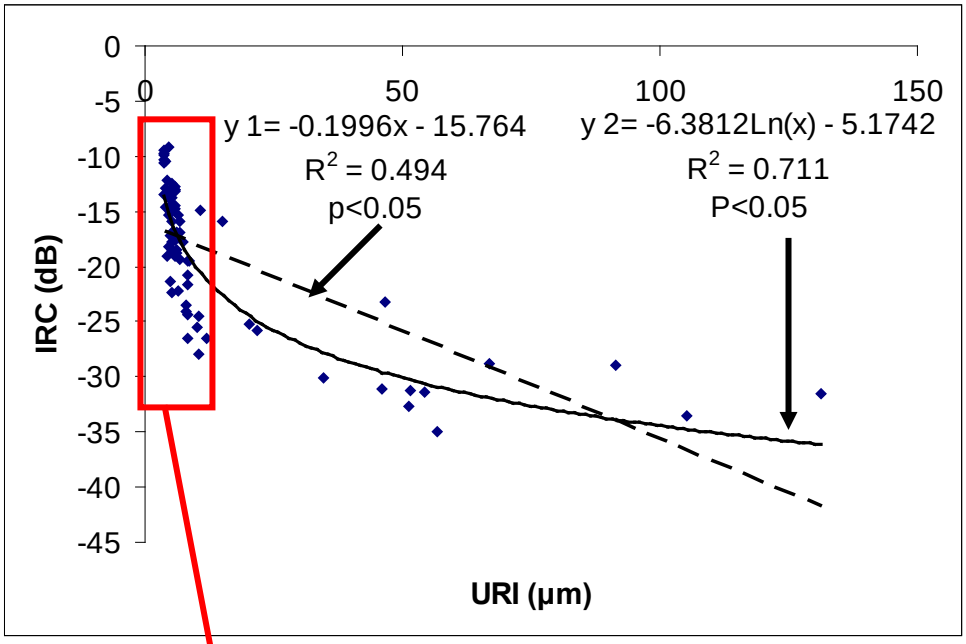

(a)

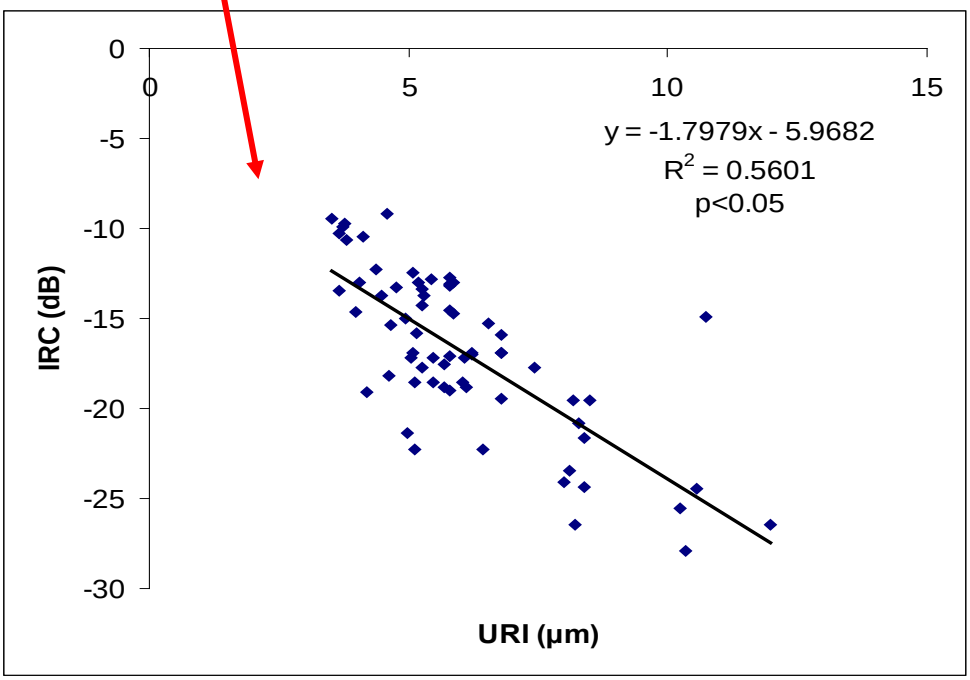

(b)

Fig 4.9. Correlations between IRC and URI in samples before and after enzyme treatments. (a) Relationship between all the samples. Dashed line represents linear estimation, while solid line represents logarithmic estimation. (b) Relationship in the region of the data points with URI value smaller than 15 µm. Linear correlations were found in both (a) and (b) ($p<0.05$, Pearson's analysis), and logarithmic relationship was found in (a) ($p<0.05$, Curve estimation).

Table 4.6. Cartilage thickness measured before and after the enzyme treatments using Vevo system. * Statistically significant difference ($p<0.05$, Paired-samples t test) before and after treatment.

Unit (mm)	Thickness before (mean± SD)	Thickness after (mean± SD)
Collagenase digest (n=20)	1.83±0.23	1.65±0.27*
Trypsin digest (n=20)	1.71±0.29	1.75±0.32

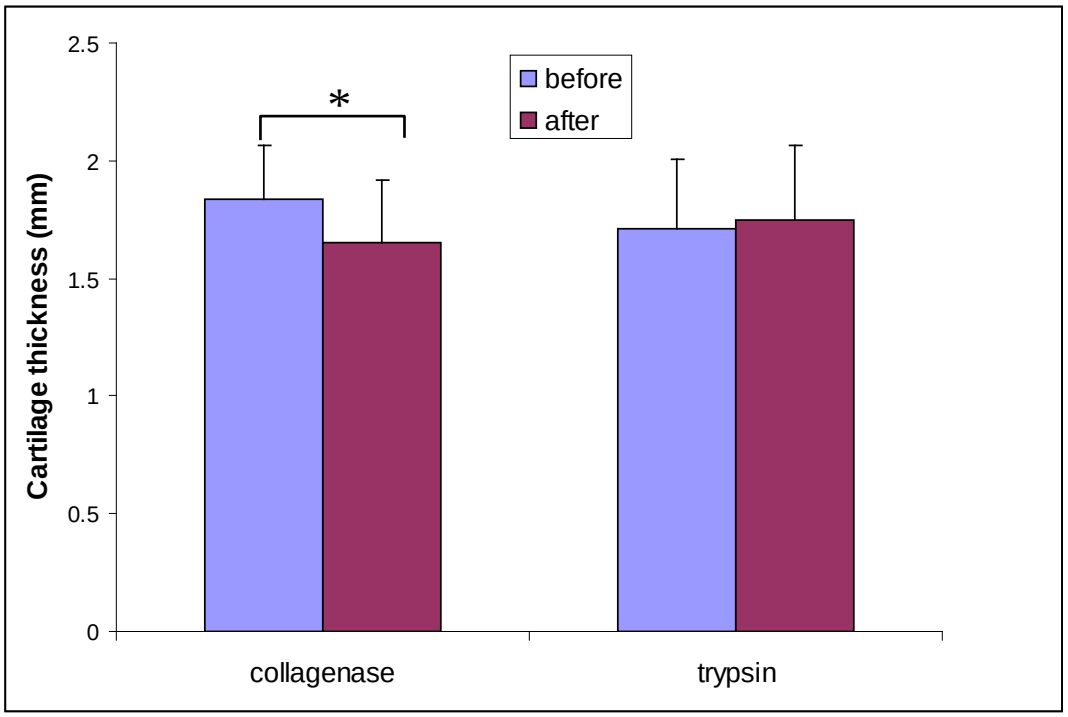

Fig 4.10. Cartilage thickness results of collagenase digestion (n=20) and trypsin digestion (n=20) groups before and after the enzyme treatments. The error bars represent the SD values for different specimens in each sample group. * Statistically significant difference ($p<0.05$, Paired-samples t test) before and after treatment.

4.5 Indentation tests

4.5.1 OCT air jet indentation test

Calibration of the air jet indentation was carried out using an electronic scale (Fig 4.11). The calibration measurements indicated highly linear relationship between the overall force applied on the sample surface measured by the electronic scale and the pressure within the pipe measured by the pressure sensor in the proportioning valve (R^2 >0.99). Since the pressure applied on the specimen surface was calculated from the overall force applied on the specimen divided by the cross-section area of the air jet, this linear relationship indicated that the pressure measured within the pipe could be used to represent the pressure applied on the specimen surface.

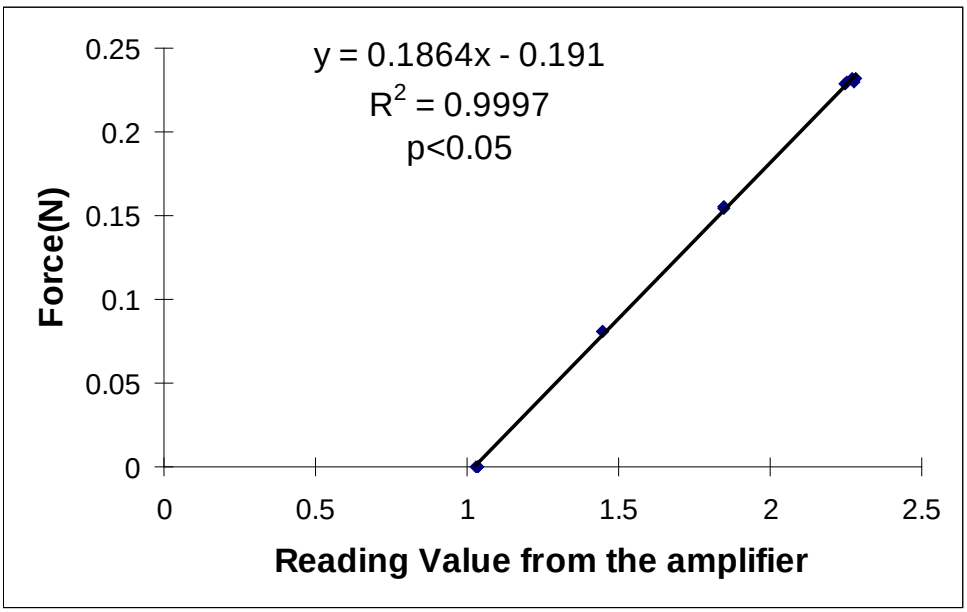

Fig 4.11. Calibration test revealing the relationship between the overall force applied on the sample and the air pressure measured within the pipe. Highly linear relationship was obtained (R^2 >0.99, p<0.05, Pearson's analysis).

A typical curve of the loading phase obtained from one normal cartilage sample is shown in Fig 4.12 (a). It was noted that the strain curve followed the pressure curve well. Fig 4.12 (b) shows that the data were fitted well with the linear regression (R^2=0.98). The reproducibility tests measured in six specimens showed a CV of 25.7%, indicating moderate reproducibility (Bae *et al.*, 2003).

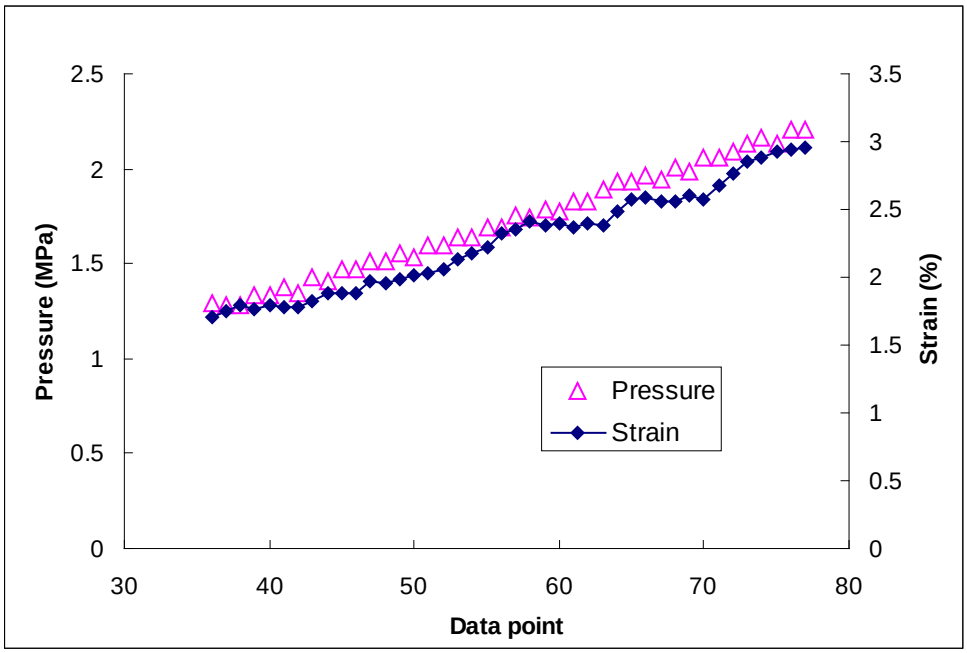

(a)

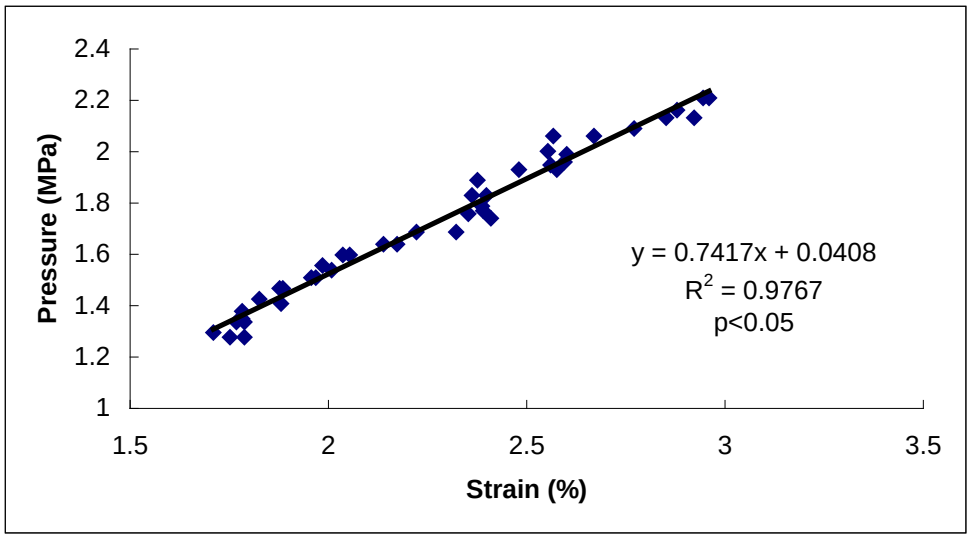

(b)

Fig 4.12. (a) A typical curve of the loading phase obtained from one cartilage sample using the OCT air jet indentation system. (b) The relationship between the pressure and strain which was fitted by a linear regression model (R^2 =0.98, p<0.05, Pearson' analysis).

The stiffness of articular cartilage specimens before and after treatment was listed in Table 4.7 and shown in Fig 4.13. Significant differences were found in both collagenase and trypsin groups before and after treatment (p<0.05). The stiffness for articular cartilage dropped by 85% and 68% after collagenase and trypsin treatments, respectively.

Table 4.7. Stiffness measured before and after treatment using OCT air jet. * Statistically significant difference (p<0.05, Paired-samples t test) before and after treatment.

Unit (MPa)	Stiffness before (mean± SD)	Stiffness after (mean± SD)
Collagenase digestion (n=20)	0.71±0.28	0.11±0.07*
Trypsin digestion (n=20)	0.73±0.28	0.23±0.13*

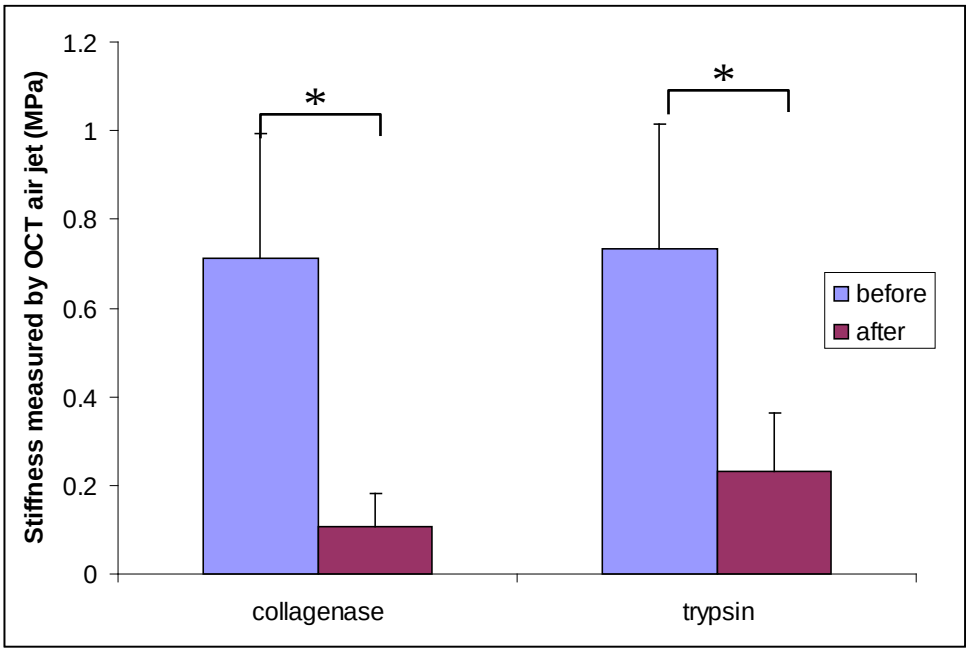

Fig 4.13. Stiffness measured before and after treatment using OCT air jet in both collagenase digestion and trypsin digestion groups. * Statistically significant difference ($p<0.05$, Paired-samples t test) before and after the enzyme treatment.

4.5.2 Ultrasound water jet indentation test

The calibration measurements indicated highly linear relationship for both load cell and pressure transducer (R^2>0.99 for applied force and load cell reading, Fig 4.14 (a); R^2=0.98 for load cell and pressure sensor reading, Fig 4.14(b)). These relationships suggested that the pressure applied on the specimen surface could be calculated using the pressure within the water pipe.

A typical curve of the loading phase obtained from one normal cartilage sample using water jet is shown in Fig 4.15 (a). Fig 4.15 (b) shows that the correlation between the force and strain was highly linear (R^2=0.99). The reproducibility measured in six specimens showed a CV of 22.4%, indicating moderate reproducibility (Bae *et al.*, 2003).

The stiffness measured by water jet before and after treatment is shown in Table 4.8 and Fig 4.16. Similar to the OCT air jet indentation test result, significant differences were found in both collagenase digestion and trypsin digestion groups before and after treatment ($p<0.05$). The stiffness dropped by 87% and 75% after collagenase and trypsin digestion, respectively.

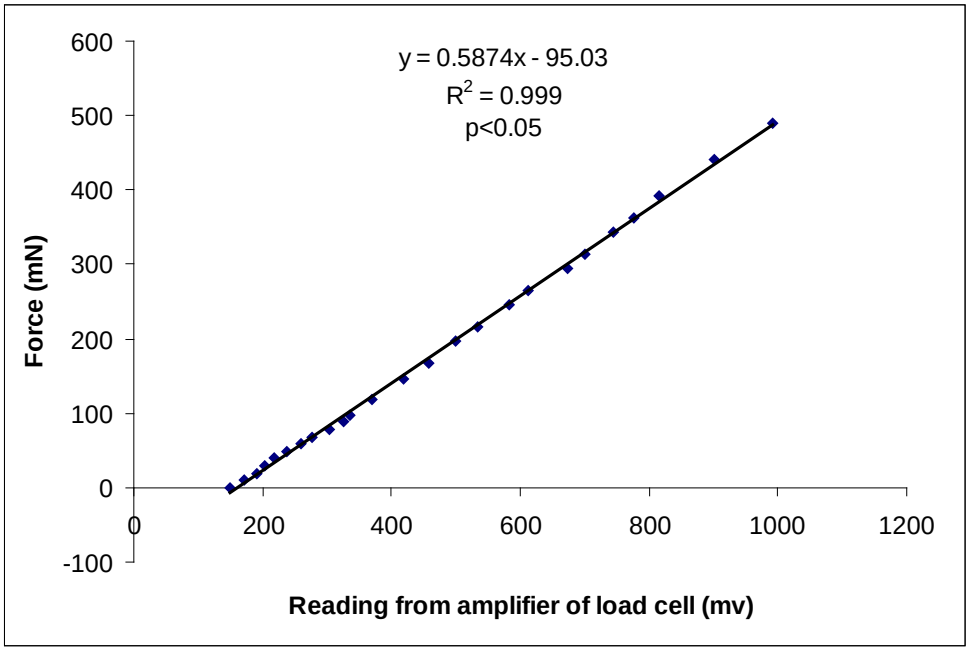

(a)

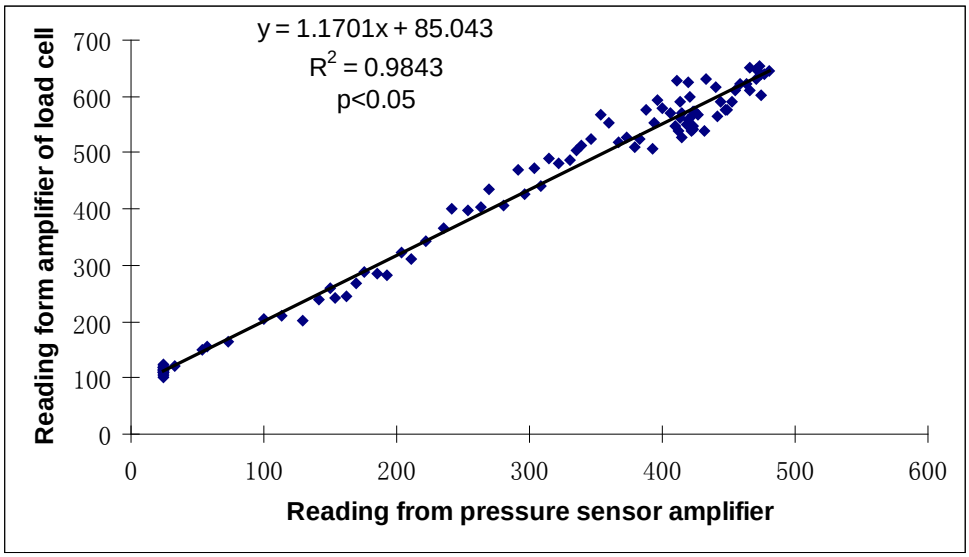

(b)

Fig 4.14. Calibration tests showed that there were linear correlations (a) between applied force and load cell reading, and (b) between load cell reading and pressure sensor output (R^2 =0.98 for both relationships, p<0.05, Pearson's analysis).

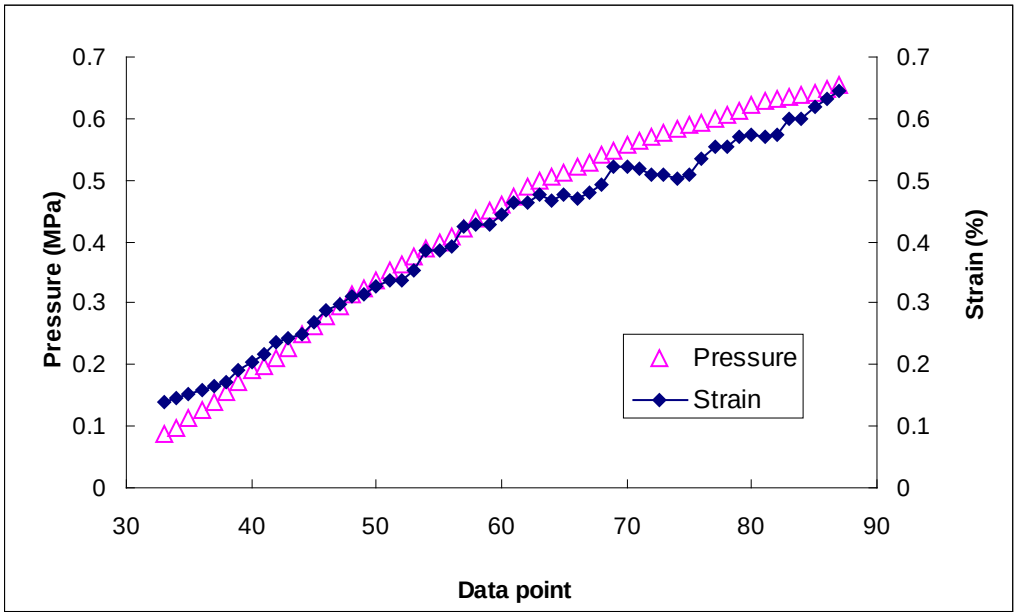

(a)

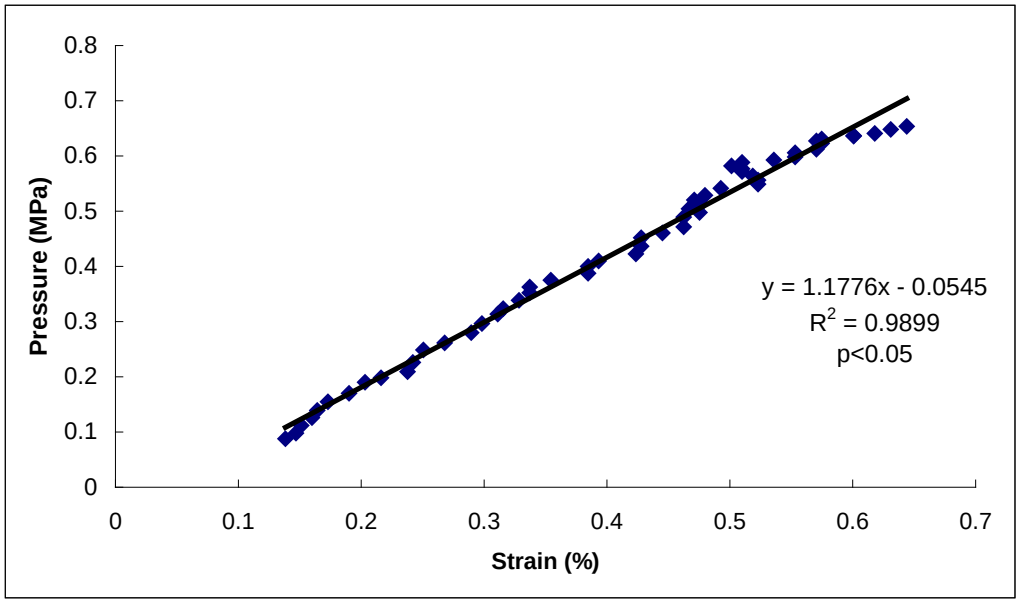

(b)

Fig 4.15. (a) A typical curve of the loading phase obtained from one cartilage sample using ultrasound water jet indentation system. (b) The relationship between the pressure and strain which was fitted by a linear regression model (R^2 =0.99, p<0.05, Pearson's analysis).

Table 4.8. Stiffness measured before and after the enzyme treatment using water jet. * Statistically significant difference ($p<0.05$, Paired-samples t test) before and after treatment.

Unit (MPa)	Stiffness before (mean± SD)	Stiffness after (mean± SD)
Collagenase digestion (n=20)	1.58±0.96	0.20±0.20*
Trypsin digestion (n=20)	1.27±0.71	0.32±0.20*

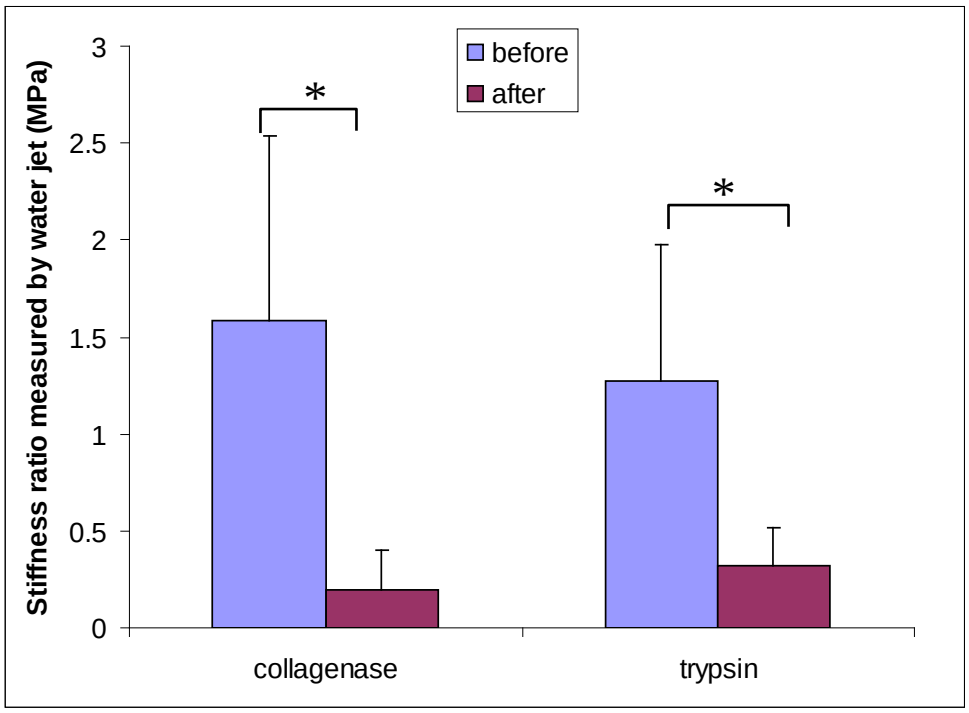

Fig 4.16. Stiffness measured before and after treatment using ultrasound water jet in both collagenase digestion and trypsin digestion groups. * Statistically significant difference ($p<0.05$, Paired-samples t test) before and after treatment.

4.5.3 Mechanical indentation test

Standard mechanical indentation was also applied to assess the stiffness of articular cartilage as a reference method. A typical curve of the loading phase obtained from one normal cartilage sample using mechanical

indentation is shown in Fig 4.17 (a). Fig 4.17 (b) shows that the relationship between the force and strain was highly linear (R^2 =0.99).

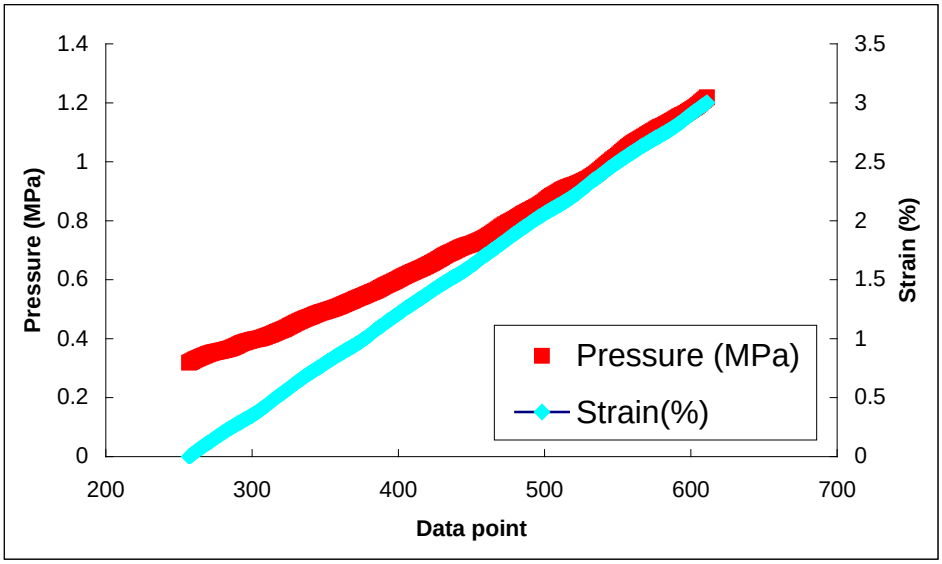

(a)

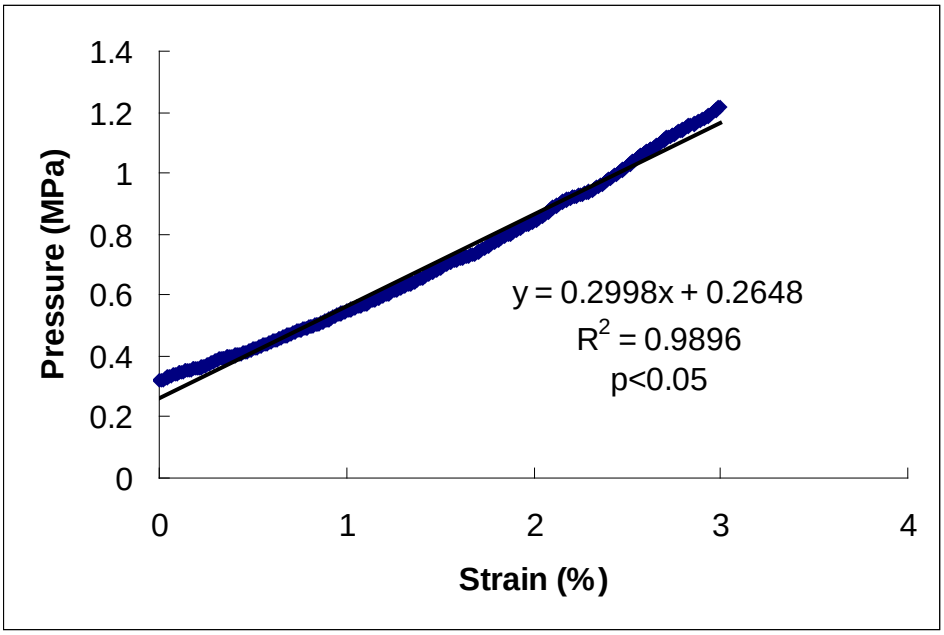

(b)

Fig 4.17. (a) A typical curve of the loading phase obtained from one cartilage sample using standard mechanical indentation system. (b) The relationship between the force and strain fitted by a linear regression model (R^2 =0.99, p<0.05, Pearson's analysis).

The stiffness values measured by standard mechanical test before and after the enzyme treatments were shown in Table 4.9 and Fig 4.18. Significant differences were found in both groups before and after treatment ($p<0.05$). For collagenase digestion and trypsin digestion groups, the stiffness dropped by 88% and 74%, respectively. The Young's modulus E before and after treatment was also obtained using standard mechanical indentation test (Table 4.10, Fig 4.19). The mean E value for samples before treatment was 1.58 ± 1.34. It also decreased significantly after the enzyme digestions.

Table 4.9. Stiffness measured before and after treatment using mechanical indentation. * Statistically significant difference ($p<0.05$, Paired-samples t test) before and after treatment.

Unit (MPa)	Stiffness before (mean± SD)	Stiffness after (mean± SD)
Collagenase digestion (n=20)	0.66±0.56	0.08±0.09*
Trypsin digestion (n=20)	0.50±0.32	0.13±0.08*

Table 4.10. Young's modulus E measured before and after treatment using mechanical indentation. * Statistically significant difference ($p<0.05$, Paired-samples t test) before and after treatment.

Unit (MPa)	E before (mean± SD)	E after (mean± SD)
Collagenase digestion (n=20)	1.89±1.74	0.24±0.30*
Trypsin digestion (n=20)	1.48±0.91	0.43±0.35*

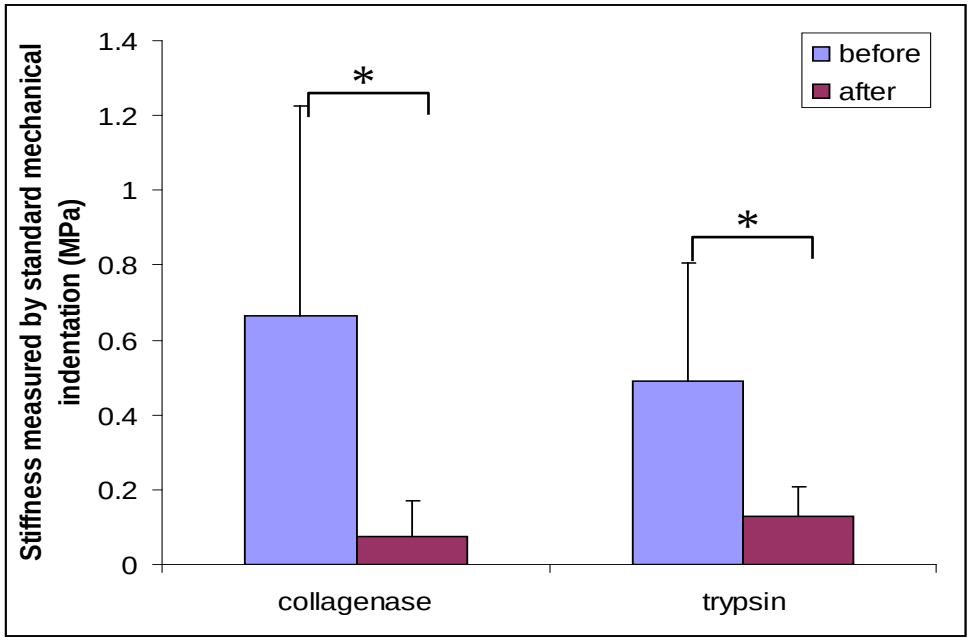

Fig 4.18. Stiffness measured before and after treatment using standard mechanical indentation in collagenase digestion and trypsin digestion groups. * Statistically significant difference ($p<0.05$, Paired-samples t test) before and after treatment.

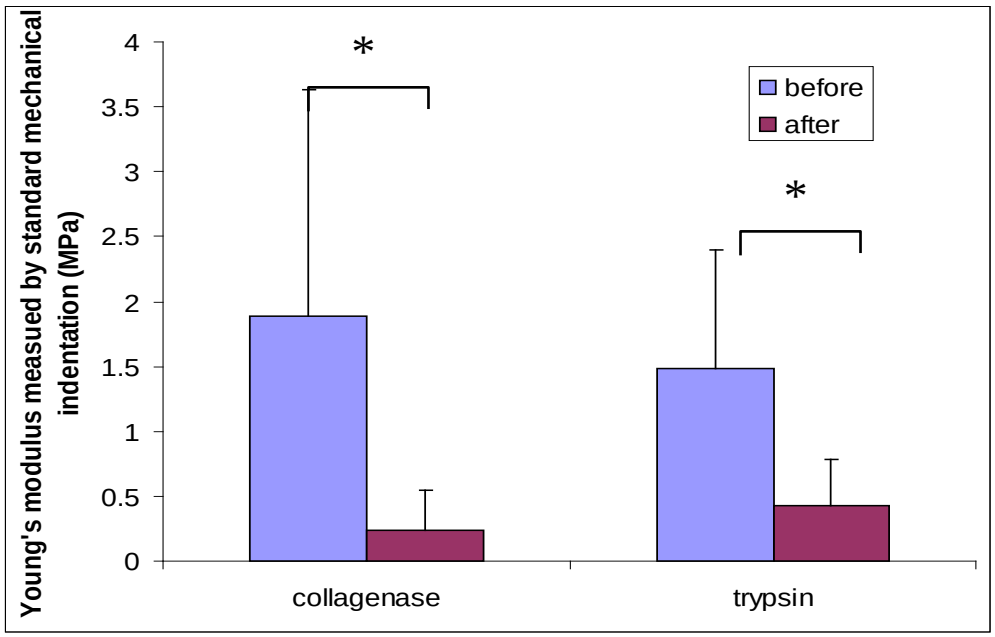

Fig 4.19. Young's modulus measured before and after treatment using standard mechanical indentation in collagenase digestion and trypsin digestion groups. * Statistically significant difference ($p<0.05$, Paired-samples t test) before and after treatment.

Since standard mechanical indentation test was employed as a reference method, the relationships between stiffness measured by air jet indentation as well as water jet indentation and stiffness (Fig 4.20) and Young's modulus measured by the mechanical indentation were explored (Fig 4.21). Pearson's analysis indicated linear relationship between the stiffness measured by the air jet and mechanical indentation as well as between the water jet and mechanical indentation ($p<0.05$, $R^2=0.69$ for correlation between air jet and mechanical indentation, and $R^2=0.71$ for that between water jet and mechanical indentation). Linear relationships were also demonstrated between the stiffness measured by air jet and water jet and the Young's modulus measured by mechanical indentation ($p<0.05$, $R^2=0.65$ for the correlation between stiffness from air jet indentation and Young's modulus from mechanical indentation, and $R^2=0.66$ for that between stiffness from water jet indentation and Young's modulus from mechanical indentation). The results showed that the air jet and water jet method were comparable to mechanical indentation test, thus indicating that the air jet and water jet indentation systems can be used as a new approach to measure the mechanical properties of articular cartilage.

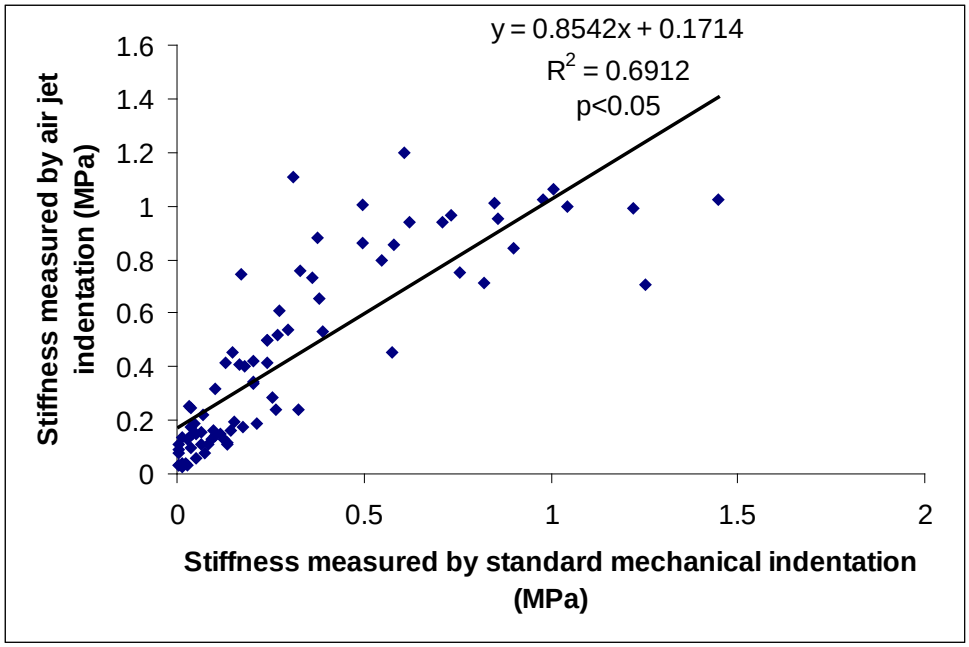

(a)

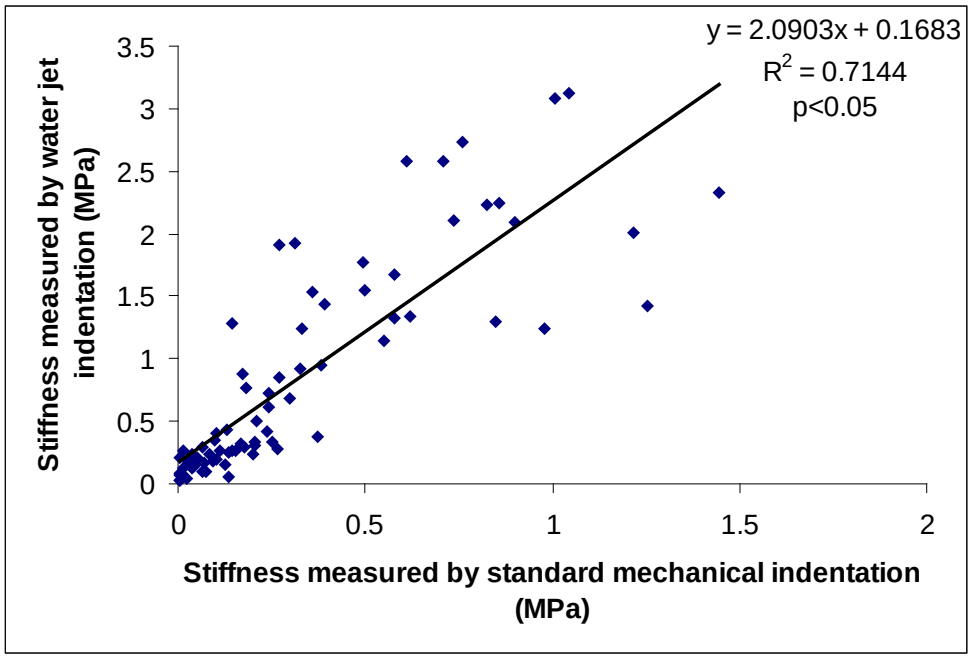

(b)

Fig 4.20. Correlations between stiffness measured by (a) OCT air jet indentation, (b) ultrasound water jet indentation system and that by standard mechanical indentation. Linear relationships were found in both comparisons ($p<0.05$, Pearson's analysis).

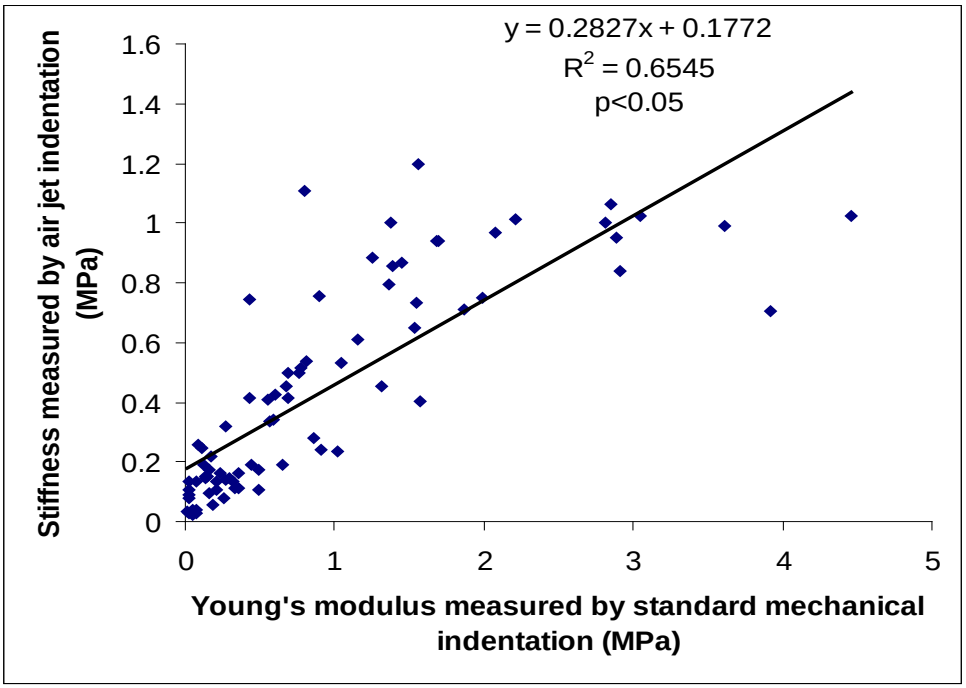

(a)

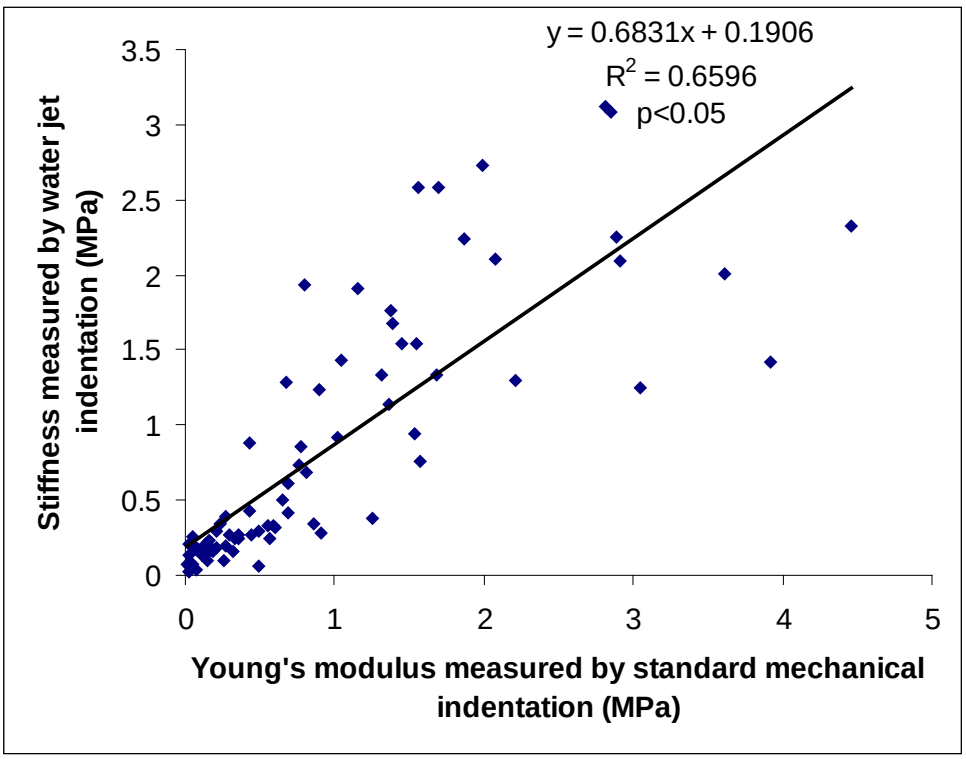

(b)

Fig 4.21. Correlations between stiffness measured by (a) OCT air jet indentation, (b) ultrasound water jet indentation system and Young's modulus measured by standard mechanical indentation. Linear relationships were found in both comparisons ($p<0.05$, Pearson's analysis).

4.6 Comparison between roughness and stiffness properties

Since the same set of articular cartilage samples were used in roughness measurements and indentation tests, the relationship between the stiffness and roughness index was investigated using both linear regression and curve fitting for both the collagenase digestion and trypsin digestion groups. The results revealed that the relationship between the stiffness, measured either by OCT air jet or ultrasound water jet indentation, and the surface roughness, indicated either by ORI or URI, was highly nonlinear for the collagenase treatment group. The relationship between stiffness and roughness index in collagenase group was shown in Fig 4.22. The result suggested that the larger roughness index the cartilage had, the smaller the stiffness of cartilage might be. To further investigate the relationships, curve fitting function provided by SPSS was applied. The results of inverse and power estimations of the relationships were plotted in Fig 4.23. The relationship between the stiffness and the surface roughness of the trypsin treatment group was more irregular and no correlation was demonstrated.

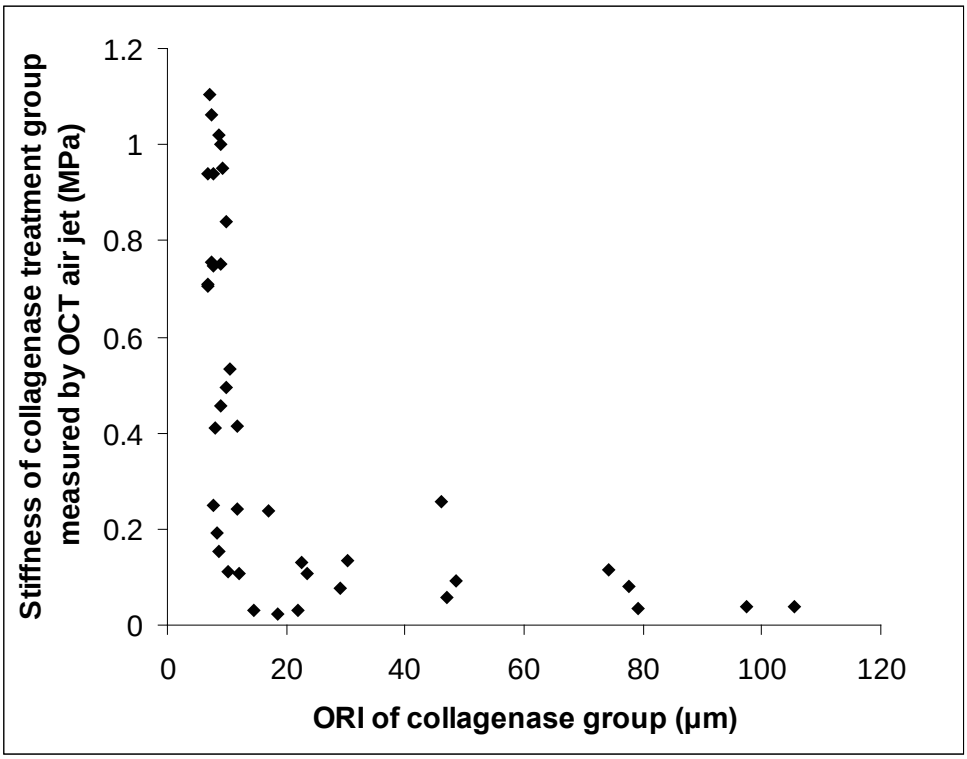

(a)

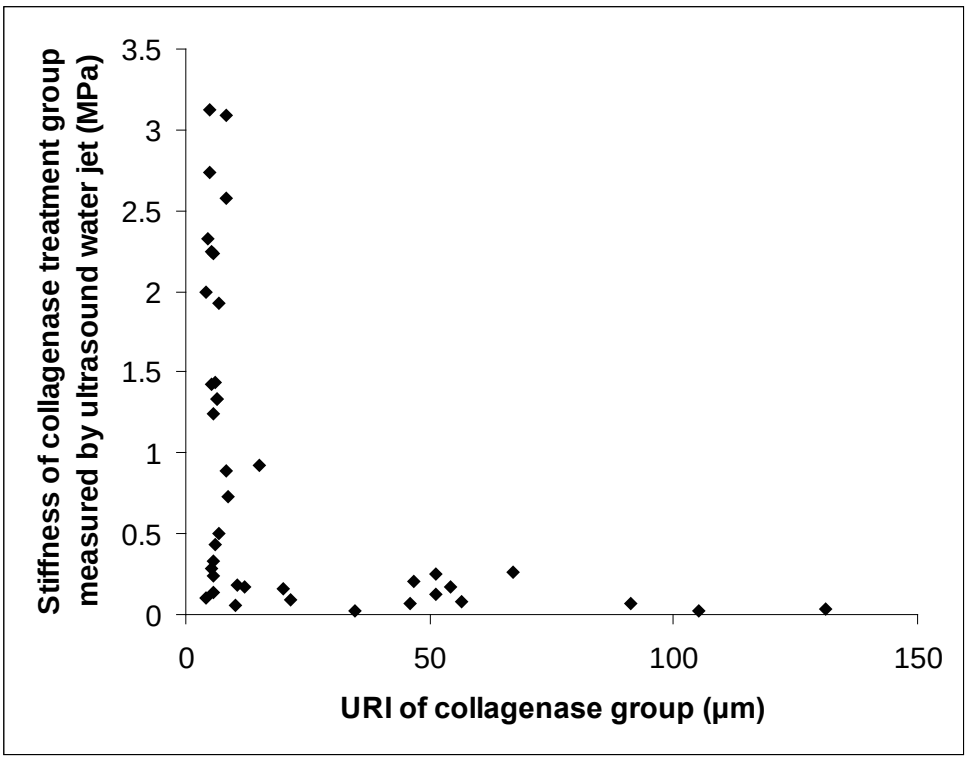

(b)

Fig 4.22. Relationships between (a) stiffness measured by OCT air jet and ORI of collagenase treatment group and (b) stiffness measured by ultrasound water jet and URI of collagenase treatment group.

Both inverse and power relationships were employed in the investigated. The curve fitting results revealed significant ($p<0.05$) inverse and power relationships in both comparisons as shown in Fig 4.23 (a) and (b) (R^2=0.58 and 0.55 for inverse and power estimation in relationship between stiffness measured by the OCT air jet indentation and ORI; R^2=0.34 and 0.50 for inverse and power estimation in relationship between stiffness measured by the water jet indentation and URI).

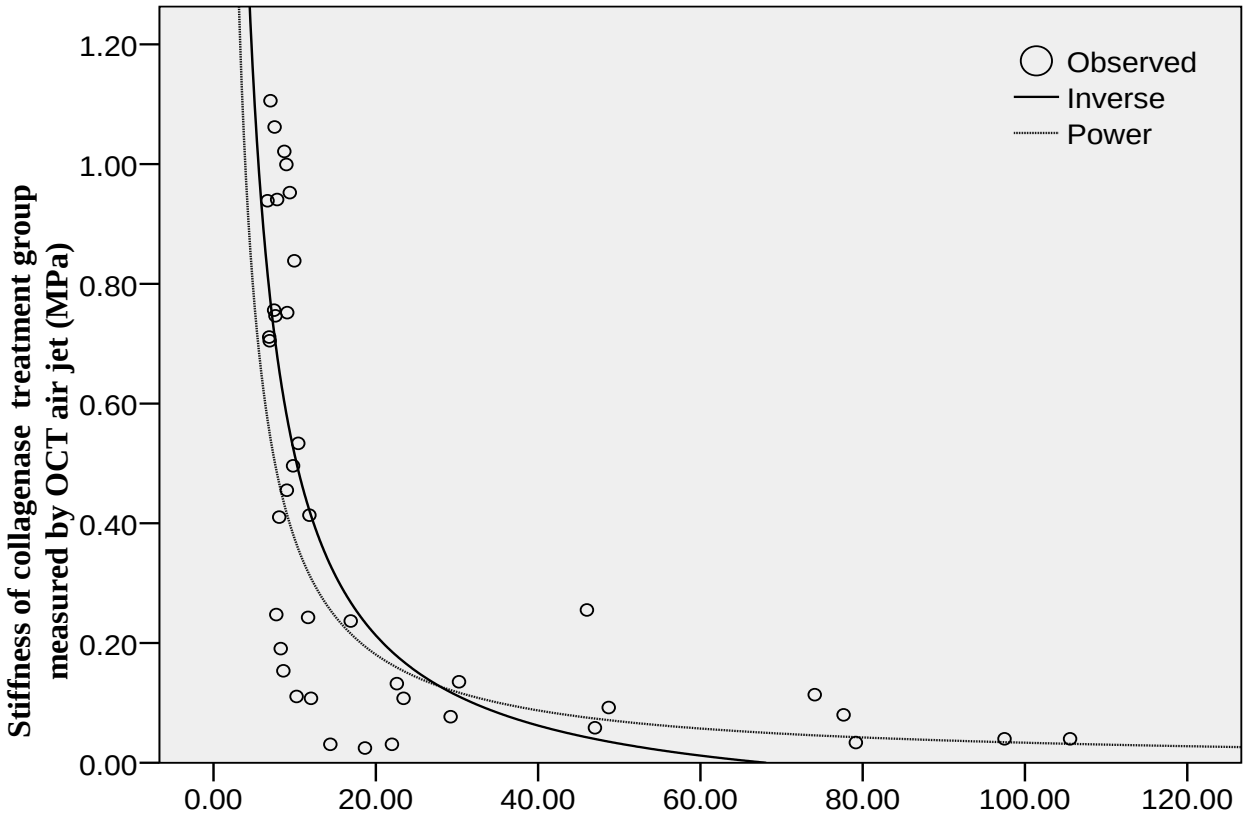

(a)

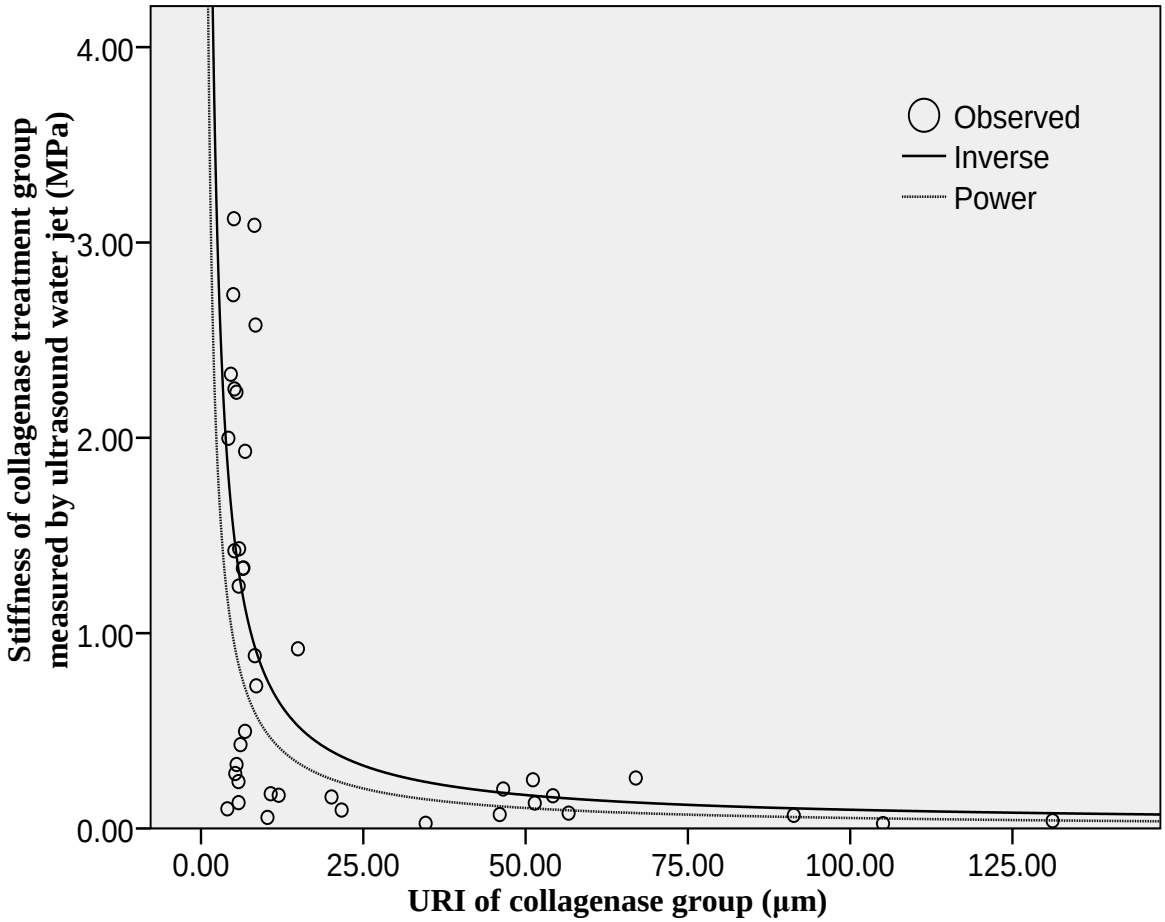

(b)

Fig 4.23. Inverse and power estimations of the relationships between (a) stiffness of collagenase group measured by the OCT air jet and ORI, (b) stiffness of collagenase group measured by the ultrasound water jet and URI. The estimation results showed significant inverse and power relationships in both comparisons ($p<0.05$).

The data points included in the Fig 4.22 and 4.23 contained the points both before and after collagenase degenerated. The result suggested that when the surface roughness was large enough (> 20μm), the stiffness would be significantly reduced. Since different cartilage samples may response to the collagenase digestion differently, the variation of the ORI and URI for collagenase digested samples may represent different degree of collagenase

degeneration. Thus these plots could be used to assess the correlation between the ORI, URI and stiffness. The correlation between the roughness index and degeneration degree should be further investigated.

4.7. Histological analysis result

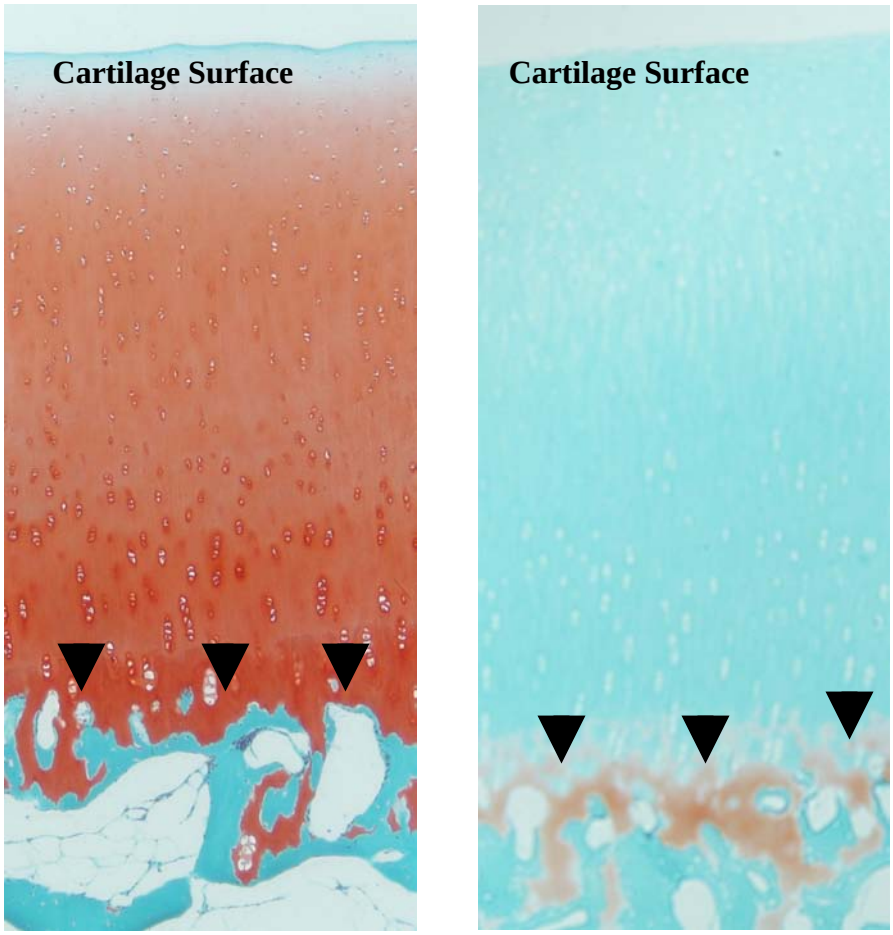

(a) (b)

Fig 4.24. Typical micrographs (×4) of articular cartilage stained with Safranine O and fast green for (a) normal sample and (b) sample after trypsin treatment. Arrowheads represent the cartilage-bone interface.

Fig 4.24 gives a typical histological presentation of a sample before and after trypsin treatment. Most of the proteoglycans were depleted after the trypsin treatment.

4.8 SEM scanning images

The typical SEM images of normal and degraded samples are shown in Fig 4.25. The SEM scanning suggested a degradation of the cartilage surface after the collagenase digestion. It was observed that the surface became much rougher and the integrity was serious damaged after the collagenase treatment (Fig 4.25(c)). Meanwhile, the effect of the trypsin treatment to the cartilage surface appeared to be minor (Fig 4.25(b)). The results of other specimens showed similar findings.

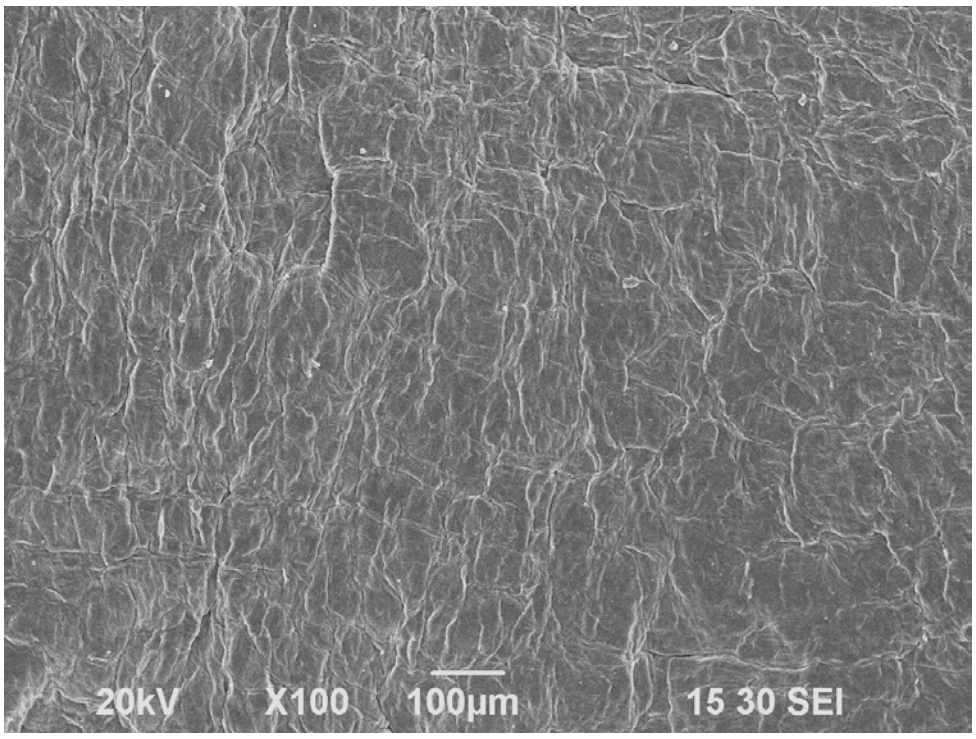

(a)

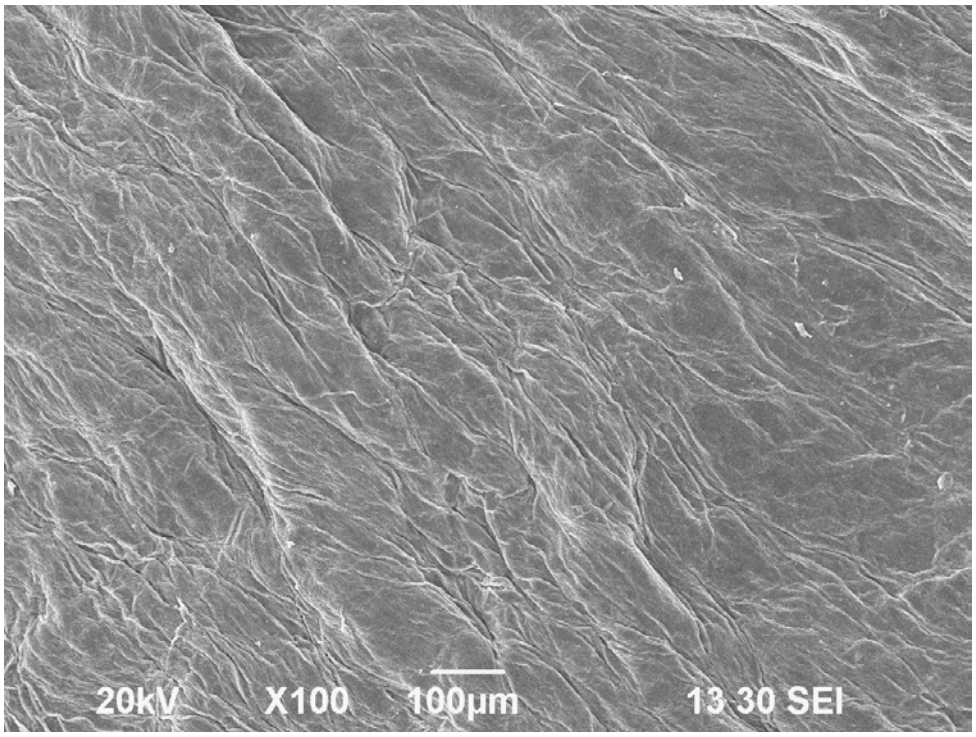

(b)

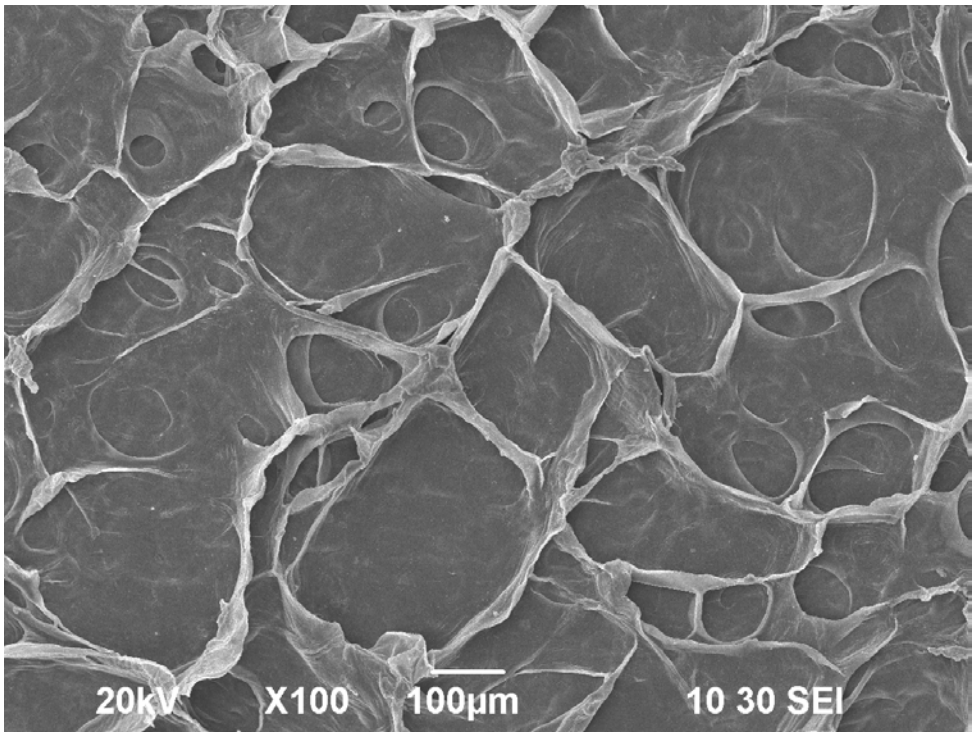

(c)

Fig 4.25. Typical SEM images (×100) of articular cartilage surface of (a) normal sample (b) trypsin digested sample, and (c) collagenase digested sample.

4.9 Summary

In this chapter, analyzed data of the study were presented. The RI result showed a significant depth dependence difference. The roughness measurement revealed a significant difference in the collagenase treatment group before and after the digestion, but not in the trypsin group. The acoustic parameter IRC had a linear relationship with the roughness index measured by the ultrasound. The stiffness of cartilage samples reduced significantly after the enzyme digestion.

Table 4.11. Summarized trends of parameter changes measured in this study. "↑" indicates a significant increase after the enzyme treatment; "↓" indicates a significant decrease after the enzyme treatment; and "--" indicates no significant change after the enzyme treatment.

Parameter	Collagenase treatment	Trypsin treatment
RI	--	--
ORI	↑	--
URI	↑	--
IA	--	--
IBS	↑	↑
IRC	↓	--
AIB	--	↓
Thickness	↓	--
Stiffness (air jet)	↓	↓
Stiffness (water jet)	↓	↓
Stiffness (mechanical indentation)	↓	↓
Young's modulus E	↓	↓

The trends of parameter change after enzyme degeneration are showed in Table 4.11. Out of the 12 parameters measured in this study, 9 showed significant change after the collagenase treatment, except for RI, IA and AIB. And six of them showed significant change after the trypsin treatment, including IBS, AIB, stiffness measured by air jet, water jet and mechanical

indentation, and Young's modulus. Among these 12 parameters, ORI, URI, IRC, AIB and thickness change could be potentially used to differentiate the collagenase and trypsin treatments, since the trends of these five parameters were different for the two treatments.

CHAPTER 5 DISCUSSION

In this chapter, experiment results of RI measurement, roughness index measurements, acoustic parameters and cartilage thickness calculation and indentation tests are discussed in separate sections.

5.1 RI measurement using OCT

The RI measurement in this study investigated depth and degeneration dependent RI of *in vitro* bovine articular cartilage. The overall mean RI of normal cartilage for different regions was 1.358±0.022, which agreed well with the value expected (1.37) for tissues with 80% water content (Madsen *et al.*, 1999). In the process of RI measurement, cartilage slices were immersed in the 0.15 M/L physiological saline, and the RI value of the saline from literature (Levin *et al.*, 2004) was employed as the standard value for calculation of RI of the articular cartilage. The RI obtained for bovine patellar cartilage in the present study was smaller than that reported by Herrmann and coworkers (Herrmann *et al.*, 1999) for human cartilage of different joints, which was 1.51 ± 0.009. The difference might be caused by the different specimens used in these two studies and different methods used for measuring RI. Unlike the speed of sound in ultrasound measurement of articular cartilage, there is very limited RI data of cartilage available in the literature. Therefore, it is hard to conclude which value would be more accurate. More studies are required to further investigate the absolute values of RI of articular cartilage from different joints and among various species.

Statistical analysis revealed that the RI of articular cartilage in different depths was significantly different ($p<0.05$), indicating that the optical properties varied in articular cartilage across different depths due to its heterogeneous structure. It was found in this study that, for the normal articular cartilage, the RI of the top, middle and deep layers was 1.361±0.032, 1.338±0.036 and 1.371±0.041. The RI of the middle layer was significantly smaller compared with the other two layers. This finding suggested that when using OCT to observe the optical properties of articular cartilage, the depth dependence should be taken into account. As described in the Methods Chapter, the top layer with 0.5 mm most likely included both superficial and middle layers of cartilage, as the superficial layer of cartilage normally occupies 10-20% of the entire thickness (Mow *et al.*, 2005; Clark, 1990; Hunziker *et al.*, 2002). Further studies could be followed to slice the cartilage into more layers with smaller thickness so that the results of RI can better match with the organization and orientation of collagen fibrils.

It is possible that the properties of cartilage may change after sliced into layers. Thus the RI may be different after cut into three layers. However, in this study, the calculation of RI is still in vitro measurement. Since the slice thickness and the difference of optical path length after install the slice between the container base and the lower surface of the glass need to be measured in the study, it is not possible to calculate the RI for different layers with intact cartilage.

As little research has been done on the depth dependent RI of cartilage, direct comparison with the literature is impracticable. Some related depth dependent properties of articular cartilage, however, have been reported earlier, including water (Shapiro *et al.*, 2001), fixed charge density (FCD) (Wang *et al.*, 2002a), proteoglycans distribution (Nieminen *et al.*, 2001), collagen fibril arrangement (Nieminen *et al.*, 2001; Arokoski *et al.*, 1996), and the speed of sound along the depth direction. Interestingly, the observed RI variation trend through different layers was similar to the optical path difference (retardation) trend along the depth direction in the canine knee articular cartilage (Fig 5.1) (Arokoski *et al.*, 1996). In cartilage sections, the retardation depends on the density of collagen structures in the specimen or the organization (orientation) pattern of collagen fibrils, or both (Modis, 1991). Although the retardation was calculated by measuring the light intensity values emerging from the analyzer (Arokoski *et al.*, 1996) and was not related to RI directly, the collagen structures density and collagen fibril arrangement change in articular cartilage may have caused similar effect on the two measurements. An earlier study reported that FCD reached the highest value in the middle layer (Wang *et al.*, 2002a), while in the present study, the middle layer of articular cartilage was found to have the smallest RI. It appears that the RI of articular cartilage may have a reverse relationship with FCD. And it was also suggested that the content of proteoglycan reaches its maximum in the middle zone (Mow *et al.*, 2005), that is, RI of articular cartilage may also have a reverse relationship with proteoglycan concentration. Furthermore, according to previous studies, the concentration of water decreases as the distance between measurement point

and cartilage surface increases (Shapiro *et al.*, 2001; Nieminen *et al.*, 2001). And the speed of sound also increases along the depth direction from superficial to deeper zones (Patil *et al.*, 2004). The RI measured in this study didn't follow a similar trend. This may indicate that concentration of water might play a less important role in determining RI than collagen network, proteoglycan or FCD. The speed of sound and the RI represent the propagating speed of acoustic and optical waves in articular cartilage, respectively. Although they were found both depth dependent according to the results of this and an earlier study (Patil *et al.*, 2004), they may be determined and affected by different factors, taking into account the complexity of the articular cartilage structure.

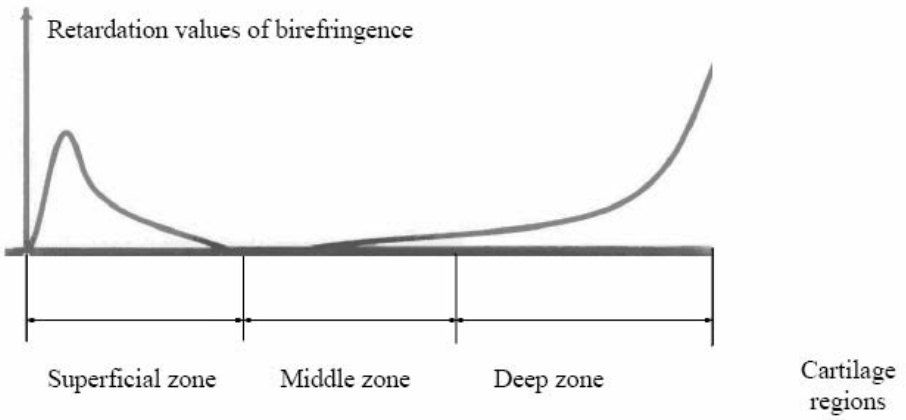

Fig 5.1. The curve representing the trend of retardation values of the birefringence of canine knee articular cartilage in different regions (Arokoski *et al.*, 1996). The regions are named according to the specimen preparation method used in the present study.

In the RI measurement, to test the effect of proteoglycan and collagen degeneration on the RI of cartilage, one group of specimens was treated with 0.25% trypsin solution at room temperature for 5 h (Zheng *et al.*,

2004b) and another group by 30 U/ml collagenase solution at 37°C for 5 h (Toyras *et al.*, 2003). In the reference studies (Zheng *et al.*, 2004b; Toyras *et al.*, 2003), it was reported that the proteoglycans were completely depleted and the collagen network significantly affected under these conditions. However, the results in this study revealed that the trypsin and collagenase treatments did not have significant effects on the RI of articular cartilage ($p>0.05$), suggesting that the degeneration of proteoglycan and collagen network would not significantly change the cartilage RI.

Previous studies on the tissue RI using OCT were mainly based on focus tracking method and optical length shifting method. The focus tracking method has been used to measure the RI of human tissues both *in vitro* and *in vivo*, employing the coherence gating properties of OCT to track the focal position as the sample moves along the optical axis. The optical length shifting method uses the ability of OCT to measure the optical path length and physical thickness of tissue specimen *in vitro* (Herrmann *et al.*, 1999; Tearney *et al.*, 1995; Wang *et al.*, 2002b). During the course of measurement, water content in the tissue may change due to vaporization, which may cause the change of tissue RI. In this study, we modified the optical length shifting method to measure the RI of cartilage which was bathed in physiological saline. Thus, the variation of tissue water content could be minimized and the RI value would be more stable and reliable during the experimental process. In addition, the proposed method did not require any specific operation for the optical system. By designing a

specimen holder as introduced earlier in this thesis, the method can be adopted with any available OCT imaging system.

5.2 Surface roughness measurement

In the surface roughness measurement, the ability of OCT and high frequency ultrasound systems to assess the surface conditions of bovine articular cartilage was investigated. A new parameter, ORI was introduced to quantify specimen surface roughness using OCT, following the principle of URI introduced in previous studies (Saarakkala *et al.*, 2004b; Saarakkala *et al.*, 2006).

A piece of glass was employed in this study to test whether the scanning process itself would induce a large system error to the result of ORI or URI. The glass surface was considered to be smooth with a small roughness index value. The ORI and URI results for glass surface were 0.68 ± 0.07 μm and 0.55 ± 0.08 μm, respectively, which were relatively small compared to the results of articular cartilage surface (approximately 7% of the average roughness index of articular cartilage). This result suggested that the system error which was probably induced by the subtle vibration of the station, the tiny disturbance in saline solution, or the limit of the resolution could be neglected for this application.

The results of ORI and URI of the emery papers both showed highly linear correlations with the emery paper grit size (R^2=0.95 for both correlations),

suggesting that both methods can be used to assess various surface conditions. In OCT cross-sectional images obtained by the Labview program in this study, two adjacent data points in the depth direction represented a distance of 0.43 μm in saline, while in RF signal obtained by the Vevo high frequency ultrasound system, the adjacent data points in the depth direction represented a distance of 1.83 μm in saline. These data suggested that the OCT system may be more sensitive at measuring roughness index. Both the equivalences of representative distance per data point were smaller than the roughness index measured for normal cartilage samples (approximately 9 μm for ORI and 6 μm for URI), suggesting that the variation of surface interface in different scanning lines could be detected.

The overall ORI value for normal articular cartilage was 8.8±1.4 μm, while the overall URI value for normal articular cartilage was 6.0±1.5 μm. These results agreed well with the URI result measured using a 20 MHz ultrasound system (Saarakkala *et al.*, 2004b), which ranged from 6.8 μm to 12.3 μm for normal articular cartilage samples. The distance equivalences per point for OCT and high frequency ultrasound system were different (0.38 μm for OCT system and 1.83 μm for high frequency ultrasound system). Thus the calculated ORI and URI value for the same sample may be different. Also the measurement sites for ORI and URI for the same sample may vary. The sum of the SD value for the ORI and URI for normal specimen was 2.9 μm. The difference between the mean ORI and URI value should still be reasonable. For the test among the digestion samples, statistical analysis

showed significant differences of roughness index in collagenase digestion group using both OCT and ultrasound ($p<0.05$). The ORI increased by 368% after collagenase digestion, while the URI increased by 602%. And the mean ORI and URI value after collagenase were 39.8 μm and 42.1 μm, respectively, despite the relatively large SD value. The difference of the collagenase degenerated mean URI and ORI was 2.3 μm, which should also be reasonable. The subsequent increase rate should also be reasonable. These dramatic changes of the surface integrity were confirmed by the results of SEM. This finding demonstrated that the superficial structure change of articular cartilage caused by collagenase digestion could be detected by OCT and ultrasound. For the trypsin digestion, there was no significant difference in the parameters before and after the treatment measured by either OCT or ultrasound ($p>0.05$), suggesting that trypsin digestion wouldn't vary the surface structure. This was confirmed by the results of SEM. The significant changes of ORI and URI in collagenase group agreed with the result of a previous study (Saarakkala *et al.*, 2004b), indicating that ORI and URI measurements could be used to assess the surface changes during cartilage degeneration.

Since OCT and high frequency ultrasound were both employed to assess the surface condition of specimen, the relationship between these two assessment methods was also investigated. The relationship between ORI and URI results for emery paper measurement demonstrated a highly linear relationship ($p<0.05$) with $R^2=0.89$. The relationship between ORI and URI results for the same set of articular cartilage samples also shown a linear

relationship (R^2 =0.74, p<0.05). These findings suggested the ORI and URI measurements were comparable.

In this study, the ORI and URI were introduced to quantify the surface integrity of articular cartilage. The cross-sectional images of articular cartilage along different directions were obtained and ORI and URI were defined as the RMS of the deviation of the surface profile in different scanning lines. This RMS surface roughness method has been commonly applied in the field of material sciences (Werber and Zappe, 2006; Collins *et al.*, 1994; Jun *et al.*, 1995; Logothetidis and Stergioudis, 1997), and was recently introduced to the ultrasonic analysis of articular cartilage surface by Saarakkala *et al.* (Saarakkala *et al.*, 2004b; 2006). To the best of our knowledge, this method has not been adapted to the OCT analysis of cartilage surface. The global contour of cartilage surface profile was eliminated by high pass filter, with the assumption that the surface disruption mainly affected the high frequency component of surface profile. Thus the measurement of ORI and URI could be more independent of the perpendicularity between the transducer and sample surface, theoretically. Since the potential for extremely compact OCT endoscopes combined with arthroscope has already been shown (Xie *et al.*, 2008), it is possible that ORI could be used as a parameter to assess the surface condition of articular cartilage *in vivo*. URI may as well be able to be measured using clinical ultrasound devices, and applied for roughness characterization of different acoustic interfaces within human tissue (Saarakkala, 2007). The

miniaturization of the ultrasound scanning probe should be further investigated.

During the measurement of ORI and URI in this study, the cartilage specimens were immersed in saline and the interface of saline-cartilage was employed for the assessment of cartilage surface conditions. If in the future, the ORI could be measured *in vivo* using endoscopes or during open knee surgery, there might be a relatively thin interstitial fluid layer covering the articular cartilage surface. Since the air-fluid interface may also induce highly reflected signals, the influence of this fluid layer on the detection of fluid-cartilage surface should be further investigated. The shrinkage of cartilage when exposed to air directly may also affect the surface roughness result. The effects of shrinkage and swelling on cartilage surface roughness could be further evaluated by varying the concentration of bathing solution during measurement.

The specimens used in this study were from the medial upper region of bovine patellar cartilage. As it was reported in a previous study that the URI value showed site-dependent variation (Laasanen *et al.*, 2005), basic studies investigating the surface roughness index at various sites are recommended to be carried out to provide reference roughness index values.

5.3 Acoustic parameters measurement

The acoustic parameters of this study were measured using the 55 MHz probe of the high frequency ultrasound system, Vevo, before and after the

enzyme treatments. Since during the study, cartilage surface was adjusted to be perpendicular to ultrasound beam, the reflection was dependent on the surface properties such as roughness and impedance (Adler *et al.*, 1992; Cherin *et al.*, 1998). And the results showed that IRC and URI obtained from the same set of samples had a significant correlation. It is believed that the collagen fibrils are the main reflectors of ultrasound at the surface of cartilage (Cherin *et al.*, 1998; Nieminen *et al.*, 2002). In this study, IRC value dropped significantly after collagenase digestion, which agreed with a previous study (Saarakkala *et al.*, 2004b), while the IRC value showed insignificant change after trypsin digestion. This result matched with the results of previous investigations that proteoglycans were considered to play an insignificant role in ultrasound reflection from cartilage surface (Nieminen *et al.*, 2002; Toyras *et al.*, 1999). The SEM results of this study also demonstrated the dramatic damage of the surface integrity induced by the collagenase treatment.

The AIB value representing the property at subchondral bone interface was also examined in this study. The values showed no significant difference for the collagenase digestion group, but significantly dropped after the trypsin digestion. The mean AIB value reduced by 2.4 dB after the trypsin digestion. The significant decrease was suggested to be caused by the depletion of proteoglycans in the articular cartilage and agreed with the result of a previous study (Wang, 2007).

The attenuation evaluation was performed using a multinarrow band algorithm. The mean value of IA increased insignificantly after removing proteoglycans from cartilage by the trypsin treatment, which was similar to the results of some previous studies (Wang, 2007; Agemura *et al.*, 1990; Toyras *et al.*, 1999). The reason that IA didn't increase significantly may be that trypsin digestion also caused the damage of the collagen network, which decreased the attenuation coefficient. However, some other studies reported a significant increase of attenuation after the digestion of proteoglycans (Joiner *et al.*, 2001; Nieminen *et al.*, 2002). This should be further investigated in future studies. The result in this study also revealed an insignificant reduction of IA after the collagenase digestion, which agreed with the result of a previous study (Nieminen *et al.*, 2002). The reduction of collagen contents may make the cartilage more transparent to ultrasound.

The current study showed that the backscatter coefficient from the middle cartilage matrix, represented by IBS, increased significantly by approximately 2.5 dB after both the enzyme degeneration. A study on the effects of drugs on rat cartilage also showed that IBS increased significantly after applying drug induced degeneration. However, it was reported that IBS value would not change significantly after digestion (Wang, 2007). Therefore, the effect of enzyme digestion on backscatter coefficients should be further investigated by using high frequency ultrasound to monitor the enzyme degenerating process.

In this study, acoustic parameters were measured before and after the enzyme treatments. Samples had to be repositioned after the treatments. Although samples were carefully adjusted to let ultrasound beam locate in the centre of the disk perpendicularly to the cartilage surface, and scanned in four different directions, this reposition might inevitably affect the outcome of the measurement. The perpendicularity of the transducer to the cartilage surface was ensured by adjusting the sample to get the maximum echo amplitude. However, the natural contour of cartilage surface may still induce an incident angle. Previous studies had investigated the effect of incident angle on the reflected and backscattered ultrasound signals (Cherin *et al.,* 2001; Wilhjelm *et al.,* 2001). The results of these studies indicated that the deflection of 2° would induce a reduction of reflection of 1.7 dB to 5 dB. These findings suggested the significant effect of incident angle on the acoustic parameters. Thus the natural cartilage contour might affect the results of the measurement. As mentioned above, the results of IRC and URI in this study were linearly correlated, particularly for small values of URI. Since during the calculation of URI the surface contour effect had been eliminated by using a high pass filter, assessing URI or ORI might provide better methods than measuring IRC to investigate the surface conditions of articular cartilage, at least theoretically. Future studies may be followed to further compare these assessment methods.

5.4 Cartilage thickness measurement

In this study, a high frequency ultrasound system Vevo was utilized to measure cartilage specimen thickness and to assess the acoustic properties

of articular cartilage. Cartilage thickness was determined with the 55 MHz transducer by calculating the time of flight and its deflection of the ultrasound signals reflected from the saline-cartilage and cartilage-bone interfaces. The mean thickness of normal cartilage samples obtained from the medial upper region of bovine patellar cartilage was 1.77 ± 0.27 mm, which agreed well with the value 1.75 ± 0.23 mm reported by a previous study (Lu *et al.*, 2009) using 20 MHz ultrasound. The cartilage thickness decreased significantly by 9.8% from 1.83 ± 0.23 mm to 1.65 ± 0.27 mm after the collagenase digestion ($p<0.05$), while increased insignificantly by 2.3% from 1.71 ± 0.29 mm to 1.75 ± 0.32 after trypsin digestion ($p>0.05$).

Collagenase is known to induce a serious damage to cartilage collagens. A previous study investigated by microscopic analysis also reported that the whole cartilage thickness reduced by 6.1% and the surface zone thickness reduced significantly by 76% after 48 h collagnease treatment with a concentration of 30U/ml (Lyyra *et al.*, 1999). And the result of Toyras *et al.*'s (Toyras *et al.*, 1999) also indicated insignificantly decreased cartilage thickness after collagenase digestion. The reduction of cartilage thickness after the collagenase may have been caused by the damage of collagen network, especially in the surface zone.

Trypsin is known to be effective for the proteoglycan digestion with a slight simultaneous effect on the collagen network (Harris *et al.*, 1972). Previous studies showed that the trypsin digestion would not affect the cartilage thickness significantly (Wang *et al.*, 2008b; Lyyra *et al.*, 1999; Lu *et al.*,

2009). They reported a mean thickness increase of 0.02 mm, 0.06 mm and 0.01 mm, respectively, after the trypsin digestion for bovine patellar cartilage. In another study, the weight of fibrillated cartilage (degenerated) reported increased when immersed in solution compared with its initial weight (Maroudas and Venn, 1977). The study of Buckwalter and Mankin (1997) also revealed that in the early degeneration stage, cartilage swelling and increase of water content would occur. The insignificant increase of cartilage thickness observed in the current study may be caused by the swelling effect after the depletion of proteoglycans.

In the current study, the cartilage thickness was calculated according to the time of flight between saline-cartilage and cartilage-bone interfaces and the speed of sound in articular cartilage. The speed of sound was assumed to be constant with the value of 1610 m/s, 1580 m/s and 1595m/s for normal, collagenase treated and trypsin treated cartilage, respectively (Laasanen *et al.*, 2002). As mentioned in the Literature Review Chapter, previous studies had already investigated the variation of the speed of sound in articular cartilage under different conditions. During the cartilage thickness measurements, samples were all immerged in physiological saline at room temperature (24.5±1°C). And the overall thickness of articular cartilage was measured with ultrasound beam perpendicular to the cartilage surface. Thus the conditions such as temperature, medium concentration, pressure applied on the sample, or different scanning layer and direction were kept as much the same as possible before and after the enzyme treatments, so that those factors would not induce the variation of speed of sound during the

measurement. Different constant values of the speed of sound were assumed for cartilage before and after the enzyme treatments, because tissue compositions have large effect on speed of sound in cartilage (Toyras *et al.*, 2003). The samples used in the measurement of speed of sound value in the reference (Laasanen *et al.*, 2002) was from the lateral upper quadrant of patella, while in the current study, the samples were from the medial upper quadrant. Although the speed of sound may vary among different measurement sites, a previous study had already demonstrated that there was no significant difference of speed of sound among four different quadrants (Patil, 2004). So using the value of speed of sound from reference study measured at lateral upper region for the calculation of thickness in the current study is reasonable. However, the reference study was carried out in unconfined geometry; the temperature and medium concentration were not specified in the reference. The differences of temperature and medium concentration between the reference study and the current study may lead to the variation of speed of sound in these two studies. These effects need to be further investigated in the future.

Further investigation employing other thickness measurement methods such as digital caliper and histology analysis would also be needed to better understand the thickness change after degeneration.

5.5 The indentation tests

In this study, the mechanical properties of bovine patellar articular cartilage were investigated by the novel OCT air jet indentation system, the

ultrasound water jet indentation system as well as the standard mechanical indentation system. The issues related to indentation tests are discussed as follows.

5.5.1 OCT air jet indentation

The OCT air jet indentation system was developed earlier by our group. Its capability of assessing the mechanical properties of soft tissue has been investigated using phantoms (Huang *et al.*, 2009). In this study, the stiffness obtained using OCT air jet indentation system showed a linear correlation with the stiffness and Young's modulus measured by the standard mechanical indentation test ($p<0.05$, Pearson's analysis). This correlation revealed that this novel OCT air jet could be used to assess the elasticity of articular cartilage.

Both collagenase digestion and trypsin digestion groups showed significant stiffness decreases after the enzyme treatments ($p<0.05$). The stiffness values of the collagenase digestion and trypsin digestion groups reduced by 85% and 68%, respectively. The digestion of proteoglycans has been considered to cause the reduction of cartilage stiffness (Qin *et al.*, 2002). And collagenase digestion could cause a serious damage to the cartilage collagens and thus disrupt the structure and network of cartilage (Laasanen *et al.*, 2002). The reduction of stiffness observed in this study agreed well with the results of previous studies (Laasanen *et al.*, 2002; Qin *et al.*, 2002; Lu *et al.*, 2009).

The OCT system employed in this study could measure the mechanical properties of tissue without a direct contact. It might induce less damage on the tissue surface than the traditional rigid contact indentation. Thus it provides the possibility for miniaturized use such as combined with an endoscope.

In this study, the reflected signals from the cartilage-bone interface could not be obtained during the air jet indentation as in the water jet case. The deformation of cartilage samples was calculated by tracking the deformation of the surface under the air jet pressure assuming that the bottom of cartilage sample was fixed and the platform remained absolutely stable during the indentation. In the real situation, there might be some subtle vertical movement of the optical probe caused by the air jet. Thus the deformation measured by this system could be inevitably larger than the actual deformation. It has been demonstrated that the detection of cartilage-bone boundary was feasible using OCT (Rogowska and Brezinski, 2002; Rogowska *et al.*, 2003). In the future, by improving the hardware of the optical source to increase the signal noise ratio of the OCT system used in the current study, or adopting the polarization-sensitive OCT with proper signal processing techniques (such as boundary detection, image enhancement and image segmentation techniques), it is possible to detect the lower interface of the cartilage attached to the subchondral bone and then obtain a more precise value of the thickness and the change of the tissue layer, i.e. deformation, during the indentation process.

It was found in the current study that the optical signals were quite sensitive to the surface movement. And the signal amplitude reduced rapidly when increasing the air jet pressure. This might be caused by the surface profile change after deformation, and the non-vertical relationship between the optical beam and the indented surface. In order to reduce the possible system noise induced by this phenomenon, the indentation rate was controlled within 2 mm/min and moving average was used when necessary during the data analysis.

In this study, the signals were obtained by A-line OCT, i.e., the surface displacement was assessed when OCT signals were measured at a single point. Cross-sectional OCT imaging could be used in the future to obtain more information such as the surface profile during the indentation. The frame rate of cross-sectional image scanning obtained by the current system would be lower than A-line scanning, since signals from different scan lines are needed to form the cross-sectional image. Thus the improvement of frame rate is necessary in order to utilize cross-sectional scanning.

Data within 3% of deformation/thickness ratio were employed for the calculation of stiffness or Young's modulus in this study. Within this ratio range, linear elasticity for most soft tissues could be assumed (Nitta and Shiina, 2002). The solid cartilage matrix was assumed to be isotropic and homogeneous in order to simplify the mechanical properties of the cartilage specimen. Only the data from the loading phase of the indentation were used for calculation to reduce the viscosity factor. More comprehensive models

would be needed to investigate the intrinsic mechanical properties of soft tissue under indentation (Hayes *et al.*, 1972; Waters, 1965). Also the air jet and specimen interaction was simplified by assuming the air jet diameter maintained the same when contacting with the cartilage surface. In the real situation, however, the air jet diameter would change and nonlinear behaviors would occur during the process of indentation. Monitoring cross-sectional image of the sample during the indentation using OCT would be a way to better understand the actual interaction profile. The stress distribution in the sample surface also needs to be further investigated. As suggested in the previous study (Lu, 2006), pressure sensor films could be employed in future studies to map the stress distribution on the interface. These efforts will help to extract the modulus of tissue specimen accurately.

5.5.2 Ultrasound water jet indentation

The ultrasound water jet indentation has been developed earlier to assess the mechanical properties of soft tissue by our group (Lu *et al.*, 2005; 2007; 2009). In this study, the stiffness obtained using this novel ultrasound water jet indentation system also had linear relationship with the stiffness and Young's modulus measured by standard mechanical indentation test ($p<0.05$, Pearson's analysis). The high correlations suggested that the water jet could be used to assess the elasticity of articular cartilage.

The stiffness of the collagenase digestion and trypsin digestion groups reduced significantly by 87% and 75%, respectively. This result was similar to the result obtained by the OCT air jet indentation system. The reasons

that might have caused the change of stiffness of articular cartilage specimen have been discussed before.

Similar to OCT air jet, ultrasound water jet also has the advantage of no direct contact with the tissue.

Using the 20 MHz ultrasound transducer, the water-cartilage and cartilage-bone interfaces could both be detected during the indentation. The deformation of cartilage layer was calculated by subtracting the deformation of these two interfaces. Compared to OCT air jet, the calculation of deformation in water jet system should be more accurate. However, the interaction of water jet and cartilage surface still needs further investigation, similar to the OCT air jet system. The linear relationship between the stiffness measured by water jet and standard mechanical indentation was obtained ($p<0.05$). The stiffness of the two tests was carried out using the similar equation. Thus, the trends of change in the two parameters should be comparable. However, since the water jet indentation test did not use a rigid indenter to compress the tissue. The actual reaction interface of water jet indentation test would be different from the standard mechanical indentation test. Thus comparing the absolute value of these two parameters would not be so meaningful. The linear correlation observed in this study together with previous results (Lu *et al.*, 2005; 2007; 2009; Lu, 2006) indicated that the water jet system could be used as a new approach to measure the mechanical properties of various soft tissues.

The deformation measured by the water jet indentation was calculated with the information of speed of sound in the cartilage tissue and the time of flight in cartilage samples. The time of flight was calculated by the difference between echoes from the interfaces using a cross correlation technique. In this study, the strain applied on the cartilage was relatively small, and only the data within 3% strain ratio were used for calculation. It was suggested that the measurement error caused by frequency dependent attenuation may be small and the deformation uncertainty was mainly caused by the variation of the speed of sound (Lu *et al.*, 2009). In this study, the speed was assumed to be constant during the indentation with the value 1610 m/s for normal articular cartilage, and 1595 m/s and 1580 m/s after trypsin and collagenase treatments, respectively (Laasanen et al., 2002) . In the real situation, however, the speed of sound may change during the indentation. It was reported in a previous study that the speed of sound increased significantly during stepwise stress relaxation compression (Ling *et al.*, 2007), while other studies showed significant reduction of speed of sound during stress-relaxation test (Nieminen *et al.*, 2006; 2007). The conflicted results may arise from different compression protocols. Also the speed of sound can be affected by different measurement sites. Is was suggested that using the predefined speed of sound 1610 m/s, may induce an error of approximately 1% of the stiffness, which should be clinically acceptable (Lu *et al.*, 2009).

In this water jet indentation system, tap water (nearly 0 M/L NaCl) was utilized for ejecting water jet. Articular cartilage swelling occurs because of

the change of Donnon osmotic pressure (Donnan, 1924; 1995) when the concentration of the bathing solution decreases. In order to reduce the strain change caused by swelling, the cartilage sample was first scanned under a low pressure (less than 1 kPa) for 15 minutes to allow the cartilage to reach equilibrate state in water, according to a previous study (Lu *et al.*, 2009). However, to better maintain the similar physiological conditions *in vivo*, normal physiological saline solution is suggested for ejecting water jet in the future studies.

Similar to the OCT air jet indentation system, in order to obtain the modulus of tissue specimen more accurately, more efforts would be needed to investigate intrinsic mechanical properties, actual interaction profile, and stress distribution on the interaction surface during the indentation using similar means as suggested for the air jet indentation.

5.6 Correlations among different parameters

In this study, a total of 12 parameters were measured in this study to characterize optical, morphological, acoustic and mechanical properties of bovine articular cartilage. In order to investigate the correlations among those different parameters, the same set of samples was employed in the roughness, acoustic parameters and mechanical parameters measurements. It was demonstrated that the acoustic parameter IRC significantly correlated to the morphological parameter URI. Linear and logarithmic relationships were found between URI and IRC measured in this study. The result suggested that when URI increased the IRC value decreased. Both

parameters could be used to represent the surface condition of articular cartilage.

The relationship between morphological and mechanical properties was also determined. A correlation was found between the roughness index and the stiffness of articular cartilage in the collagenase digestion group. Inverse and power relationships were found in the collagenase digestion group both between ORI and stiffness measured by OCT air jet and between URI and stiffness measured by ultrasound water jet, revealing that when roughness index increases the stiffness would decrease.

It was found in this study that collagenase treatment induced the increase of roughness index and the decrease of stiffness while trypsin treatment also induced the decrease of stiffness but not the roughness index. The results also suggested that with morphological (roughness index) and mechanical information (stiffness), one could tell whether an articular cartilage sample was from the normal, collagenase digested or trypsin digested group. According to previous studies, in the early degeneration stage of articular cartilage, collagen network change is relatively minor and proteoglycan aggregation decreases. In advanced degeneration stage, surface or deep defects can be observed (Mow VC, 1991). The results in this study suggested that after collagenase degeneration, the articular cartilage was close to the advanced or late degeneration stage of OA; while after trypsin degeneration, the articular cartilage was more similar to the early degeneration stage of OA. With the information of different articular

cartilage parameters under various conditions and proper modeling technique, it is possible to establish a novel OA scoring system. And since morphological, acoustic and mechanical properties could all be taken into consideration in the system, it may improve the accuracy of OA diagnosis. More systematic studies and modeling technique would be needed in order to achieve this goal.

5.7 Experimental protocols

Previous studies showed that cryopreservation storage and thawing of articular cartilage samples would not affect the acoustic properties (Kiefer *et al.*, 1989; Agemura *et al.*, 1990). In the current study, the same set of samples was employed in the surface roughness measurement using both OCT and ultrasound, then was examined using the OCT air jet, ultrasound water jet and standard mechanical indentation tests both before and after the enzyme treatment. It was reported that cartilage samples could nearly fully recover by immersing in physiological for half an hour after various tests (Bae *et al.*, 2006), using cartilage thickness as a indicator. In this study, the samples were immersed in physiological saline at room temperature (24.5±1°C) between each test. The total interval time for each sample between tests may add up to several hours. Also the OCT air jet, ultrasound water jet and standard mechanical indentations were performed on the samples in series. These experiment arrangements may induce some unknown effects on the morphological, acoustic or mechanical properties of articular cartilage. The possible effect may need to be carefully examined in future studies.

5.8 Summary

In this chapter, discussions were made on the results of the optical, morphological, acoustic and mechanical properties of articular cartilage, assessed by OCT and high frequency ultrasound systems. Possible reasons leading to those results were explored in details and limitations for each test were addressed. Important findings obtained in this study and suggested future works are introduced in the next chapter.

CHAPTER 6 CONCLUSIONS AND FUTURE STUDIES

6.1 Conclusions

The depth and degeneration dependences of articular cartilage RI were investigated in this study using OCT for the bovine patella specimens detached from the subchondral bone. It was found that the RI was significantly different among the three layers for both normal and enzymes treated articular cartilage, while, the trypsin and collagenase treatments didn't lead to significant change in RI. It was suggested that the depth dependence of articular cartilage RI should be taken into consideration in the studies of its optical properties.

The ability of OCT and ultrasound to assess the cartilage surface roughness was also investigated, using parameters ORI and URI, respectively. Both measurements showed significant increase of roughness index in collagenase digestion group. No significant difference was observed in trypsin digestion group, suggesting that collagenase could affect the surface condition of articular cartilage. The roughness index obtained using OCT and ultrasound showed a linear relationship in both emery paper and articular cartilage studies. The results suggested that OCT and ultrasound could be used for the surface condition assessment of articular cartilage.

The acoustic parameters of articular cartilage including the surface, the cartilage matrix, and the cartilage-bone interface were investigated by high frequency ultrasound system before and after the enzyme treatments. The

IRC value dropped significantly after the collagenase digestion, but only changed insignificantly after the trypsin treatment. The IRC result of the whole cartilage samples had a linear correlation with URI obtained from the same sample set. The result of AIB value showed a significant decrease in trypsin digestion group. The evaluation of IA revealed an insignificant increase after the trypsin digestion and an insignificant decrease after the collagenase digestion. The IBS result showed a significant increase in both groups by approximately 2.5 dB.

The articular cartilage thickness measurement using the high frequency ultrasound system showed that the two enzymes caused different effect on the thickness. The mean value for normal cartilage thickness was 1.77 ± 0.27 mm obtained in this study. The cartilage thickness decreased significantly by 9.8% from 1.83 ± 0.23 mm to 1.65 ± 0.27 mm after collagenase digestion, but increased insignificantly by 2.3% from 1.71 ± 0.29 mm to 1.75 ± 0.32 after trypsin digestion.

The indentation tests showed that both air jet and water jet measured stiffness had linear relationships with the stiffness and Young's modulus obtained by the standard mechanical indentation. The correlations suggested that the OCT air jet and ultrasound water jet indentation tests could be used to assess the elasticity of soft tissue. According to the result, collagenase and trypsin digestions induced significant reduction of stiffness by 85% and 68%, respectively, as detected by the OCT air jet, and 87% and 75%, respectively, as detected by the ultrasound water jet. The reference results of

the standard mechanical indentation showed reductions of 88% and 74% for the collagenase and trypsin treatment groups, respectively.

Since the surface roughness and stiffness were measured on the same sample set, the relationships between the morphological and mechanical properties were also investigated in this study. Significant ($p<0.05$) inverse or power relationships between ORI and the stiffness measured by OCT air jet were obtained in the collagenase treatment group. Similarly, there was an inverse or power relationship between URI and the stiffness measured by ultrasound water jet.

6.2 Future studies

The following future studies are suggested based on the present study.

For the study of RI value of articular cartilage, further investigations are needed to obtain the absolute RI values of articular cartilage from different articulating sites, different joints and from various species. The role of different cartilage components in determining the cartilage RI needs to be further investigated as well.

Since ORI and URI measurements are relatively new in the assessment of articular cartilage, the clinical value of these parameters needs to be further investigated. The roughness index results obtained by OCT or ultrasound could be compared to those by other roughness determination apparatus. Future studies of roughness index in different cartilage sites and various

species need to be conducted in order to investigate cartilage surface under different conditions. Besides the enzyme induced degenerated cartilage, other degenerated samples such as spontaneously degenerated or external operation induced degenerated cartilage can be included in the surface roughness study. Also factors such as scanning range, sampling frequency, distance between interval scanning lines, and wavelength of OCT or frequency of ultrasound transducer need to be further studied to see their effect on the roughness index result.

For the OCT air jet and ultrasound water jet indentation tests, the interaction between the air jet and water jet and sample surface needs further study. In this study, the deformation profile during the indentation was assumed to be the same as using the rigid cylindrical indenter. However, the behaviors of air and water on the sample surface in the real situation need to be observed. Using cross-sectional OCT images or B-mode ultrasound images of the surface profile could help to observe the actual interaction. During the ultrasound water jet indentation, the water flow was controlled manually. In order to better control the fluid speed and pressure within the pipe, a proportioning valve may be desired to control and adjust the fluid automatically, as in the case of the OCT water jet. The relationships between the applied force on the sample surface and the indentation speed, and the distance between the jet head and sample surface could be further studied. The stress distribution on the interaction surface can be mapped using pressure sensor films. Finite element models can be built in future studies to simulate the interaction between the air or water jet and the soft

tissue. Intrinsic mechanical properties of cartilage can also be extracted using accurately controlled creep tests (Lu, 2006).

In the case of OCT air jet, the deformation of cartilage was estimated by measuring the deformation of surface interface. In order to monitor the deformation of samples more accurately, reflected signals from the cartilage-bone interface would be needed. Necessary noise reduction and signal processing techniques are also necessary in order to detect the cartilage-bone boundary in OCT images.

Since the potential for extremely compact OCT endoscopes combined with arthroscope has already been shown (Xie *et al.*, 2008), it is possible that OCT could be used to assess the condition of articular cartilage *in vivo*, using the parameters like ORI and using OCT air jet indentation system. In the future, portable OCT probe for *in vivo* tissue investigation can hopefully be developed.

Ultrasound may also potentially be used as clinical devices, measuring the surface conditions by obtaining the URI parameter and using portable ultrasound water jet to assess the mechanical properties. Also clinically used sterilized saline pump may be an alternative to eject the liquid.

The possible effects arising from indentation tests and the immersing of the samples in physiological saline at room temperature for several hours on the

morphological, acoustic and mechanical properties of articular cartilage also need to be carefully examined in future studies.

In summary, OCT and ultrasound could be used as useful tools to quantitatively investigate the optical (OCT), morphological, acoustic (ultrasound) and mechanical properties of articular cartilage. The combination of these two techniques may provide a comprehensive assessment of articular cartilage and has a bright future in the field of *in vivo* tissue studies.

REFERENCES

Abdel-Hamid M Z, Chang C H, Chan Y S, Lo Y P, Huang J W, Hsu K Y and Wang C J 2006 Arthroscopic evaluation of soft tissue injuries in tibial plateau fractures: Retrospective analysis of 98 cases *Arthroscopy-the Journal of Arthroscopic and Related Surgery* **22** 669-75

Adams S B, Herz P R, Stamper D L, Roberts M J, Bourquin S, Patel N A, Schneider K, Martin S D, Shortkroff S, Fujimoto J G and Brezinski M E 2006 High-resolution imaging of progressive articular cartilage degeneration *Journal of Orthopaedic Research* **24** 708-15

Adler R S, Dedrick D K, Laing T J, Chiang E H, Meyer C R, Bland P H and Rubin J M 1992 Quantitative Assessment of Cartilage Surface-Roughness in Osteoarthritis Using High-Frequency Ultrasound *Ultrasound in Medicine and Biology* **18** 51-8

Agemura D H, Obrien W D, Olerud J E, Chun L E and Eyre D E 1990 Ultrasonic Propagation Properties of Articular-Cartilage at 100 Mhz *Journal of the Acoustical Society of America* **87** 1786-91

Al-Ahalabi S A, Culshaw B and Davies D E N 1983 Partially coherent sources in interferometric sensors *Proceedings of the First International Conference on Optical Fibre Sensors*

Appleyard R C, Swain M V, Khanna S and Murrell G A C 2001 The accuracy and reliability of a novel handheld dynamic indentation probe for analysing articular cartilage *Physics in medicine and biology* **46** 541-50

Armstrong C G and Mow V C 1982 Variations in the intrinsic mechanical properties of human articular cartilage with age, degeneration, and water content *The Journal of Bone and Joint Surgery* **64** 88-94

Arokoski J P A, Hyttinen M M, Lapvetelainen T, Takacs P, Kosztbaczky B, Modis L, Kovanen V and Helminen H J 1996 Decreased birefringence of the superficial zone collagen network in the canine knee (stifle) articular cartilage after long distance running training, detected by quantitative polarised light microscopy *Annals of the Rheumatic Diseases* **55** 253-64

Ateshian G A, Soslowsky L J and Mow V C 1991 Quantitation of Articular Surface-Topography and Cartilage Thickness in Knee Joints Using Stereophotogrammetry *Journal of biomechanics* **24** 761-76

Athanasiou K A, Rosenwasser M P, Buckwalter J A, Malinin T I and Mow V C 1991 Interspecies comparisons of in situ intrinsic mechanical

properties of distal femoral cartilage *Journal of Orthopaedic Research* **9** 330-40

Bader D L and Bowker P 1983 Mechanical Characteristics of Skin and Underlying Tissues Invivo *Biomaterials* **4** 305-8

Bader D L and Kempson G E 1994 The short-term compressive properties of adult human articular cartilage *Biomedical materials and engineering* **4** 245-56

Bader D L, Kempson G E, Egan J, Gilbey W and Barrett A J 1992 The effects of selective matrix degradation on the short-term compressive properties of adult human articular cartilage *Biochimica et biophysica acta* **1116** 147-54

Bae W C, Lewis C W, Levenston M E and Sah R L 2006 Indentation testing of human articular cartilage: Effects of probe tip geometry and indentation depth on intra-tissue strain *Journal of biomechanics* **39** 1039-47

Bae W C, Temple M A, Amiel D, Coutts R D, Niederauer G G and Sah R L 2003 Indentation testing of human cartilage - Sensitivity to articular surface degeneration *Arthritis and rheumatism* **48** 3382-94

Bank R A, Soudry M, Maroudas A, Mizrahi J and TeKoppele J M 2000 The increased swelling and instantaneous deformation of osteoarthritic cartilage is highly correlated with collagen degradation *Arthritis and rheumatism* **43** 2202-10

Barthez P Y, Bais R J and Vernooij J C M 2007 Effect of ultrasound beam angle on equine articular cartilage thickness measurement *Veterinary Radiology & Ultrasound* **48** 457-9

Bashir A, Gray M L, Hartke J and Burstein D 1999 Nondestructive imaging of human cartilage glycosaminoglycan concentration by MRI *Magnet Reson Med* **41** 857-65

Batiste D L, Kirkley A, Laverty S, Thain L M F, Spouge A R and Holdsworth D W 2004 Ex vivo characterization of articular cartilage and bone lesions in a rabbit ACL transection model of osteoarthritis using MRI and micro-CT *Osteoarthr Cartilage* **12** 986-96

Behrens F, Kraft E L and Oegema T R 1989 Biochemical-Changes in Articular-Cartilage after Joint Immobilization by Casting or External Fixation *Journal of Orthopaedic Research* **7** 335-43

Benedek T G 2006 A history of the understanding of cartilage *Osteoarthr Cartilage* **14** 203-9

Bolin F P, Preuss L E, Taylor R C and Ference R J 1989 Refractive-Index of Some Mammalian-Tissues Using a Fiber Optic Cladding Method *Appl Optics* **28** 2297-303

Boppart S A, Bouma B E, Pitris C, Tearney G J, Fujimoto J G and Brezinski M E 1997 Forward-imaging instruments for optical coherence tomography *Optics Letters* **22** 1618-20

Borrelli J, Torzilli P A, Grigiene R and Helfet D L 1997 Effect of impact load on articular cartilage: Development of an intra-articular fracture model *Journal of Orthopaedic Trauma* **11** 319-26

Bouma B E, Tearney G J, Compton C C and Nishioka N S 2000 High-resolution imaging of the human esophagus and stomach in vivo using optical coherence tomography *Gastrointest Endosc* **51** 467-74

Brezinski M E 2006 *Optical coherence tomography: principles and applications*: Elsevier Inc.)

Brown C C, Hughes S W, Crawford R W and Oloyede A 2007 Ultrasound Assessment of Articular Cartilage: Analysis of the Frequency Profile of Reflected Signals from Naturally and Artificially Degraded Samples *Connective Tissue Research* **48** 277-85

Brown C P, Hughes S W, Crawford R W and Oloyede A 2008 Joint laminate degradation assessed by reflected ultrasound from the cartilage surface and osteochondral junction *Physics in medicine and biology* **53** 4123-35

Buckwalter J A and Mankin H J 1997 Articular cartilage .2. Degeneration and osteoarthrosis, repair, regeneration, and transplantation *Journal of Bone and Joint Surgery-American Volume* **79A** 612-32

Burstein D, Bashir A and Gray M L 2000 MRI techniques in early stages of cartilage disease *Investigative Radiology* **35** 622-38

Burstein D and Gray M 2003 New MRI techniques for imaging cartilage *Journal of Bone and Joint Surgery-American Volume* **85A** 70-7

Chao J and Kalunian K 2008 Ultrasonography in osteoarthritis: recent advances and prospects for the future *Curr Opin Rheumatol* **20** 560-4

Chen A C, Bae W C, Schinagl R M and Sah R L 2001a Depth- and strain-dependent mechanical and electromechanical properties of full-thickness bovine articular cartilage in confined compression *Journal of biomechanics* **34** 1-12

Chen S S, Falcovitz Y H, Schneiderman R, Maroudas A and Sah R L 2001b Depth-dependent compressive properties of normal aged human

femoral head articular cartilage: relationship to fixed charge density *Osteoarthritis and cartilage / OARS, Osteoarthritis Research Society* **9** 561-9

Cherin E, Saied A, Laugier P, Netter P and Berger G 1998 Evaluation of acoustical parameter sensitivity to age-related and osteoarthritic changes in articular cartilage using 50-MHz ultrasound *Ultrasound in Medicine and Biology* **24** 341-54

Cherin E, Saied A, Pellaumail B, Loeuille D, Laugier P, Gillet P, Netter P and Berger G 2001 Assessment of rat articular cartilage maturation using 50-MHz quantitative ultrasonography *Osteoarthr Cartilage* **9** 178-86

Chiang E H, Laing T J, Meyer C R, Boes J L, Rubin J M and Adler R S 1997 Ultrasonic characterization of in vitro osteoarthritic articular cartilage with validation by confocal microscopy *Ultrasound in Medicine and Biology* **23** 205-13

Cho N, Tsukada T and Takahashi M 1995 Measurement of Surface-Roughness with Small Waviness by Contact Stylus Instrument Correcting Specimen Orientation *Int J Jpn S Prec Eng* **29** 74-9

Chu C R, Izzo N J, Irrgang J J, Ferretti M and Studer R K 2007 Clinical diagnosis of potentially treatable early articular cartilage degeneration using optical coherence tomography *Journal of Biomedical Optics* **12** 051703

Chu C R, Lin D, Geisler J L, Chu C T, Fu F H and Pan Y T 2004 Arthroscopic microscopy of articular cartilage using optical coherence tomography *Am J Sport Med* **32** 699-709

Clark J M 1990 The Organization of Collagen Fibrils in the Superficial Zones of Articular-Cartilage *J Anat* **171** 117-30

Cohn N A, Emelianov S Y, Lubinski M A and ODonnell M 1997a An elasticity microscope .1. Methods *Ieee Transactions on Ultrasonics Ferroelectrics and Frequency Control* **44** 1304-19

Cohn N A, Emelianov S Y and ODonnell M 1997b An elasticity microscope .2. Experimental results *Ieee Transactions on Ultrasonics Ferroelectrics and Frequency Control* **44** 1320-31

Collins G W, Letts S A, Fearon E M, Mceachern R L and Bernat T P 1994 Surface-Roughness Scaling of Plasma Polymer-Films *Phys Rev Lett* **73** 708-11

Dashefsky J H 1987 Arthroscopic measurement of chondromalacia of patella cartilage using a microminiature pressure transducer *Arthroscopy* **3** 80-5

Davis J, Bliss C and Szivek J 2006 Optical coherence tomography development and use to identify articular cartilage tissue and cell stratification. *Journal of Investigative Medicine* **54** S114

Demarteau O, Pillet L, Inaebnit A, Borens O and Quinn T M 2006 Biomechanical characterization and in vitro mechanical injury of elderly human femoral head cartilage: comparison to adult bovine humeral head cartilage *Osteoarthr Cartilage* **14** 589-96

Donnan F G 1924 The theory of membrane equilibria *Chem Rev* **1** 73-90

Donnan F G 1995 Theory of Membrane Equilibria and Membrane-Potentials in the Presence of Non-Dialyzing Electrolytes - a Contribution to Physical-Chemical Physiology (Reprinted from Zeitshrift Fur Elektrochemie Und Angewandte Physikalische Chemie, Vol 17, Pg 572, 1911) *J Membrane Sci* **100** 45-55

Drexler W, Stamper D, Jesser C, Li X D, Pitris C, Saunders K, Martin S, Lodge M B, Fujimoto J G and Brezinski M E 2001 Correlation of collagen organization with polarization sensitive imaging of in vitro cartilage: Implications for osteoarthritis *Journal of Rheumatology* **28** 1311-8

Eder K, Schmitt R and Muller-Rath R 2008 Imaging of artificial cartilage with optical coherence tomography *Optics in Tissue Engineering and Regenerative Medicine II* **6858** J8580

Federico S and Herzog W 2008 On the anisotropy and inhomogeneity of permeability in articular cartilage *Biomechanics and Modeling in Mechanobiology* **7** 367-78

Fergusonpell M, Hagisawa S and Masiello R D 1994 A Skin Indentation System Using a Pneumatic Bellows *J Rehabil Res Dev* **31** 15-9

Fink M A and Cardoso J F 1984 Diffraction Effects in Pulse-Echo Measurement *Ieee T Son Ultrason* **31** 313-29

Forman M D, Malamet R and Kaplan D 1983 A survey of osteoarthritis of the knee in the elderly *The Journal of rheumatology* **10** 282-7

Forster H and Fisher J 1996 The influence of loading time and lubricant on the friction of articular cartilage *Proceedings of the institution of mechanical engineers part b journal of engineering manufacture* **210** 109-19

Fortin M, Soulhat J, Shirazi-Adl A, Hunziker E B and Buschmann M D 2000 Unconfined compression of articular cartilage: Nonlinear behavior and comparison with a fibril-reinforced biphasic model

Journal of Biomechanical Engineering-Transactions of the Asme **122** 189-95

Fournier C, Bridal S L, Berger G and Laugier P 2001 Reproducibility of skin characterization with backscattered spectra (12-25 MHz) in healthy subjects *Ultrasound in Medicine and Biology* **27** 603-10

Fournier C, Bridal S L, Coron A and Laugier P 2003 Optimization of attenuation estimation in reflection for in vivo human dermis characterization at 20 MHz *Ieee Transactions on Ultrasonics Ferroelectrics and Frequency Control* **50** 408-18

Gahm T and Witte S 1986 Measurement of the Optical-Thickness of Transparent Tissue Layers *Journal of Microscopy-Oxford* **141** 101-10

Galbraith P C and Bryant J T 1989 Effects of Grid Dimensions on Finite-Element Models of an Articular Surface *Journal of biomechanics* **22** 385-93

Giraudeau B, Gomez M A and Defontaine M 2003 Assessing the reproducibility of quantitative ultrasound parameters with standardized coefficient of variation or intraclass correlation coefficient: a unique approach *Osteoporosis International* **14** 614-5

Gluer C C, Blake G, Lu Y, Blunt B A, Jergas M and Genant H K 1995 Accurate Assessment of Precision Errors - How to Measure the Reproducibility of Bone Densitometry Techniques *Osteoporosis International* **5** 262-70

Grassi W and Cervini C 1998 Ultrasonography in rheumatology: an evolving technique *Annals of the Rheumatic Diseases* **57** 268-71

Guilak F, Ratcliffe A, Lane N, Rosenwasser M P and Mow V C 1994 Mechanical and Biochemical-Changes in the Superficial Zone of Articular-Cartilage in Canine Experimental Osteoarthritis *Journal of Orthopaedic Research* **12** 474-84

Guilak F, Ratcliffe A and Mow V C 1995 Chondrocyte Deformation and Local Tissue Strain in Articular-Cartilage - a Confocal Microscopy Study *Journal of Orthopaedic Research* **13** 410-21

Guo X, Lam W L and Zheng Y P 2005 Rapid and quantified decalcification of bone: apparatus and methods **No. 10/510,450**

Han C W, Chu C R, Adachi N, Usas A, Fu F H, Huard J and Pan Y 2003a Analysis of rabbit articular cartilage repair after chondrocyte implantation using optical coherence tomography *Osteoarthr Cartilage* **11** 111-21

Han L H, Noble J A and Burcher M 2003b A novel ultrasound indentation system for measuring biomechanical properties of in vivo soft tissue *Ultrasound in Medicine and Biology* **29** 813-23

Harris E D, Jr., Parker H G, Radin E L and Krane S M 1972 Effects of proteolytic enzymes on structural and mechanical properties of cartilage *Arthritis and rheumatism* **15** 497-503

Hattori K, Ikeuchi K, Morita Y and Takakura Y 2005a Quantitative ultrasonic assessment for detecting microscopic cartilage damage in osteoarthritis *Arthritis Res Ther* **7** R38-46

Hattori K, Takakura Y, Ishimura M, Habata T, Uematsu K and Ikeuch K 2004 Quantitative arthroscopic ultrasound evaluation of living human cartilage *Clinical Biomechanics* **19** 213-6

Hattori K, Takakura Y, Ishimura M, Tanaka Y, Habata T and Ikeuchi K 2005b Differential acoustic properties of early cartilage lesions in living human knee and ankle joints *Arthritis and rheumatism* **52** 3125-31

Hayes W C, Herrmann G, Mockros L F and Keer L M 1972 A Mathematical Analysis for Indentation Tests of Articular Cartilage *Journal of biomechanics* **5** 541-51

Herrmann J M, Pitris C, Bouma B E, Boppart S A, Jesser C A, Stamper D L, Fujimoto J G and Brezinski M E 1999 High resolution imaging of normal and osteoarthritic cartilage with optical coherence tomography *Journal of Rheumatology* **26** 627-35

Herz P, Bourquin S, Hsiung P L, Ko T, Schneider K, Fujimoto J, Adams S, Roberts M, Patel N and Brezinski M 2003 Imaging of cartilage degeneration in vivo using ultrahigh resolution OCT *Optical Coherence Tomography and Coherence Techniques* **5140** 152-4

Hildebra.Bp, Gordon R L and Allen E V 1974 Instrument for Measuring Roughness of Supersmooth Surfaces *Appl Optics* **13** 177-80

Hu K, Radhakrishnan P, Patel R V and Mao J J 2001 Regional Structural and Viscoelastic Properties of Fibrocartilage upon Dynamic Nanoindentation of the Articular Condyle *Journal of Structural Biology* **136** 46-52

Huang D, Swanson E A, Lin C P, Schuman J S, Stinson W G, Chang W, Hee M R, Flotte T, Gregory K, Puliafito C A and Fujimoto J G 1991 Optical Coherence Tomography *Science* **254** 1178-81

Huang Y P 2004 Ultrasonic Assessment of Post-radiotheraoy Fibrosis MPhil Thesis *Jockey Club Rehabilitation Engineering Center*

Huang Y P, Zheng Y P, Wang S Z, Chen Z P, Huang Q H and He Y H 2009 An optical coherenece tomography (OCT)-based air jet indentation system for measuring mechanical properties of soft tissues *Measurement Science and Technology* 015805

Huisman H J and Thijssen J M 1996 Precision and accuracy of acoustospectrographic parameters *Ultrasound in Medicine and Biology* **22** 855-71

Hunziker E B 1992 *Articular cartilage and osteoarthritis*, ed K E Kuettner, *et al.* (New York: Raven Press)

Hunziker E B, Quinn T M and Hauselmann H J 2002 Quantitative structural organization of normal adult human articular cartilage *Osteoarthr Cartilage* **10** 564-72

Jackle S, Gladkova N, Feldchtein F, Terentieva A, Brand B, Gelikonov G, Gelikonov V, Sergeev A, Fritscher-Ravens A, Freund J, Seitz U, Schroder S and Soehendra N 2000 In vivo endoscopic optical coherence tomography of esophagitis, Barrett's esophagus, and adenocarcinoma of the esophagus *Endoscopy* **32** 750-5

Jaffre B, Watrin A, Loeuille D, Gillet P, Netter P, Laugier P and Saied A 2003 Effects of antiinflammatory drugs on arthritic cartilage - A high-frequency quantitative ultrasound study in rats *Arthritis and rheumatism* **48** 1594-601

Jago J R and Whittingham T A 1992 The Use of Measured Acoustic Speed Distributions in Reflection Ultrasound Ct *Physics in medicine and biology* **37** 2139-42

Jin H and Lewis J L 2004 Determination of Poisson's ratio of articular cartilage by indentation using different-sized indenters *Journal of Biomechanical Engineering-Transactions of the Asme* **126** 138-45

Joiner G A, Bogoch E R, Pritzker K P, Buschmann M D, Chevrier A and Foster F S 2001 High frequency acoustic parameters of human and bovine articular cartilage following experimentally-induced matrix degradation *Ultrasonic Imaging* **23** 106-16

Julkunen P, Kiviranta P, Wilson W, Jurvelin J S and Korhonen R K 2007 Characterization of articular cartilage by combining microscopic analysis with a fibril-reinforced finite-element model *Journal of biomechanics* **40** 1862-70

Julkunen P, Korhonen R K, Herzog W and Jurvelin J S 2008 Uncertainties in indentation testing of articular cartilage: A fibril-reinforced poroviscoelastic study *Med Eng Phys* **30** 506-15

Jun M C, Kim Y S, Han M K, Kim J W and Kim K B 1995 Polycrystalline Silicon Oxidation Method Improving Surface-Roughness at the Oxide Polycrystalline Silicon Interface *Appl Phys Lett* **66** 2206-8

Jurvelin J S, Buschmann M D and Hunziker E B 2003 Mechanical anisotropy of the human knee articular cartilage in compression *Proceedings of the Institution of Mechanical Engineers, Part H: Journal of Engineering in Medicine* **217** 215-9

Jurvelin J S, Rasanen T, Kolmonen P and Lyyra T 1995 Comparison of Optical, Needle Probe and Ultrasonic Techniques for the Measurement of Articular-Cartilage Thickness *Journal of biomechanics* **28** 231-5

Kaleva E, Saarakkala S, Toyras J, Nieminen H J and Jurvelin J S 2008 In-Vitro Comparison of Time-Domain, Frequency-Domain and Wavelet Ultrasound Parameters in Diagnostics of Cartilage Degeneration *Ultrasound in medicine & biology* **34** 155-9

Kaplan P A, Matamoros A and Anderson J C 1990 Sonography of the Musculoskeletal System *Am J Roentgenol* **155** 237-45

Karpie J C and Chu C R 2006 Imaging of articular cartilage *Operative Techniques in Orthopaedics* **16** 279-85

Kempson G E, Muir H, Pollard C and Tuke M 1973 The tensile properties of the cartilage of human femoral condyles related to the content of collagen and glycosaminoglycans *Biochimica et Biophysica Acta (BBA) - General Subjects* **297** 456-72

Kiefer G N, Sundby K, Mcallister D, Shrive N G, Frank C B, Lam T and Schachar N S 1989 The Effect of Cryopreservation on the Biomechanical Behavior of Bovine Articular-Cartilage *Journal of Orthopaedic Research* **7** 494-501

Kikuchi T, Sakuta T and Yamaguchi T 1998 Intra-articular injection of collagenase induces experimental osteoarthritis in mature rabbits *Osteoarthr Cartilage* **6** 177-86

Kiviranta P, Lammentausta E, Toyras J, Kiviranta I and Jurvelin J S 2008 Indentation diagnostics of cartilage degeneration *Osteoarthr Cartilage* **16** 796-804

Kiviranta P, Rieppo J, Korhonen R K, Julkunen P, Toyras J and Jurvelin J S 2006 Collagen network primarily controls Poisson's ratio of bovine articular cartilage in compression *Journal of Orthopaedic Research* **24** 690-9

Korhonen R K, Laasanen M S, Toyras J, Rieppo J, Hirvonen J, Helminen H J and Jurvelin J S 2002 Comparison of the equilibrium response of

articular cartilage in unconfined compression, confined compression and indentation *Journal of biomechanics* **35** 903-9

Kuroki H, Nakagawa Y, Mori K, Kobayashi M, Yasura K, Okamoto Y, Mizuno Y, Ando K, Ikeuchi K and Nakamura T 2006 Maturation-dependent change and regional variations in acoustic stiffness of rabbit articular cartilage: an examination of the superficial collagen-rich zone of cartilage *Osteoarthr Cartilage* **14** 784-92

Kuroki H, Nakagawa Y, Mori K, Kobayashi M, Yasura K, Okamoto Y, Suzuki T, Nishitani K and Nakamura T 2008 Ultrasound properties of articular cartilage in the tibio-femoral joint in knee osteoarthritis: relation to clinical assessment (International Cartilage Repair Society grade) *Arthritis Res Ther* **10** ar2452

Kuroki H, Nakagawa Y, Mori K, Ohba M, Suzuki T, Mizuno Y, Ando K, Takenaka M, Ikeuchi K and Nakamura T 2004 Acoustic stiffness and change in plug cartilage over time after autologous osteochondral grafting: correlation between ultrasound signal intensity and histological score in a rabbit model *Arthritis Res Ther* **6** R492-R504

Laasanen M S, Saarakkala S, Toyras J, Rieppo J and Jurvelin J S 2005 Site-specific ultrasound reflection properties and superficial collagen content of bovine knee articular cartilage *Physics in medicine and biology* **50** 3221-33

Laasanen M S, Toyras J, Hirvonen J, Saarakkala S, Korhonen R K, Nieminen M T, Kiviranta I and Jurvelin J S 2002 Novel mechano-acoustic technique and instrument for diagnosis of cartilage degeneration *Physiological Measurement* **23** 491-503

Laasanen M S, Toyras J, Vasara A, Saarakkala S, Hyttinen M M, Kiviranta I and Jurvelin J S 2006 Quantitative ultrasound imaging of spontaneous repair of porcine cartilage *Osteoarthr Cartilage* **14** 258-63

Langsjo T K, Hyttinen M, Pelttari A, Kiraly K, Arokoski J and Helminen H J 1999 Electron microscopic stereological study of collagen fibrils in bovine articular cartilage: volume and surface densities are best obtained indirectly (from length densities and diameters) using isotropic uniform random sampling *J Anat* **195** 281-93

Laurent D, Wasvary J, Rudin M, O'Byrne E and Pellas T 2003 In vivo assessment of macromolecular content in articular cartilage of the goat knee *Magnet Reson Med* **49** 1037-46

Lawrence J S, Bremner J M and Bier F 1966 Osteo-Arthrosis - Prevalence in Population and Relationship between Symptoms and X-Ray Changes *Annals of the Rheumatic Diseases* **25** 1-24

Lee C L, Huang M H, Chai C Y, Chen C H, Su J Y and Tien Y C 2008 The validity of in vivo ultrasonographic grading of osteoarthritic femoral condylar cartilage: a comparison with in vitro ultrasonographic and histologic gradings *Osteoarthr Cartilage* **16** 352-8

Legare A, Garon M, Guardo R, Savard P, Poole A R and Buschmann M D 2002 Detection and analysis of cartilage degeneration by spatially resolved streaming potentials *Journal of Orthopaedic Research* **20** 819-26

Leung K S, Qin L, Leung M C T, Fu L L K and Chan C W 1999 Partial patellectomy induces a decrease in the proteoglycan content in the remaining patellar articular cartilage. An experimental study in rabbits *Clin Exp Rheumatol* **17** 597-600

Levin G G, Kovalev A A, Minaev V L and Sukhorukov K A 2004 Error in measuring dry cell mass with a computerized interference microscope *Measurement Techniques* **47** 412-6

Li X D, Martin S, Pitris C, Ghanta R, Stamper D L, Harman M, Fujimoto J G and Brezinski M E 2005 High-resolution optical coherence tomographic imaging of osteoarthritic cartilage during open knee surgery *Arthritis Res Ther* **7** R318-R23

Li X D, Stamper D, Patel N, Saunders K, Plummer S, Schenck J, Rogowska L, Fujimoto J and Brezinski M 2001 OCT imaging of the musculoskeletal and cardiovascular systems *Saratov Fall Meeting 2001: Optical Technologies in Biophysics and Medicine III* **4707** 9-15

Ling H Y, Zheng Y P and Patil S G 2007 Strain dependence of ultrasound speed in bovine articular cartilage under compression in vitro *Ultrasound in Medicine and Biology* **33** 1599-608

Link T M, Steinbach L S, Ghosh S, Ries M, Lu Y, Lane N and Majumdar S 2002 Osteoarthritis: MR Imaging Findings in Different Stages of Disease and Correlation with Clinical Findings *Radiology* **226** 373 - 81

Lizzi F L, Greenebaum M, Feleppa E J, Elbaum M and Coleman D J 1983 Theoretical Framework for Spectrum Analysis in Ultrasonic Tissue Characterization *Journal of the Acoustical Society of America* **73** 1366-73

Logothetidis S and Stergioudis G 1997 Studies of density and surface roughness of ultrathin amorphous carbon films with regards to

thickness with x-ray reflectometry and spectroscopic ellipsometry *Appl Phys Lett* **71** 2463-5

Lu M H 2006 Development of a noncontact ultrasound indentation system for measuring tissue material properties using water jet Ph.D Thesis *Department of Health Technology and Informatics*

Lu M H, Zheng Y P and Huang Q H 2005 A novel noncontact ultrasound indentation system for measurement of tissue material properties using water jet compression *Ultrasound in Medicine and Biology* **31** 817-26

Lu M H, Zheng Y P and Huang Q H 2007 A novel method to obtain modulus image of soft tissues using ultrasound water jet indentation: A phantom study *IEEE Transactions on Biomedical Engineering* **54** 114-21

Lu M H, Zheng Y P, Huang Q H, Ling H Y, Wang Q, Bridal S L, Qin L and Mak A F 2009 Noncontact Evaluation of Articular Cartilage Degeneration Using a Novel Ultrasound Water Jet Indentation System *Annals of Biomedical Engineering* **37** 164-75

Lyons T J, McClure S F, Stoddart R W and McClure J 2006 The normal human chondro-osseous junctional region: evidence for contact of uncalcified cartilage with subchondral bone and marrow spaces *Bmc Musculoskeletal Disorders* **7**

Lyyra T, Arokoski J P A, Oksala N, Vihko A, Hyttinen M, Jurvelin J S and Kiviranta I 1999 Experimental validation of arthroscopic cartilage stiffness measurement using enzymatically degraded cartilage samples *Physics in medicine and biology* **44** 525-35

Madsen S J, Chu E A and Wong B J F 1999 The optical properties of porcine nasal cartilage *IEEE Journal of Selected Topics in Quantum Electronics* **5** 1127-33

Mak A F, Lai W M and Mow V C 1987 Biphasic Indentation of Articular-Cartilage .1. Theoretical-Analysis *Journal of biomechanics* **20** 703-14

Mankin H J and Thrasher A Z 1975 Water-Content and Binding in Normal and Osteoarthritic Human Cartilage *Journal of Bone and Joint Surgery-American Volume* **A 57** 76-80

Mansfield J C, Ugryumova N, Knapp K M and Matcher S J 2006 The collagen structure of equine articular cartilage, characterized using polarization-sensitive optical coherence tomography and non-linear microscopy - art. no. 604715 *Fourth International Conference on Photonics and Imaging in Biology and Medicine, Pts 1 and 2* **6047** 4715

Maroudas A and Venn M 1977 Chemical composition and swelling of normal and osteoarthrotic femoral head cartilage. II. Swelling. pp 399-406

Mathiesen O, Konradsen L, Torp-Pedersen S and Jorgensen U 2004 Ultrasonography and articular cartilage defects in the knee: an in vitro evaluation of the accuracy of cartilage thickness and defect size assessment *Knee Surgery Sports Traumatology Arthroscopy* **12** 440-3

Mattson L and Wagberg P 1993 Assessment of Surface Finish on Bulk Scattering Materials - a Comparison between Optical Laser Stylus and Mechanical Stylus Profilometers *Precis Eng* **15** 141-9

Modest V E, Murphy M C and Mann R W 1989 Optical Verification of a Technique for Insitu Ultrasonic Measurement of Articular-Cartilage Thickness *Journal of biomechanics* **22** 171-6

Modis L 1991 *Organization of the Extracellular Matrix: A Polarization Microscopic Approach* (Boca Raton: CRC Press)

Morrison E 1995 A Prototype Scanning Stylus Profilometer for Rapid Measurement of Small Surface-Areas *Int J Mach Tool Manu* **35** 325-31

Moskowitz R W, Altman R D, Hochberg M C, Buckwalter J A and Goldberg V M 2007 *Osteoarthritis: Diagnosis and Medical/ Surgical Management* (Philadelphia: LIPPINCOTT WILLIAMS)

Mow V and Guo X E 2002 Mechano-electrochemical properties of articular cartilage: Their inhomogeneities and anisotropies *Annual Review of Biomedical Engineering* **4** 175-209

Mow V C, Gu W Y and Chen F H 2005 *Basic Orthopaedic Biomechanics and Mechano-Biology - 3rd ed*, ed V Mow, Huiskes, R

Mow V C, Kuei S C, Lai W M and Armstrong C G 1980 Biphasic Creep and Stress-Relaxation of Articular-Cartilage in Compression - Theory and Experiments *Journal of Biomechanical Engineering-Transactions of the Asme* **102** 73-84

Mow VC Z W, Ratcliffe A ed 1991 *Structure and function of articular cartilage and meniscus* (New York: Raven Press)

Mui L W, Engelsohn E and Umans H 2007 Comparison of CT and MRI in patients with tibial plateau fracture: can CT findings predict ligament tear or meniscal injury? *Skeletal Radiology* **36** 145-51

Myers E R, Lai W M and Mow V C 1984 A Continuum Theory and an Experiment for the Ion-Induced Swelling Behavior of Articular-Cartilage *Journal of Biomechanical Engineering-Transactions of the Asme* **106** 151-8

Myers S L, Dines K, Brandt D A, Brandt K D and Albrecht M E 1995 Experimental Assessment by High-Frequency Ultrasound of Articular-Cartilage Thickness and Osteoarthritic Changes *Journal of Rheumatology* **22** 109-16

Narmoneva D A, Wang J Y and Setton L A 1999 Nonuniform swelling-induced residual strains in articular cartilage *Journal of biomechanics* **32** 401-8

Narmoneva D A, Wang J Y and Setton L A 2001 A noncontacting method for material property determination for articular cartilage from osmotic loading *Biophysical Journal* **81** 3066-76

Nassif N A, Pierce M C, Park B H, Cense B and de Boer J F 2004 Evaluation of osteoarthritis progression using polarization-sensitive optical coherence tomography *Advanced Biomedical and Clinical Diagnostic Systems Ii* **5318** 170-5

Nieminen H J, Julkunen P, Toyras J and Jurvelin J S 2007 Ultrasound speed in articular cartilage under mechanical compression *Ultrasound in Medicine and Biology* **33** 1755-66

Nieminen H J, Saarakkala S, Laasanen M S, Hirvonen J, Jurvelin J S and Toyras J 2004 Ultrasound attenuation in normal and spontaneously degenerated articular cartilage *Ultrasound in Medicine and Biology* **30** 493-500

Nieminen H J, Toyras J, Laasanen M S and Jurvelin J S 2006 Acoustic properties of articular cartilage under mechanical stress *Biorheology* **43** 523-35

Nieminen H J, Toyras J, Rieppo J, Nieminen M T, Hirvonen J, Korhonen R and Jurvelin J S 2002 Real-time ultrasound analysis of articular cartilage degradation in vitro *Ultrasound in Medicine and Biology* **28** 519-25

Nieminen M T, Rieppo J, Toyras J, Hakumaki J M, Silvennoinen J, Hyttinen M M, Helminen H J and Jurvelin J S 2001 T-2 relaxation reveals spatial collagen architecture in articular cartilage: A comparative quantitative MRI and polarized light microscopic study *Magnet Reson Med* **46** 487-93

Nieminen M T, Toyras J, Rieppo J, Hakumaki J M, Silvennoinen J, Helminen H J and Jurvelin J S 2000 Quantitative MR microscopy of

enzymatically degraded articular cartilage *Magnet Reson Med* **43** 676-81

Nissi M J, Rieppo J, Toyras J, Laasanen M S, Kiviranta I, Nieminen M T and Jurvelin J S 2007 Estimation of mechanical properties of articular cartilage with MRI - dGEMRIC, T-2 and T-1 imaging in different species with variable stages of maturation *Osteoarthr Cartilage* **15** 1141-8

Nitta N and Shiina T 2002 A visualization of nonlinear elasticity property of tissues by ultrasound *Electronics and Communications in Japan* **85** 9-18

Ophir J, Cespedes I, Ponnekanti H, Yazdi Y and Li X 1991 Elastography - a Quantitative Method for Imaging the Elasticity of Biological Tissues *Ultrasonic Imaging* **13** 111-34

Pan Y T, Li Z G, Xie T Q and Chu C R 2003 Hand-held arthroscopic optical coherence tomography for in vivo high-resolution imaging of articular cartilage *Journal of Biomedical Optics* **8** 648-54

Park S, Hung C T and Ateshian G A 2004 Mechanical response of bovine articular cartilage under dynamic unconfined compression loading at physiological stress levels *Osteoarthr Cartilage* **12** 65-73

Park S, Nicoll S B, Mauck R L and Ateshian G A 2008 Cartilage mechanical response under dynamic compression at physiological stress levels following collagenase digestion *Annals of Biomedical Engineering* **36** 425-34

Passariello R, Trecco F, Depaulis F, Bonanni G, Masciocchi C and Zobel B B 1983 Computed-Tomography of the Knee-Joint - Technique of Study and Normal Anatomy *Journal of Computer Assisted Tomography* **7** 1035-42

Patel N A, Zoeller J, Stamper D L, Fujimoto J G and Brezinski M E 2005 Monitoring osteoarthritis in the rat model using optical coherence tomography *IEEE T Med Imaging* **24** 155-9

Patil S G 2004 Measurement of the Sound Speed in Articular Cartilage In-Vitro MPhil Thesis *Jockey Club Rehabilitation Engineering Center*

Patil S G, Zheng Y P, Wu J Y and Shi J 2004 Measurement of depth-dependence and anisotropy of ultrasound speed of bovine articular cartilage in vitro *Ultrasound in Medicine and Biology* **30** 953-63

Pellaumail B, Watrin A, Loeuille D, Netter P, Berger G, Laugier P and Saied A 2002 Effect of articular cartilage proteoglycan depletion on high frequency ultrasound backscatter *Osteoarthr Cartilage* **10** 535-41

Peterfy C G, Dicarlo J C and Kothari M 2007 *Osteoarthritis : diagnosis and medical/surgical management 4th edition,* ed R W Moskowitz, *et al.* (Philadelphia: Lippincott Williams & Wilkins)

Pethica J B, Hutchings R and Oliver W C 1983 Hardness Measurement at Penetration Depths as Small as 20-Nm *Philosophical Magazine a-Physics of Condensed Matter Structure Defects and Mechanical Properties* **48** 593-606

Podoleanu A G 2005 Optical coherence tomography *British Journal of Radiology* **78** 976-88

Poon C Y and Bhushan B 1995 Comparison of surface roughness measurements by stylus profiler, AFM and non-contact optical profiler *Wear* **190** 76-88

Qin L, Zheng Y P, Leung C T, Mak A, Choy W Y and Chan K M 2002 Ultrasound detection of trypsin-treated articular cartilage: its association with cartilaginous proteoglycans assessed by histological and biochemical methods *J Bone Miner Metab* **20** 281-7

Rapp S R, Rejeski W J and Miller M E 2000 Physical function among older adults with knee pain: The role of pain coping skills *Arthrit Care Res* **13** 270-9

Rauscher I, Stahl R, Cheng J, Li X, Huber M B, Luke A, Majumdar S and Link T M 2008 Meniscal Measurements of T1 and T2 at MR Imaging in Healthy Subjects and Patients with Osteoarthritis *Radiology* **249** 591-600

Ribbens W B 1969 Interferometric Surface Roughness Measurement *Appl Optics* **8** 2173-6

Risbud M V and Sittinger M 2002 Tissue engineering: advances in in vitro cartilage generation *Trends in biotechnology* **20** 351-6

Roberjot V, Bridal S L, Laugier P and Berger G 1996 Absolute backscatter coefficient over a wide range of frequencies in a tissue-mimicking phantom containing two populations of scatterers *Ieee Transactions on Ultrasonics Ferroelectrics and Frequency Control* **43** 970-8

Roberts M J, Adams S B, Patel N A, Stamper D L, Westmore M S, Martin S D, Fujimoto J G and Brezinski M E 2003 A new approach for assessing early osteoarthritis in the rat *Anal Bioanal Chem* **377** 1003-6

Rogowska J and Brezinski M E 2002 Image processing techniques for noise removal, enhancement and segmentation of cartilage OCT images *Physics in medicine and biology* **47** 641-55

Rogowska J, Bryant C M and Brezinski M E 2003 Cartilage thickness measurements from optical coherence tomography *J Opt Soc Am A* **20** 357-67

Romano F L, Ambrosano, G. M., Magnani, M. B, Nouer, D. F. 2005 Analysis of the Coefficient of Variation in Shear and Tensile Bond Strength Tests *J Appl Oral Sci* **13** 243-6

Roth V and Mow V C 1980 The Intrinsic Tensile Behavior of the Matrix of Bovine Articular-Cartilage and Its Variation with Age *Journal of Bone and Joint Surgery-American Volume* **62** 1102-17

Saarakkala S 2007 Pre-Clinical Ultrasound Diagnostics of Articular Cartilage and Subchondral Bone Ph.D Thesis *Faculty of Natural and Environmental Sciences*

Saarakkala S, Korhonen R K, Laasanen M S, Toyras J, Rieppo J and Jurvelin J S 2004a Mechano-acoustic determination of Young's modulus of articular cartilage *Biorheology* **41** 167-79

Saarakkala S, Laasanen M S, Jurvelin J S and Toyras J 2006 Quantitative ultrasound imaging detects degenerative changes in articular cartilage surface and subchondral bone *Physics in medicine and biology* **51** 5333-46

Saarakkala S, Toyras J, Hirvonen J, Laasanen M S, Lappalainen R and Jurvelin J S 2004b Ultrasonic quantitation of superficial degradation of articular cartilage *Ultrasound in medicine & biology* **30** 783-92

Saied A, Cherin E, Gaucher H, Laugier P, Gillet P, Floquet J, Netter P and Berger G 1997 Assessment of articular cartilage and subchondral bone: Subtle and progressive changes in experimental osteoarthritis using 50 MHz echography in vitro *Journal of Bone and Mineral Research* **12** 1378-86

Schinagl R M, Gurskis D, Chen A C and Sah R L 1997 Depth-dependent confined compression modulus of full-thickness bovine articular cartilage *J Orthop Res* **15** 499-506

Schmitt J M 1999 Optical coherence tomography (OCT): a review *Selected Topics in Quantum Electronics, IEEE Journal of* **5** 1205-15

Senzig D A, Forster F K and Olerud J E 1992 Ultrasonic-Attenuation in Articular-Cartilage *Journal of the Acoustical Society of America* **92** 676-81

Setton L A, Tohyama H and Mow V C 1998 Swelling and curling behaviors of articular cartilage *Journal of Biomechanical Engineering-Transactions of the Asme* **120** 355-61

Shapiro E M, Borthakur A, Kaufman J H, Leigh J S and Reddy R 2001 Water distribution patterns inside bovine articular cartilage as visualized by H-1 magnetic resonance imaging *Osteoarthr Cartilage* **9** 533-8

Shingleton W D, Hodges D J, Brick P and Cawston T E 1996 Collagenase: a key enzyme in collagen turnover *Biochemistry and cell biology/ Biochimie et biologie cellulaire* **74** 759-75

Song Y, Greve J M, Carter D R, Koo S and Giori N J 2006 Articular cartilage MR imaging and thickness mapping of a loaded knee joint before and after meniscectomy *Osteoarthr Cartilage* **14** 728-37

Spagnolo G S and Paoletti D 1996 Digital speckle correlation for on-line real-time measurement *Optics Communications* **132** 24-8

Suh J K F, Youn I and Fu F H 2001 An in situ calibration of an ultrasound transducer: a potential application for an ultrasonic indentation test of articular cartilage *Journal of biomechanics* **34** 1347-53

Swagerty D L and Hellinger D 2001 Radiographic assessment of osteoarthritis *American Family Physician* **64** 279-86

Tarhan S, Unlu Z and Goktan C 2003 Magnetic resonance imaging and ultrasonographic evaluation of the patients with knee osteoarthritis: a comparative study *Clin Rheumatol* **22** 181-8

Tearney G J, Brezinski M E, Bouma B E, Boppart S A, Pitris C, Southern J F and Fujimoto J G 1997 In vivo endoscopic optical biopsy with optical coherence tomography *Science* **276** 2037-9

Tearney G J, Brezinski M E, Southern J F, Bouma B E, Hee M R and Fujimoto J G 1995 Determination of the Refractive-Index of Highly Scattering Human Tissue by Optical Coherence Tomography *Optics Letters* **20** 2258-60

Thomas R H, Resnick D, Alazraki N P, Daniel D and Greenfield R 1975 Compartmental Evaluation of Osteoarthritis of Knee - Comparative Study of Available Diagnostic Modalities *Radiology* **116** 585-94

Thompson R C, Oegema T R, Lewis J L and Wallace L 1991 Osteoarthrotic Changes after Acute Transarticular Load - an Animal-Model *Journal of Bone and Joint Surgery-American Volume* **73A** 990-1001

Tomlins P H and Wang R K 2005 Theory, developments and applications of optical coherence tomography *Journal of Physics D-Applied Physics* **38** 2519-35

Toyras J, Laasanen M S, Saarakkala S, Lammi M J, Rieppo J, Kurkijarvi J, Lappalainen R and Jurvelin J S 2003 Speed of sound in normal and degenerated bovine articular cartilage *Ultrasound in Medicine and Biology* **29** 447-54

Toyras J, Nieminen H J, Laasanen M S, Nieminen M T, Korhonen R K, Rieppo J, Hirvonen J, Helminen H J and Jurvelin J S 2002 Ultrasonic characterization of articular cartilage *Biorheology* **39** 161-9

Toyras J, Rieppo J, Nieminen M T, Helminen H J and Jurvelin J S 1999 Characterization of enzymatically induced degradation of articular cartilage using high frequency ultrasound *Physics in medicine and biology* **44** 2723-33

Ugryumova N, Attenburrow D P, Winlove C P and Matcher S J 2005 The collagen structure of equine articular cartilage, characterized using polarization-sensitive optical coherence tomography *Journal of Physics D-Applied Physics* **38** 2612-9

Ugryumova N, Gangnus S V and Matcher S J 2006 Variable-angle-of-incidence polarization-sensitive optical coherence tomography: its use to study the 3-D collagen structure of equine articular cartilage. - art. no. 60792C *Coherence Domain Optical Methods and Optical Coherence Tomography in Biomedicine X* **6079** C792

Ugryumova N and Matcher S J 2006 Innovative application of optical techniques to comprehensive study the etiology of osteoarthritis - art. no. 616308 *Saratov Fall Meeting 2005: Optical Technologies in Biophysics and Medicine VII* **6163** 16308

Ugryumova N and Matcher S J 2007 Novel optical imaging technique to determine the 3D structure of collagen fibers in articular cartilage: variable-incidence-angle polarization-sensitive optical coherence tomography. In: *Autumn Meeting of the British-Society-for-Matrix-Biology*, (Keele, ENGLAND: Blackwell Publishing) pp A20-1

Vanderkraan P M, Vitters E L, Vanbeuningen H M, Vandeputte L B A and Vandenberg W B 1990 Degenerative Knee-Joint Lesions in Mice after a Single Intraarticular Collagenase Injection - a New Model of Osteoarthritis *Journal of Experimental Pathology* **71** 19-31

Vannah W M, Drvaric D M, Hastings J A, Strand J A and Harning D M 1999 A method of residual limb stiffness distribution measurement *J Rehabil Res Dev* **36** 1-7

Venkatesh R 2006 Minimal invasive techniques in the management of tibial plateau fractures *Current Orthopaedics* **20** 411-7

Verteramo A and Seedhom B B 2004 Zonal and directional variations in tensile properties of bovine articular cartilage with special reference to strain rate variation *Biorheology* **41** 203-13

Wagner A, Aurich M, Sieber N, Stoessel M, Wetzel W D, Schmuck K, Lohmann M, Reime B, Metge J, Coan P, Bravin A, Arfelli F, Rigon L, Menk R H, Heitner G, Irving T, Zhong Z, Muehleman C and Mollenhauer J A 2004 Options and limitations of joint cartilage imaging: DEI in comparison to MRI and sonography *Nucl Instrum Meth A* **548** 47-53

Wang C C B, Guo X E, Sun D N, Mow V C, Ateshian G A and Hung C T 2002a The functional environment of chondrocytes within cartilage subjected to compressive loading: A theoretical and experimental approach *Biorheology* **39** 11-25

Wang Q 2007 Ultrasonic Characterization of Transient and Inhomogeneous Swelling Behavior and Progeressive Degeneration of Articular Cartilage Ph.D Thesis *Department of Health Technology and Informatics*

Wang Q, Zheng Y P, Leung G, Lam W L, Guo X, Lu H B, Qin L and Mak A F T 2008a Altered osmotic swelling behavior of proteoglycan-depleted bovine articular cartilage using high frequency ultrasound *Physics in medicine and biology* **53** 2537-52

Wang Q, Zheng Y P, Qin L, Huang Q H, Lam W L, Leung G, Guo X and Lu H B 2008b Real-time ultrasonic assessment of progressive proteoglycan depletion in articular cartilage *Ultrasound in Medicine and Biology* **34** 1085-92

Wang Q, Zheng Y P, Qin L, Huang Q H, Lam W L, Leung G, Guo X and Lu H B 2008c Ultrasonic assessment of progressive proteoglycan depletion of articular cartilage in real-time *Ultrasound in Medicine and Biology* **In print**

Wang X Y, Zhang C P, Zhang L S, Xue L L and Tian J G 2002b Simultaneous refractive index and thickness measurements of bio tissue by optical coherence tomography *Journal of Biomedical Optics* **7** 628-32

Waters N E 1965 The Indentation of Thin Rubber Sheets by Spherical Indentors *Brit J Appl Phys* **16** 557-63

Watrin-Pinzano A, Ruaud J P, Olivier P, Grossin L, Gonord P, Blum A, Netter P, Guillot G, Gillet P and Loeuille D 2005 Effect of proteoglycan depletion on T2 mapping in rat patellar cartilage *Radiology* **234** 162-70

Welsing R T C, van Tienen T G, Ramrattan N, Heijkants R, Schouten A J, Veth R F H and Buma P 2008 Effect on tissue differentiation and articular cartilage degradation of a polymer meniscus implant - A 2-year follow-up study in dogs *Am J Sport Med* **36** 1978-89

Werber A and Zappe H 2006 Tunable, membrane-based, pneumatic micro-mirrors *J Opt a-Pure Appl Op* **8** S313-S7

Wheaton A J, Dodge G R, Borthakur A, Kneeland J B, Schumacher H R and Reddy R 2005 Detection of changes in articular cartilage proteoglycan by T-1p, magnetic resonance imaging *Journal of Orthopaedic Research* **23** 102-8

Wilhjelm J E, Pedersen P C and Jacobsen S M 2001 The influence of roughness, angle, range, and transducer type on the echo signal from planar interfaces *IEEE Transactions on Ultrasonics Ferroelectrics and Frequency Control* **48** 511-21

Xie T Q, Ahn Y C, Chen Z P and Peavy G 2008 In vitro 3D articular cartilage imaging using endoscopic spectral domain optical coherence tomography (SD-OCT) with a GRIN (gradient index) lens rod based probe - art. no. 684730 *Coherence Domain Optical Methods and Optical Coherence Tomography in Biomedicine XII* **6847** 84730

Xie T Q, Guo S G, Chen Z P and Peavy G M 2007 Regional polarization sensitivity of articular cartilage by using polarization sensitive optical coherence tomography - art. no. 64292O. In: *Conference Coherence Domain Optical Methods and Optical Coherence Tomography in Biomedicine XI*, ed J G I J A T V V Fujimoto (San Jose, CA: Spie-Int Soc Optical Engineering) p O4292

Xie T Q, Guo S G, Rao B, Chen Z P and Peavy G M 2005 Cartilage disease diagnosis by conventional and polarization-sensitive optical coherence tomography *Coherence Domain Optical Methods and Optical Coherence Tomography in Biomedicine IX* **5690** 556-62

Xie T Q, Guo S G, Zhang J, Chen Z P and Peavy G M 2006a Determination of characteristics of degenerative joint disease using optical coherence tomography and polarization sensitive optical coherence tomography *Lasers in Surgery and Medicine* **38** 852-65

Xie T Q, Guo S G, Zhang J, Chen Z P and Peavy G M 2006b Directional polarization sensitivity of articular cartilage by optical coherence tomography *Coherence Domain Optical Methods and Optical Coherence Tomography in Biomedicine X* **6079** E792

Xie T Q, Guo S G, Zhang J, Chen Z P and Peavy G M 2006c Use of polarization-sensitive optical coherence tomography to determine

the directional polarization sensitivity of articular cartilage and meniscus *Journal of Biomedical Optics* **11** 8

Yasura K, Mizuno Y, Nakagawa Y, Mori K, Takenaka M, Ohashi T, Yamada K, Kobayashi M, Ando K, Kuroki H, Suzuki T, Ikeuchi K, Tsutsumi S and Nakamura T 2007 Estimation of the mechanical property of meniscus using ultrasound: Examinations of native meniscus and effects of enzymatic digestion *Journal of Orthopaedic Research* **25** 884-93

Yelin E and Callahan L F 1995 The economic cost and social and psychological impact of musculoskeletal conditions. National Arthritis Data Work Groups *Arthritis and rheumatism* **38** 1351-62

Youn J I 2008 Evaluation of morphological changes in degenerative cartilage using 3-D Optical Coherence Tomography *Journal of the Optical Society of Korea* **12** 98-102

Youn J I, Akkin T and Milner T E 2004 Electrokinetic measurement of cartilage using differential phase optical coherence tomography *Physiological Measurement* **25** 85-95

Zhang M, Zheng Y P and Mak A F T 1997 Estimating the effective Young's modulus of soft tissues from indentation tests - nonlinear finite element analysis of effects of friction and large deformation *Med Eng Phys* **19** 512-7

Zhang Y Q and Jordan J M 2008 Epidemiology of osteoarthritis *Rheum Dis Clin N Am* **34** 515-29

Zhang Y Q, Xu L, Nevitt M C, Aliabadi P, Yu W, Qin M W, Lui L Y and Felson D T 2001 Comparison of the prevalence of knee osteoarthritis between the elderly Chinese population in Beijing and whites in the United States - The Beijing osteoarthritis study *Arthritis and rheumatism* **44** 2065-71

Zheng Y P, Bridal S L, Shi J, Saied A, Lu M H, Jaffre B, Mak A F T and Laugier P 2004a High resolution ultrasound elastomicroscopy imaging of soft tissues: system development and feasibility *Physics in medicine and biology* **49** 3925-38

Zheng Y P, Ding C X, Bai J, Mak A F T and Qin L 2001 Measurement of the layered compressive properties of trypsin-treated articular cartilage: an ultrasound investigation *Med Biol Eng Comput* **39** 534-41

Zheng Y P, Lu M H and Wang Q 2006a Ultrasound elastomicroscopy using water jet and osmosis loading: Potentials for assessment for articular cartilage *Ultrasonics* **44** e203-9

Zheng Y P, Mak A F, Lau K P and Qin L 2002 An ultrasonic measurement for in vitro depth-dependent equilibrium strains of articular cartilage in compression *Physics in medicine and biology* **47** 3165-80

Zheng Y P and Mak A F T 1996 An ultrasound indentation system for biomechanical properties assessment of soft tissues in-vivo *IEEE Transactions on Biomedical Engineering* **43** 912-8

Zheng Y P, Patil S and Wang Q 2006b Ultrasound speed in articular cartilage under different bathing saline concentration *Advanced Nondestructive Evaluation I, Pts 1 and 2, Proceedings* **321-323** 972-7

Zheng Y P, Shi J, Qin L, Patil S G, Mow V C and Zhou K Y 2004b Dynamic depth-dependent osmotic swelling and solute diffusion in articular cartilage monitored using real-time ultrasound *Ultrasound in medicine & biology* **30** 841-9